LAPPEENRANTA UNIVERSITY OF TECHNOLOGY
LUT School of Technology
LUT Chemtech

Noora Pehrman

SLURRY FLOWS IN PROGRESSIVE CAVITY AND IN HOSE PUMPS

Examiners: Professor Tuomas Koiranen
M.Sc. (Tech.) Jarmo Partanen

ACKNOWLEDGEMENTS

This Master's thesis was done for Flowrox Oy between January and October 2014 in Lappeenranta.

I would like to thank my supervising professor Tuomas Koiranen for guidance and for giving me good advices during this thesis. I would also like to thank my second supervisor Jarmo Partanen for guidance and help to organize the experiments in Flowrox Oy. Also, Esa Paavola deserves thanks for his help in the experiments.

I would also like to thank my lovely family for all that support that I have had during my life, especially during my university years.

Last but definitely not least, I would like to thank all my friends. Thanks for your support, encouragement, and existence. Friends, you are the best, and I am very grateful to have you all in my life.

Noora Pehrman

Lappeenranta, 21th October 2014

TIIVISTELMÄ

Lappeenrannan teknillinen yliopisto
Teknillinen tiedekunta
LUT Kemiantekniikka

Noora Pehrman

Lietevirtaukset epäkeskoruuvipumpussa ja letkupumpussa

Diplomityö

2014

74 sivua, 39 kuvaa, 8 taulukkoa ja 5 liitettä

Tarkastajat: Prof. Tuomas Koiranen
DI Jarmo Partanen

Hakusanat: letkupumppu, ruuvipumppu, painepiikki, reologia

Tämän diplomityön tarkoituksena oli tutkia, kuinka pumpattavan lietteen viskositeetti ja reologia vaikuttavat pumppaukseen peristalttisessa letkupumpussa sekä epäkeskoruuvipumpussa. Lisäksi työssä tutkittiin letkupumpun aiheuttamia painepiikkejä. Painepiikkejä tutkittiin pumppaamalla erilaisia lietteitä sekä käyttämällä erilaisia putkimateriaaleja. Työssä käytetyille pumpuille määritettiin paine- ja tehokäyrät. Epäkeskoruuvipumpulle määritettiin myös $NPSH_R$-käyrä.

Kirjallisuusosa keskittyi käsittelemään fluidien jaottelua eri reologia-tyyppeihin sekä teorioihin ja malleihin, joilla eri reologia-tyypit voidaan tunnistaa. Erityishuomio diplomityössä kiinnitettiin ei-newtonisiin fluideihin, joita käytettiin myös työn kokeellisessa osassa. Lisäksi kirjallisuusosa käsitteli työssä käytettyjä pumppuja, pumppujen mitoitukseen käytettäviä parametreja sekä painepiikkejä.

Diplomityön kokeellisessa osassa käytettiin tärkkelys-, bentoniitti- ja karboksimetyyliselluloosa-lietteitä. Lietteitä pumpattiin Flowroxin peristalttisella letkupumpulla (LPP-T32) sekä epäkeskoruuvipumpulla (C10/10). Jokaisesta pumpatusta lietteestä otettiin näyte, josta määritettiin lietteen konsentraatio, viskositeetti ja reologia-tyyppi. Käytetyt putkistomateriaalit painepiikki-kokeissa olivat teräs- ja kumiputki sekä pulsaation vaimentimen prototyyppi.

Pulsaatio kokeet osoittivat, että alhaisella painetasolla kumiputki ja pulsaation vaimentimen prototyyppi vaimensivat pulsaatiota selvästi paremmin kuin teräsputki. Painetason ja pumpun pyörimisnopeuden kasvaessa erot eri materiaalien välillä hävisivät. Liete-kokeissa painepiikit olivat erilaisia riippuen lietteen reologiasta ja viskositeetista. Kokeiden perusteella lietteiden reologia ei kuitenkaan merkittävästi vaikuttanut pumppujen tehon kulutukseen tai hyötysuhteeseen.

ABSTRACT

Lappeenranta University of Technology
LUT School of Technology
LUT Chemtech

Noora Pehrman

Slurry flows in progressive cavity and in hose pumps

Master's thesis

2014

74 pages, 39 figures, 8 tables, and 5 appendices

Examiners: Prof. Tuomas Koiranen
M. Sc. (Tech.) Jarmo Partanen

Keywords: hose pump, screw pump, pressure pulsation, rheology

The aim of this thesis was to research how slurry's viscosity and rheology affect to pumping in peristaltic hose pump and in eccentric progressive cavity pump. In addition, it was researched the formed pressure pulsation in hose pump. Pressure pulsation was studied by pumping different slurries and by using different pipe materials. Pressure and power curves were determined for both used pumps. It was also determined $NPSH_R$ curve for the progressive cavity pump.

Literature part of the thesis considered to distribute fluids to different rheology types, as well as theories and models to identify different rheology types. Special attention was paid to non-Newtonian fluids, which were also used in experimental part of this thesis. In addition, the literature part discusses about pumps, parameters for pump sizing, and pressure pulsation in hose pump.

Starch, bentonite, and carboxymethyl cellulose slurries were used in the experimental part of this thesis. The slurries were pumped with Flowrox peristaltic hose pump (LPP-T32) and eccentric progressive cavity pump (C10/10). From the each slurry was taken a sample, and the samples were analyzed for concentration, viscosity and rheology type. The used pipe materials in pressure pulsation experiments were steel and elastic, and it was also used a prototype of pulsation dampener.

The pulsation experiments indicated that the elastic pipe and the prototype of pulsation dampener attenuated pressure pulsation better than the steel pipe at low pressure levels. The differences between different materials disappeared when pressure level and pump rotation speed increased. In slurry experiments, pulsation was different depending on rheology and viscosity of the slurry. According to experiments, the rheology did not significantly affect to pump power consumption or efficiency.

LIST OF ABBREVIATIONS AND SYMBOLS

ABBREVIATIONS

CMC	Carboxymethyl Cellulose
CR	Controlled Strain Rate
CS	Controlled Stress
LPP	Larox Peristaltic Pump
NaOH	Sodium hydroxide
NPSH	Net Positive Suction Head
$NPSH_A$	Net Positive Suction Head Available
$NPSH_R$	Net Positive Suction Head Required
PCP	Progressive Cavity Pump
PDP	Positive Displacement Pump
PVS	Polyvinyl Siloxane

SYMBOLS

A_i	Calculational area	bar·s
A_p	Area of the pipe	m^2
A_{pl}	Are of the plane	m^2
du_x/dy	Velocity gradient	1/s
d	Pipe diameter	m
dy	Distance between planes	m
F	Shear force	Pa
f	Friction factor	-
G	Shear modulus	-
g	Standard gravity (9.81 m/s^2)	m/s^2
H	Pump head	m
H_{fl}	Dynamic friction loss of the suction pipe	m
H_{sh}	Suction height	m
I	Voltage	V
K	Index parameter	-
L	Pipe length	m
l	Distance between pressure meters	m
m	Mass of the solid	g
m_{tot}	Mass of the total mixture	g
n	Index parameter	-
n	Number of data points	-
P_e	Electric pump power	W
P_{theo}	Theoretical pump power	W
p	Fluid pressure	Pa
p_a	Atmospheric pressure	Pa
p_n	Pulsation cycle pressure	bar
p_d	Pump discharge pressure	Pa

p_s	Static pressure of the vessel	Pa
p_{sc}	Pump suction pressure	Pa
p_{vp}	Vapor pressure of the fluid	Pa
p_0	Pressure below the peak	bar
$\bar{p}_A$	Time averaged pressure in pulsation cycle	bar
$\bar{p}$	Average pressure	bar
q_v	Volume flow	m^3/s
Re	Reynold's number	-
t_{tot}	Pressure peak cycle	s
U	Current	A
u_x	Velocity x-direction	m/s
v	Fluid flow velocity	m/s
w	Concentration	wt-%
Z	Suction height	m
$\dot{\gamma}$	Shear rate	1/s
Δp	Pressure difference of the suction and the discharge	Pa
Δp_{fri}	Frictional losses	Pa
Δp_{losses}	Pressure losses	Pa
Δp_{minor}	Minor losses	Pa
ζ	Minor coefficient	-
η	Pump efficiency	-
λ	Relaxation time	s
μ	Dynamic viscosity	Pa·s
ρ	Density of the fluid	kg/m^3
ρ_w	Density of water	kg/m^3
τ	Shear stress	Pa
τ_y	Yield stress	Pa
$\dot{\tau}$	Time derivative	Pa/s

TABLE OF CONTENTS

1 INTRODUCTION

Nowadays it is difficult to find a process or a plant where are no pumps. A pump is known as a device that can be used to transfer liquids and in some cases to change fluid pressure. Pump is one of the most common machines in the modern industry due to its important role in processes. The knowledge of the earliest pumps varies depending on the source. According to Abulencia and Theodore (2009), the earliest forms of pumps were used in 3000 B.C.E. in Mesopotamia. These first pumps were water wheels (also known as Persian wheels) containing buckets for water. When the wheel was rotating, the buckets were immersed in water and they were automatically emptied when they achieved their highest point in the rotating wheel. [1,2]

The pumps can be classified into several groups (dynamic, positive displacement etc.). Each group contains numbers of pumps whose operation principles are slightly different. The most general and best-known pump is a centrifugal pump. However, centrifugal pumps work best in dilute solutions. Problems in pumping will occur when the solid content and the fluid viscosity increase. For thick fluids (slurries), suitable pumps are positive displacement pumps. Positive displacement pumps are self-priming pumps, which have a displacement chamber or chambers. The chamber displaces corresponding quantity of liquid and transfers it forward along the pipe.

Fluids are divided into Newtonian and non-Newtonian fluids. The distribution is based on Newton's law of viscosity. Theory suggest that Newtonian fluids follows the law and non-Newtonian do not. Non-Newtonian fluids are divided further into smaller groups depending on their rheological properties. The purpose of this thesis was to research how different rheologies of slurries affect to the pumping. The used pumps were Flowrox peristaltic hose pumps (LPP-T32) and progressive cavity pump (C10/10). In addition of traditional pumping, this thesis examined pressure pulsation in hose pump. The experimental part of this thesis was done in Flowrox Oy in Lappeenranta.

2 POSITIVE DISPLACEMENT PUMPS

The fluid transfer pumps can be divided into three main categories according to their operating principle: [3]

- positive displacement pumps (PDP or PD-pump)
- dynamic pumps
- other pumps

Positive displacement pumps are not as well-known as the centrifugal pumps. Centrifugal pumps belong to the group of dynamic pumps. The basic difference between centrifugal and PD-pump is that PD-pump creates flow and the centrifugal pump creates pressure. [4] The selection between centrifugal or positive displacement pump depends on the fluid composition. For example, centrifugal pumps are used in applications, which need a wide capacity range (0.01-400 m^3/min) and a wide range of pump head. [5] Instead, positive displacement pumps are applied for fluids that have high viscosity, high pressure, low velocity, and low shear [6].

All positive displacement pumps work in principle at the same way. Displacement chamber displaces the liquid and transfers it to the pressurized discharge pipe. PD-pumps have an expanding cavity on the suction side and a decreasing cavity on the discharge side. In suction side, liquid expands and flows to discharge pipe. At the same time when the liquid flows, the cavity collapses. [4] PD-pumps can be divided into rotary and reciprocating pumps depending on the nature of movement of the pressure-producing members. In Figure 1, the classification of displacement pumps is presented.

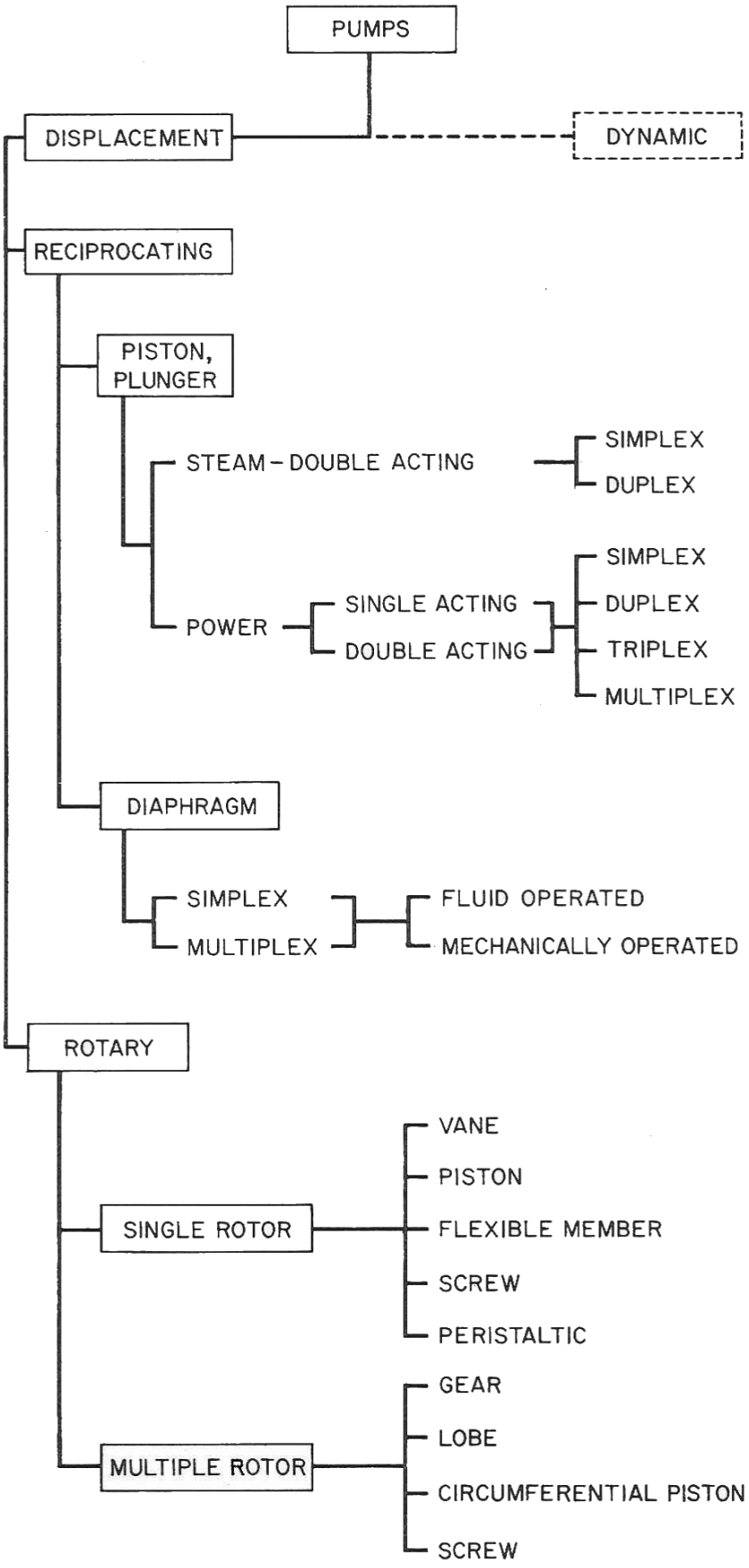

Figure 1. Classification of positive displacement pumps [2].

Vane, piston, flexible member, lobe, gear, circumferential piston, and screw pumps are rotary pumps. Rotary pumps must be able to handle fluids, which consist of liquid and vapor. Majority of rotary pumps are self-priming. [2,7] The most common reciprocating pumps are piston and plunger pumps, which are still divided into steam and power pumps. Piston pump can be direct-/indirect-acting, horizontal/vertical, single-/double-acting or simplex/duplex/multiplex type. Diaphragm (simplex or duplex) pumps are also included for the group of reciprocating pumps. [7,8]

In rotary positive displacement pumps the rotating vane, screw, or gear traps transfers liquid from suction side and forces it to discharge side. Rotary pumps are applied for systems, which need a high suction lift and self-priming properties. In rotary pumps usually occur backflow, which can be noticed as a "slippage" in characteristic curve of PD-pumps. The characteristic curve of PD-pump is presented later in Figure 11 in Chapter 5.2. The clearances between rotating and stationary parts should keep to a minimum to prevent or minimize backflow. [8]

This research is focused on progressive cavity and peristaltic hose pumps, which are both rotary positive displacement pumps.

2.1 Progressive cavity pump

Progressive cavity pump (PCP) is a single and eccentric screw pump, which is applied for challenging conditions. Typical applications for PC-pumps are pulp and paper industry, water and wastewater treatment, chemical and mining industry. Especially PCPs are suitable for pumping slurries and pastes. PC-pumps are one of the most used artificial lift system in low deep wells because they have many important properties. PC-pumps can pump heavy oils and endure both large concentrations of sand and high amounts of gases. PC-pump is also known as a mono pump, an eccentric screw pump, and a "worm pump". [9,10]

The working principle of progressive cavity pump is based on eccentricity of stator and rotor. Between rotor and stator are formed cavities where the fluid will flow. In PC-pump, cavities are moving forward at the same time with the fluid due to rotor rotation. [2] There can be both single and multiple acting PC-pumps. Multiple screw pumps have multiple external screw threads and single screw

pump has only one thread. [11] The main components of progressive cavity pump are shown in Figure 2.

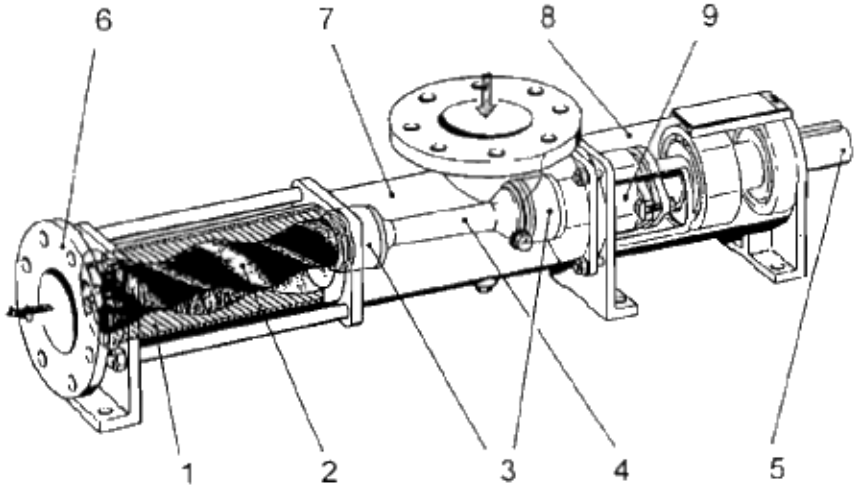

Figure 2. Principle of progressive cavity pump. 1) stator; 2) rotor; 3) cardan coupling; 4) cardan shaft; 5) drive shaft; 6) discharge flange; 7) pump housing; 8) bearing housing; 9) seal housing. [12]

PCP consists of rotor and stator. According to Pessoa *et al*. (2009), the material of stator may be steel or some elastomer but the rotor is made of metal. The internal surface of the stator consists of several helices without eccentricity. The internal surface of rotor has one less helical than in stator, and one-step in rotor is equal to half the stator's step. [9] The steps of rotor and stator are represented in Figure 3.

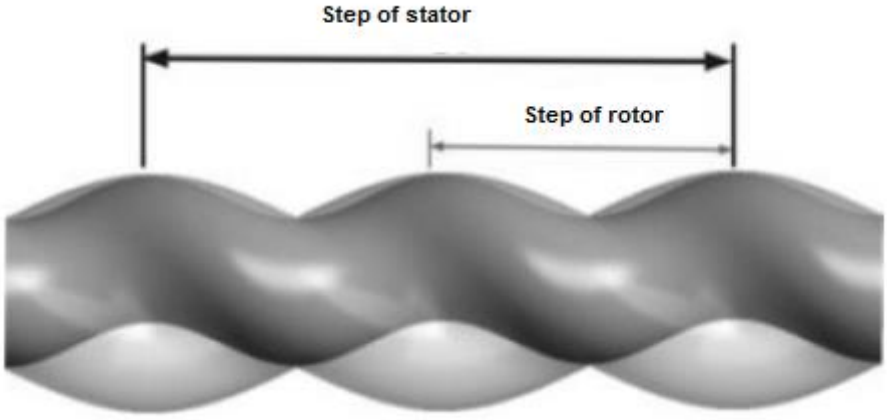

Figure 3. Stator and rotor steps in progressive cavity pump [9].

2.2 Peristaltic hose pump

Hose pump belongs to the group of peristaltic pumps. Hose pumps have a hose inside the pump casing where the fluid is flowing. Hose pumps can be used, for example, in chemical process industries, steel factories, and breweries. [13]

The main components of the hose pump are a hose and a rotor. Operating principle of the hose pump is based on peristaltic effect in pump. The working cycle of hose pump begins when in suction side is formed negative pressure, which sucks fluid into hose. When rotor rotates, it compresses and flattens the hose and pushes fluid forward. After compression, hose returns back to its original form creating negative pressure conditions on the suction side of pump. [14] In Figure 4, the stages of fluid moving in hose in hose pump are shown.

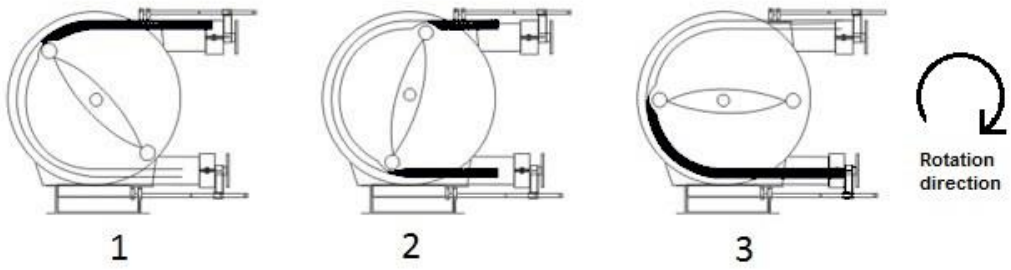

Figure 4. The operating principle of a hose pump. The numbers 1-3 represent the stages of the operating. 1) Fluid exits from discharge side 2) new cycle starts when suction side sucks fluid into hose 3) Rotor pushes fluid forward in the hose. The fluid inside the hose is shaded. [15]

2.3 Flowrox Oy

Flowrox Oy manufactures valves and pumps for challenging conditions for heavy industries. Typical industries, where Flowrox supplies its products, are especially mining and mineral processes. The products are also used in energy and environment industries, which need corrosion resistant products. Flowrox has head office in Lappeenranta and branch office in Kouvola. In addition, Flowrox has subsidiaries in Maryland (USA), in Sydney (Australia), in Johannesburg (South Africa), in Moscow (Russia), and in Shanghai (China). [14]

The company was established in 1977 and its original name was Larox Oy. In 1993, Larox established a subsidiary called Larox Flowsys Oy and six years later,

it became associated company of Larox Oy. In 2011, company changed its name to Flowrox Oy. [14]

Flowrox manufactures pinch, knife gate, and rotary disc valves. In addition, Flowrox produces peristaltic hose pumps and progressive cavity pumps. A more detailed discussion of the Flowrox's pumps is shown next. [14]

2.3.1 Flowrox eccentric progressive cavity pump

Flowrox has a wide selection of progressive cavity pumps, which can be divided into four series: C-, EL-, E- and D-series. The C-series are intended for the most demanding applications, for example, for pulp and paper, mining and minerals, and chemical industries. E-models can be used in various industrial applications, and EL-models are made for environmental applications (wastewater treatment). EL-models withstand high particle sizes. Instead of, D-series is for dosing applications. [16] The series differ from each other in size and material. The pumps inside materials can be varied depending on the properties of pumped fluid.

A special feature of Flowrox PC-pumps is the "2/3 spiral technology". Generally, PC-pump has a round rotor and a round stator. In 2/3 spiral technology PC-pump has an elliptic rotor and stator which have an elastomer layer in the inner surface. Using a spiral stator, thickness of the elastomer through the stator is same unlike in conventional stator where the thickness varies. When thickness is same through the stator, there is less backflow. In addition, the spiral technology enables to use more pressure, higher flow per revolution, and the lifetime of rotor and stator are longer. The spiral technology is used in series E and C, and the round technology is used in series EL and D. [17] The round shape and the spiral stators are represented in Figure 5.

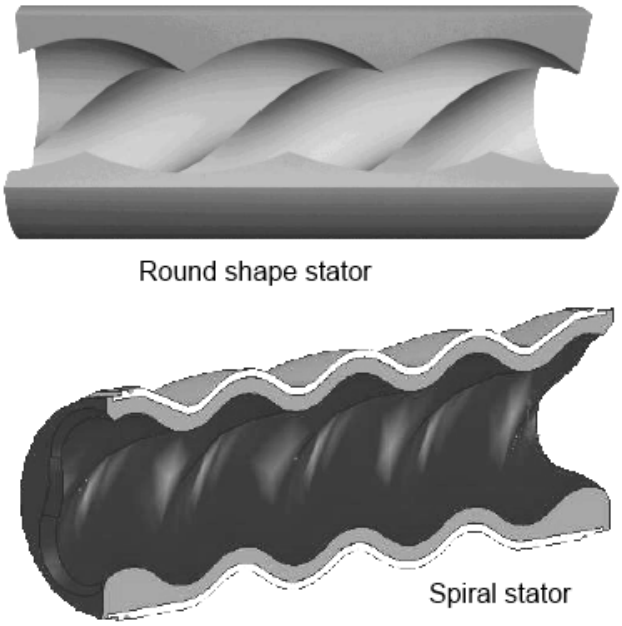

Figure 5. Round shape and spiral stators in Flowrox PC-pumps [10].

Rotors of Flowrox PC-pumps are made of a hard-coated stainless steel, stainless steel, or hard-coated carbon steel. The material of stator depends on the composition of pumped fluid. [10] In Table I, the suitable stator materials for different fluids are presented.

Table I Stator materials for various compounds containing fluids [10].

Material	Composition of fluid
Nitrile butadiene rubber (NBR)	Oil and fat
Natural rubber (NR)	Extremely abrasive
Nitrile rubber (NBRF)	Food grade
Ethylene propylene diene monomer (EPDM)	Chemicals
VITON (Synthetic rubber)	Aggressive chemicals

2.3.2 Flowrox's peristaltic hose pump

Flowrox has three different series of LP-pumps and the series are designed for the different applications. The series are:

- LPP-T for transferring
- LPP-D for dosing
- LPP-M for metering

LP-pumps can be used in many applications depending on the pumped media. In Table II, some example applications for LP-pumps are shown. [18]

Table II Typical applications for Flowrox LP-pumps [18].

Application/media	Industry
Paints, acids, resins	Chemical process industries
Metal concentrates & flocculants	Mining & metal industry
Slurries, sludge, mud, additivies	Water & effluent treatment
GCC, PCC, Talc, Chaolin, TiO_2	Pigments & fillers
Lime, waste, slurries	Energy production
Paper coatings, glues, additivies	Pulp & paper industry
Filtering & filtration aids, diatomaceous earth, starch	Food & Beverage industry
Mortars, plasters, bentonite, cement	Construction industry
Drilling mud, waste sludge	Oil & Offshore

Flowrox LP-pumps have several advantages: high-pressure capability, no overheating at high continuous flow rates, low energy consumption, easy maintenance, and low operating cost. Other benefits of LP-pumps are: no wear and corrosion, dry run capability, self-priming up to 9.5 meters, exact flow per revolution irrespective of the pipeline pressure, accurate flow, and no mixing or shearing of the medium. In addition, in LP-pumps only the hose is in contact with medium, no gland water, or packing, full vacuum capability, no backward flow and possibility to change the direction of the pumping. [14,19] The mechanical structure of Flowrox LP-pump is presented in Figure 6.

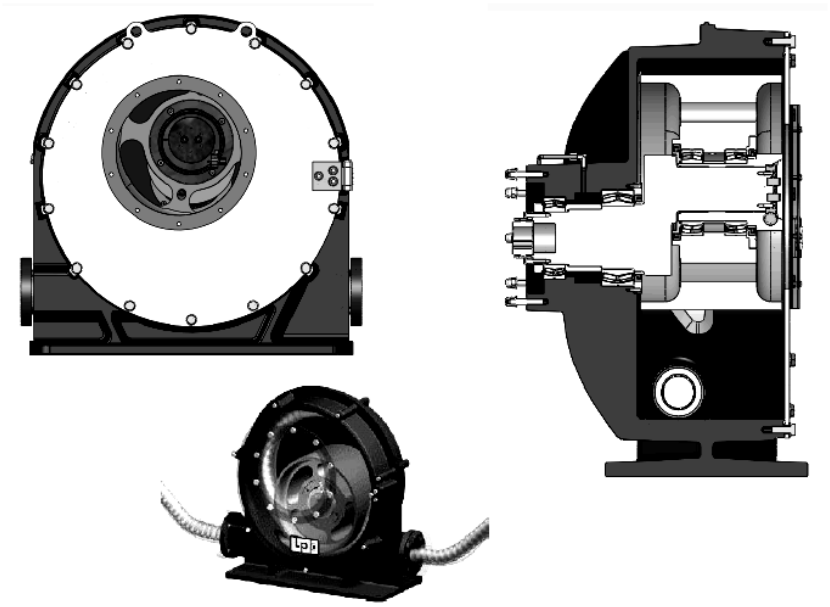

Figure 6. Mechanical structure of Flowrox LP-pump [13].

In summer 2012, Flowrox brought onto the market the world's largest hose pump, LPP-T100. This LP-pump has maximum flow of 100 m^3/h and its maximum pressure is 10.0 bar. Using the rolling technology, the pump will deliver 31 liters per 360° working period. In one service period, LPP-T100 uses only 25 liters lubricant, which is 25% of the normal lubricant consumption. The lubricant is placed in the pump when changing the hose, otherwise the lubricant will not be added. [14,20]

3 FLOW CONTROL IN POSITIVE DISPLACEMENT PUMPS

The methods to control positive displacement pump differ from the methods to control centrifugal pumps. Throttling does not work in PD-pumps, whereas centrifugal pumps are easy to control by throttling the discharge or suction. [21] Positive displacement pumps can be controlled only by varying the flow through the pump. The flow can be control by either speed control or bypass control. [22]

3.1 Speed control

The speed control is an easy method to control positive displacement pump because the flow rate of PD-pump is proportional to speed. Practically this means that the slower the rotation speed of the pump is, the lower the flow rate through the pump is. [21] Simply, the rotation speed of the pump is changed when is wanted to change the flow rate of the system.

3.2 Bypass control

Bypass control, also called recycle control, is another method to control flow in positive displacement pumps. In this method, some part of the flow is routed back to the suction source or to the separated surge tank. The operation is based on separated process measurement devices, which are connected to the control valve. Measurement devices measure different variables in the process, for example pressure in the process or the liquid level in the tank. When one variable changes, a signal is transmitted to the control valve. According to the signal, the valve either opens or closes. [21,22] In Figure 7, the system procedure of bypass control in positive displacement pump is presented.

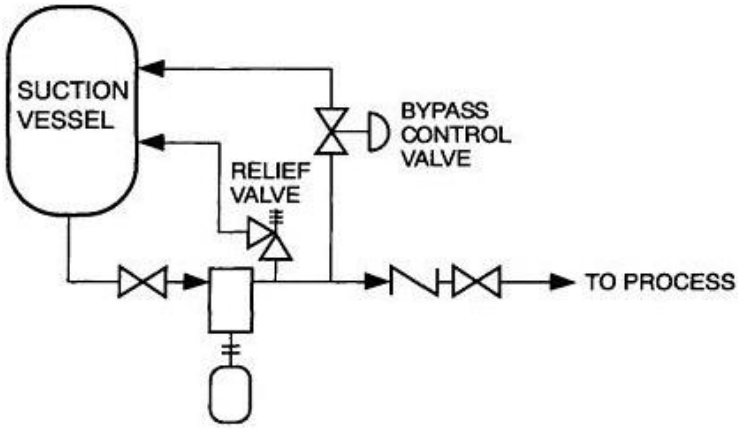

Figure 7. The bypass control system in positive displacement pumps. After pumping, some part of the fluid is recycled back. [22]

4 PRESSURE PULSATION IN HOSE PUMPS

The pressure fluctuations in the piping systems are called pressure pulsation and they are usually caused by the pump itself [23]. It is argued that there is not a pulseless pump but the intensity of pulsation varies a lot between different pumps. Both hydraulic motion systems and chemical injection pumps cause pulsation in the pumping system. Especially a hose pump can indicate pulsating discharge flow, which causes fluctuations in the pressure. Pressure pulsation can also be called pressure spikes or just pulsation.

4.1 The formation of the pulsation

Hose pump works by taking a certain amount of a pumped fluid between the compressing element and then pushing the fluid forward in the hose. The fluid pressure is higher than the pressure in the pumping system. Pressure changes in the system when the pumped fluid is transferred to the system. This action causes fluctuations in pressure, which can be described as sinusoidal pattern. Graph of sinusoidal pattern is presented in Figure 8. [24]

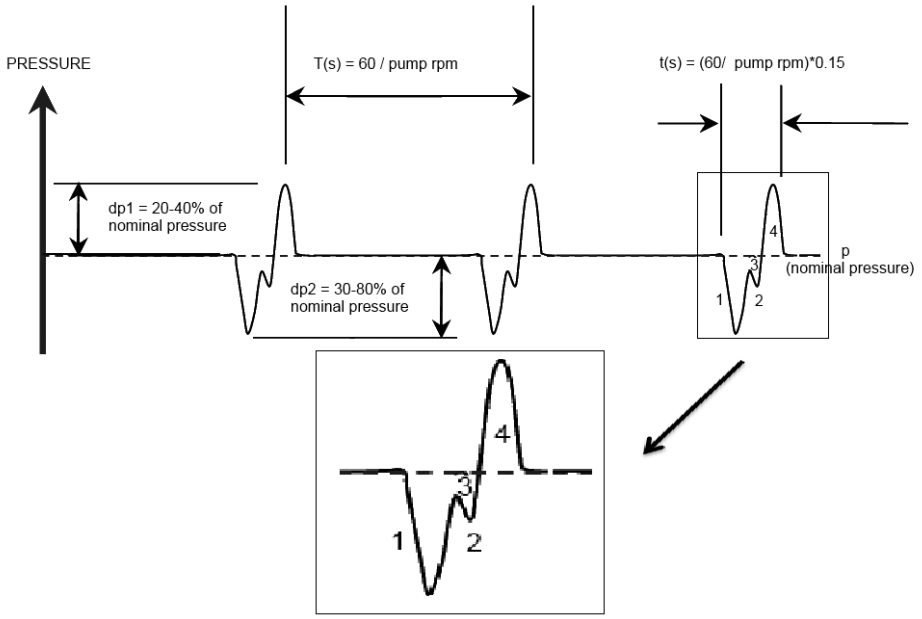

Figure 8. Theoretical LP-pump pulsation chart at pump outlet. The stages of pulsation: 1) pressure drops as medium velocity reduces when rotor closes outlet port; 2) pressure increases back to static pressure head when outlet port is closed by rotor and medium velocity is 0; 3) rotor starts to leave outlet port and hose in the pump is pressurized; 4) new pumping cycle starts and medium velocity increases. T(s)= duration of one pump cycle, dp1= pressure rise from nominal pressure, dp2= pressure drop from nominal pressure. [25]

The pump discharges the fluid as the cycles wherein pressure does not stay constant. The fluctuations in fluid pressure cause waves, which move through the fluid until they reach a bend or a restriction in the pipe. When the wave encounters some obstacle, some of the wave's energy is transferred to the obstacle and the rest is reflected back against the flow coming from the pump. [24]

4.2 Disadvantages of the pulsation

Pressure pulsation can cause disadvantages for the whole piping system. Pulsation causes mechanical fatigue and radiated noise. The noise can be defined to structure-borne and fluid-borne noises. The structure-borne noise is direct mechanical vibration, which is caused by the pump. Instead of, the fluid-borne noise is due to tension between flowing fluid and the pipe wall. [26] In long-term, both noises reduce pipeline's lifetime.

4.3 Methods to reduce pulsation

The best method to reduce pulsation would be to optimize pump operation in such a way that the pulsation does not even occur. However, in this thesis examined the methods to reduce pressure pulsation. Next is presented some examples for that.

4.3.1 Pulsation dampener

Pulsation in pumping system can be avoided by using a pulsation dampener. A pulsation dampener adsorbs pipe vibration, water hammering, and pressure fluctuations in the system. A dampener is also used as a tank for fluid thermal expansion. The dampener is connected to the pump outlet to control pressure and volume fluctuations of the pump. [27]

The basic pulsation dampener consists of a chamber containing a diaphragm or a cylinder-containing bladder. In the diaphragm case, the diaphragm divides the chamber into two parts. The other part contains compressed air or gas (for example nitrogen), and the other the fluid being pumped. Diaphragm prevents contact between fluid and gas in the system. During pump discharge, process fluid enters to the dampener and compresses gas, and gas adsorbs the shock. After that, pressure of the fluid decreases and gas expands when it forces the fluid back into the pumping system. [18,24] In Figure 9, the design of the pulsation dampener is presented.

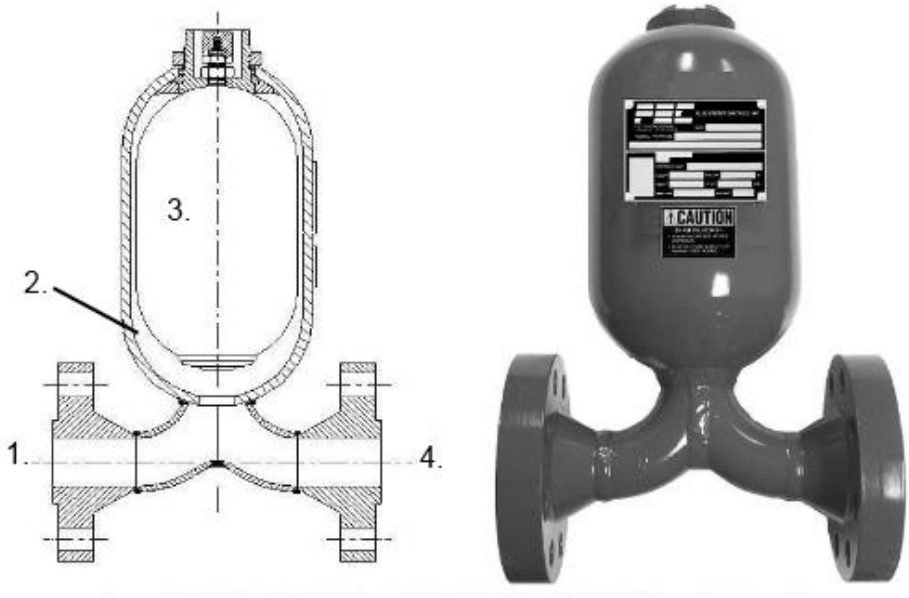

Figure 9. Pulsation dampener for reducing pressure spikes. 1) dampener inlet; 2) the part of the chamber in which the fluid flows; 3) compressed air or gas, which adsorbs the shock; 4) dampener outlet. [24]

4.3.2 Multiple rollers

One solution to reduce pulsation in hose pump is to use multiple rollers in rotor. Many hose pump has two or three rollers but some pumps have even six or eight rollers. In this context, the space in the hose, where the fluid is between two rollers, is called a pillow. Instead of, the area of the hose, which is compressed by the roller, is called a void. By using multiple rollers in hose pump, the pillow and void volumes are almost the same. Consequently, each pillow fills the void between pillows in opposite channel. This generates almost a pulseless flow. [28]

4.3.3 Design of the compressing element

According to Hermanus and Vrielink (2007), pressure pulsations can be avoided by designing the element, which compresses the hose, correctly. In the patent, the distance between the compressing element and the compressed surface is either smaller or equal to the length of the intermediate part. Usually, the distance between these elements is bigger. So, when the local compression ends and when the pressing element approaches the end of the outlet side, there occurs an increase in the volume of the hose at this outlet side. This phenomenon occurs relatively quickly and it is uncontrolled, which causes temporary change of speed

in the medium flow and at the inlet side. Pressure pulsation occurs due to the result of these problems. [29] The draft of the hose pump design is shown in Figure 10.

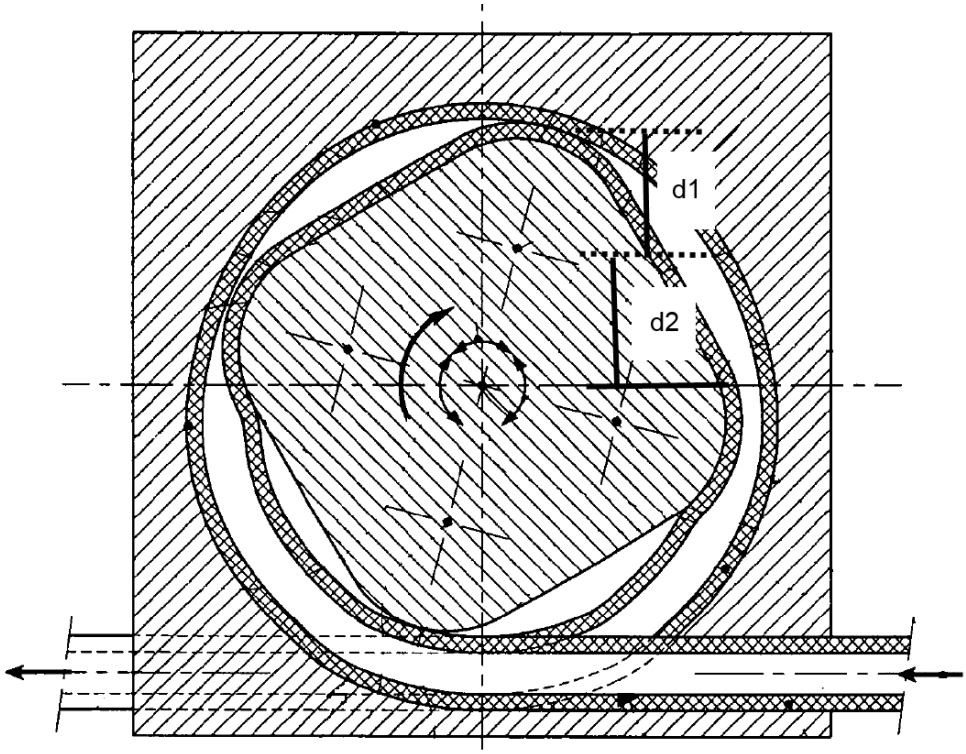

Figure 10. Hose pump, where the distance between the compressing element (rotor) and the surface of the hose (d1) is smaller/equal to the distance between the hub and the compressing element (d2) [29].

The pressure pulsations can be reduced by designing the distance between the compressing rotor and the compressed surface of the hose such a way that the distance is smaller or equal to the intermediate part. In addition, the use of an elastic hose, which returns its original form slowly, is preferred. This reduces the sudden change in the flow. [29]

5 PUMP PERFORMANCE

The operation of pumps can be described for example by some pump curves, by some equations and parameters, and by NPSH values. With these variables, the operation of pump can be designed and evaluated before the pump is built in order to avoid pumping problems.

5.1 Pump parameters

The pump operation can be described by some basic parameters. The most important parameters and the equations are presented below. [30]

Volume flow

$$q_v = v \cdot A_p \tag{1}$$

where
- q_v volume flow, m^3/s
- v fluid flow velocity, m/s
- A_p area of the pipe, m^2

Theoretical pump power

$$P_{theo} = \rho \cdot g \cdot H \cdot q_v = \Delta p \cdot q_v \tag{2}$$

where
- P_{theo} theoretical pump power, W
- ρ density of the fluid, kg/m^3
- q_v volume flow, m^3/s
- g standard gravity (9.81 m/s^2), m/s^2
- H pump head, m
- Δp pressure difference of the suction and the discharge, Pa

Usually the real power of the pump is higher than the calculated theoretical power [31]. The actual power of the pump can be calculated by multiplying the electric current and the voltage of the pump motor.

$$P_e = I \cdot U \tag{3}$$

where
- P_e electric pump power, W
- I voltage, V
- U current, A

The efficiency of the pump is calculated as the ratio of theoretical and electric pump powers.

$$\eta = \frac{P_{theo}}{P_e} \tag{4}$$

where η pump efficiency, -
P_{theo} theoretical pump power, W
P_e electric pump power, W

The efficiency of the pump takes into accounts the electrical failures and mechanical losses, which occur in pumping [32].

5.2. Pump curves

Different pump curves are used when are examined the operation of the pump. Next are presented the characteristic, pressure, and power curves of the pumps. The curves are mostly for centrifugal pumps but they can also apply for positive displacement pumps.

Characteristic curve

The characteristic curve describes the relation between the volume flow and pump head. In Figure 11, the Q-H curves of both centrifugal and positive displacement pumps are shown. As from the Figure 11 can be noticed, in the case of positive displacement pump, the pumping height does not affect for the flow rate. This is due to that the pump transfers certain volume of fluid for each cycle. The only factor that effects to the flow rate is the rotation speed at which the positive displacement pump operates. [8] The real characteristic curve does not follow the ideal curve in the case of PD-pumps when so-called “slippage” occurs. The slippage is the result of the backflow, which cause capacity reduction. The backflow is due to high discharge pressures. [30]

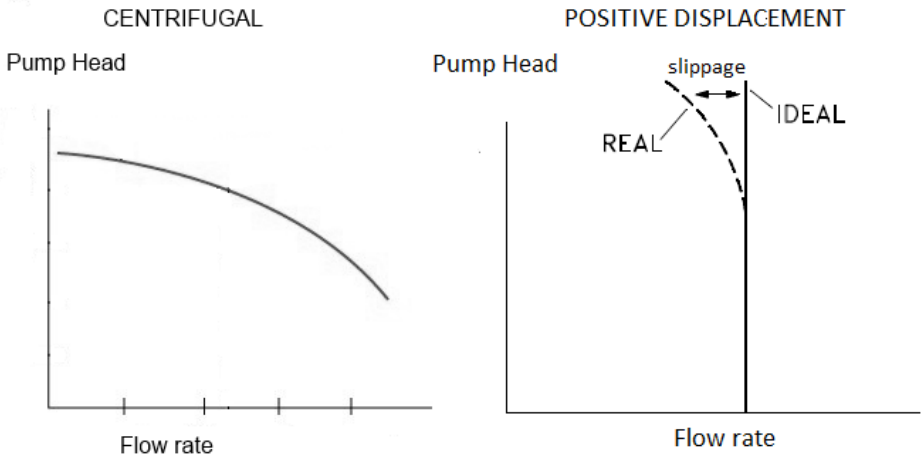

Figure 11. The characteristic curves of centrifugal and positive displacement pumps [30].

Pressure curve

The effect of the pressure to the flow rate can be described by the pressure curve. The example of pressure curve is presented in Figure 12. From the figure can be noticed that the flow rate decreases when the pressure increases. The pressure rise makes the pumping more difficult and heavier. The pump's rotation speed or power needs to increase that the flow rate stays constant when the pressure increases.

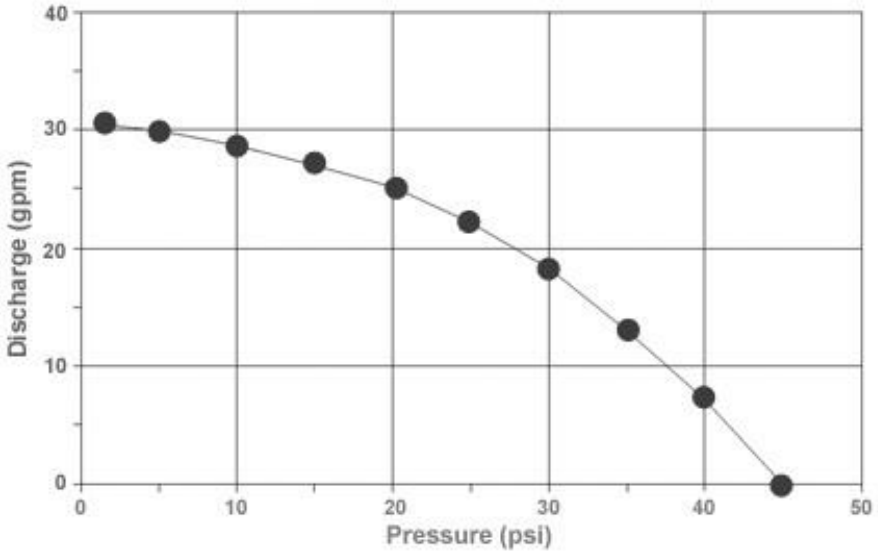

Figure 12. Pump pressure curve. Flow rate/discharge is presented as gallons per minute (gpm) and pressure as pounds per square inch (psi). [33]

Power curve

Power curve presents pump's power as the function of the flow rate. In Figure 13 are shown different pump curves. The power curve is shown at the bottom of the figure. The power is shown on y-axel on the right-hand side of the figure. In the figure is also shown the efficiency curve, which describes the ratio of pump power and electric power. Figure 13 shows that the power increases when the capacity increases also.

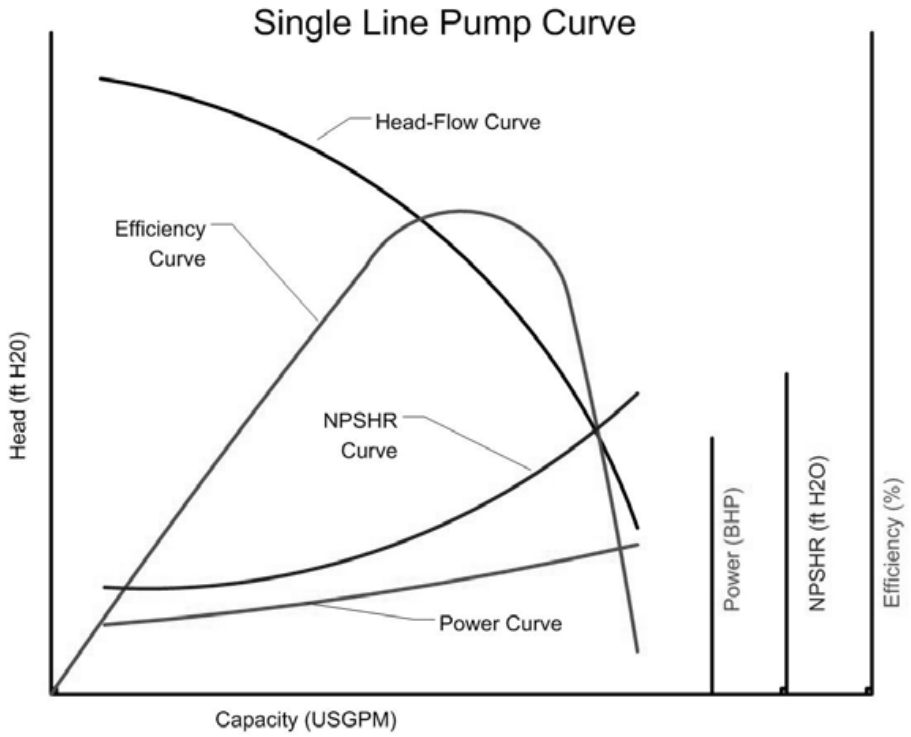

Figure 13. Different pump curves. In the figure are shown head-flow, efficiency, $NPSH_R$, and power curves. [34]

5.3 Net positive suction head

Sometimes the pressure in the pump inlet (suction side) decreases below the evaporation pressure of the fluid. Then part of the liquid is vaporized and it forms steam bubbles. The bubbles are migrated with the liquid flow to the pump. When the bubbles come to the area where the pressure is higher than the vapor pressure, the bubbles will collapse back into liquid. Each of the collapse creates a strong pressure impulse, which can cause serious damage in pump material. This phenomenon from the forming is called *cavitation*. Cavitation can be observed

from a crackling noise. Mostly the damages occur in suction side of the pump impeller where the pressure begins to rise. [35]

The term net positive suction head (NPSH) indicates how high the pressure should be in the pump inlet that the pump does not cavitate. There are two different type of NPSH: $NPSH_A$ and $NPSH_R$. $NPSH_A$ means the absolute pressure at the suction port of the pump and it is function of the whole system, which must be calculated. Instead, $NPSH_R$ is the minimum pressure that is required at the suction port of the pump to keep the pump from cavitating and the value is given by the pump manufacturer. [8,36]

$$NPSH_A \geq NPSH_R \tag{5}$$

As it represented in Equation (5), the $NPSH_A$ must always be greater (or even equal) than $NPSH_R$ because there must be more suction side pressure available than the pump requires. It is also recommended that $NPSH_A/NPSH_R$ ratio should be between 1.1-2.5 or even more. [35,36,37]

$NPSH_A$ can be calculated [16]

$$NPSH_A = \frac{p_s + p_a - p}{\rho \cdot g} + \frac{v^2}{2g} - H_{fl} + H_{sh} \tag{6}$$

where

p_s	static pressure of the vessel (open vessel p_s=0), Pa
p_a	atmospheric pressure, Pa
p	pressure of the fluid, Pa
ρ	density of the fluid, kg/m^3
g	standard gravity (9.81 m/s^2), m/s^2
v	fluid flow velocity, m/s
H_{fl}	dynamic friction loss of the suction pipe (-0.6..1 m), m
H_{sh}	suction height, m

When calculating the $NPSH_A$ value, following things must be considered. First, it must be found out if the vessel is open or closed. This affects to the pressure of the vessel; if the vessel is open, the pressure is 0. In addition, it must be taken into account the location of the pump compared to the vessel. If the vessel is at higher level than the pump, the suction height is positive and if the pump is higher than the vessel the suction height is negative. [16,38] In Figure 14, the scheme of the open tank system is shown.

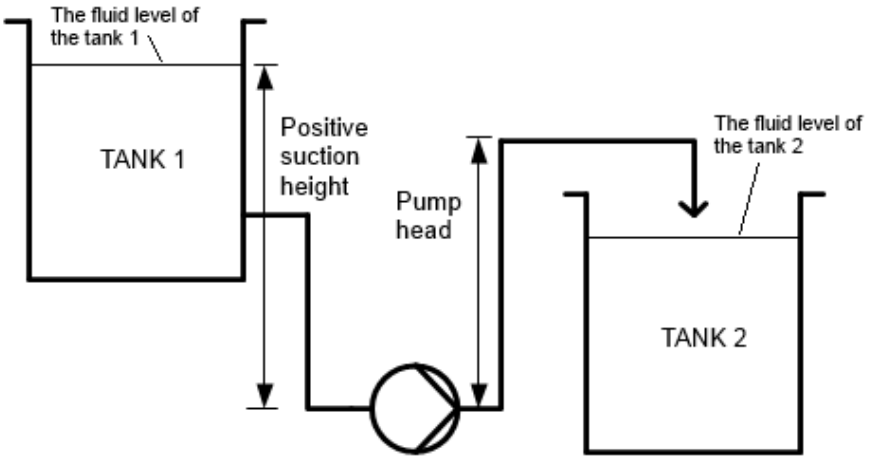

Figure 14. Scheme of the pumping system where both tanks are open and the tank 1 is higher than tank 2. [16]

The $NPSH_R$ value is presented as the head of pumped liquid in pumps. The $NPSH_R$ values are published by manufacturers as capacity and other the pump curves. [39,40] The $NPSH_R$ value can be determined in three different ways: [40]

- The pump suction is throttled or the water is heated to vary the vapor pressure
- The suction is taken from a suction sump and the suction is throttled or the pump is placed on the level, which height can be controlled
- In the suction vessel are created a vacuum

According to Hydraulic Standard Institute (1983), the $NPSH_R$ point can be observed from the audible cavitation noise or 3% drop in pump capacity [11].The most common way is to use 3% drop in pump head. The illustration of capacity drop in centrifugal pump is shown in Figure 15. The shape of $NPSH_R$ curve is roughly a lazy "U" [41].The example of $NPSH_R$ curve is shown earlier in Figure 13.

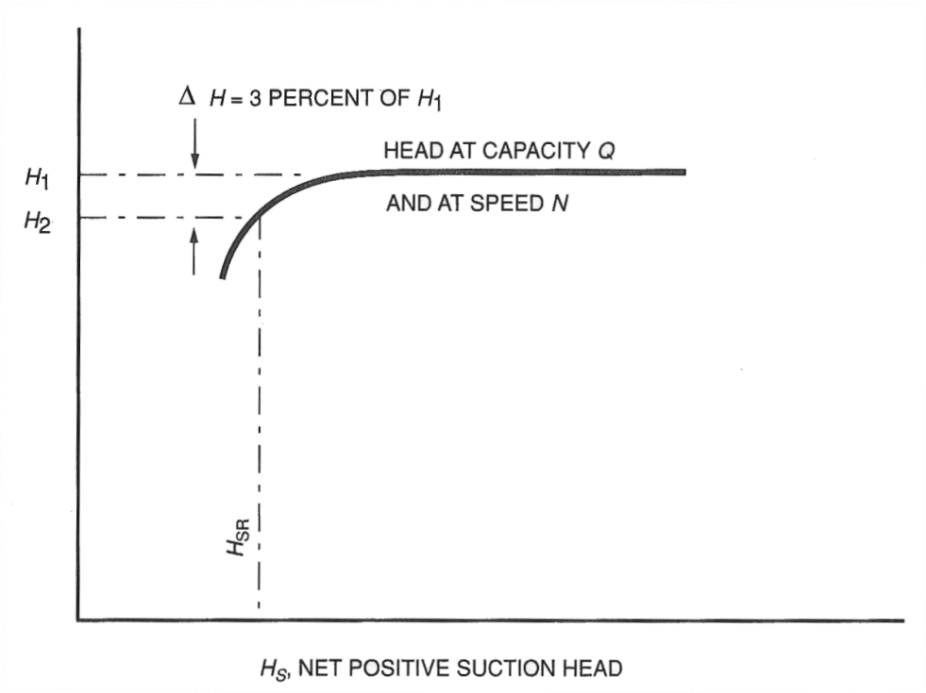

Figure 15. Illustration of capacity drop in centrifugal pump from which the cavitation can be observed. In figure Q=constant capacity, ΔH= 3 % drop of capacity. [42]

Cavitation is preferred to avoid in pumping because the internal part of the pump can damage when vapor bubbles collapse back into liquid [1]. However, cavitation can be utilized in ultrasonic cleaning. In ultrasonic cleaning small cavitation, bubbles are formed due to ultrasound, which is derived to water. The formed cavitation bubbles cause intense pressure shocks, which remove dirt, grease, and other impurities. [43]

6 RHEOLOGY

According to Harris (1977) “Rheology may be defined as the study of relationships between “stress” and corresponding “strain” in a non-rigid substance.” [44] Practically rheology examines transformations of fluid flows by measuring flow ability when the fluid is mixed or moved. In other words, in rheology it is examined the viscosities of the fluids.

The fluids can be divided into Newtonian and non-Newtonian fluids. The classification of fluids is based on Newton’s law of viscosity, which describes that the stress is proportional to the corresponding time derivative of strain. The viscosity is a variable, which characterizes the frictional forces between particles in the fluid. The frictional forces are trying to prevent the movement of the particles. The viscosity can define as tenacity, which is due to intermolecular cohesion of the liquid. The viscosity can be described by two variables: *dynamic viscosity* and *kinematic viscosity*. The dynamic viscosity is defined as the ratio between shear stress and shear rate and kinematic viscosity is the dynamic viscosity, which is divided by the density of the fluid. [5,44]

6.1 Newtonian fluid

In the definition of Newton’s Viscous Law is considered a thin layer of fluid between two parallel planes whose distance from each other is *dy* and the surface area of each plane is A. When the fluid is applied to the shear force F in steady state conditions, causes the shear force an equal opposite force in fluid, which balances the state. [45] The scheme of the situation described above is represented in Figure 16.

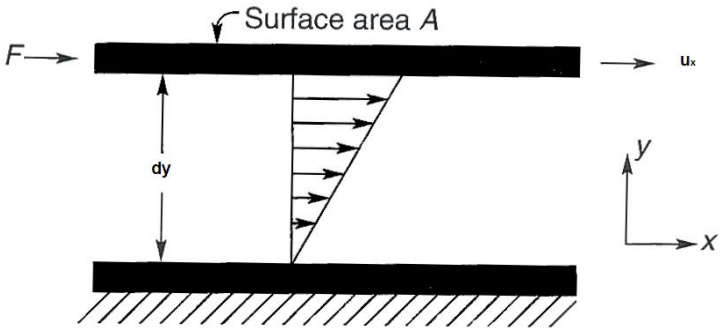

Figure 16. The scheme of Newtonian flow, where F= force affecting to planes, A= surface are of the plane, dy= distance between planes and u_x= velocity x-direction [45].

The situation described in Figure 16 can also describe by the equation. In Equation (7), the shear rate is presented by the velocity gradient (du/dy), which is vertical to the shear stress.

$$\frac{F}{A_{pl}} = \tau = \mu\left(-\frac{du_x}{dy}\right) = \mu\dot{\gamma} \tag{7}$$

where
F	shear force, Pa
A_{pl}	surface area of the plane, m^2
τ	shear stress, Pa
μ	dynamic viscosity, Pa·s
du_x/dy	velocity gradient, 1/s
$\dot{\gamma}$	shear rate, 1/s

Previous equation can be presented simply as the *Newton's law of viscosity*

$$\mu = \frac{\tau}{\dot{\gamma}} \tag{8}$$

where
μ	dynamic viscosity, Pa·s
τ	shear stress, Pa
$\dot{\gamma}$	shear rate, 1/s

In Newtonian fluids, the stress, which is acting to the material, is proportional to the corresponding shear rate. This property is called the viscosity. The viscosity has several properties: it is independent of time and strain, which is measured from any reference state and it, is independent of time derivatives or integrals. [44] In the classification, Newtonian fluids follow the Newton's law of viscosity and the non-Newtonian do not.

6.2 Non-Newtonian fluid

A non-Newtonian fluid is a fluid, which does not exhibit Newtonian characteristics. These kinds of fluids are for example high-viscosity liquids, polymers, colloids, gels and concentrated slurries, such as polyvinyl siloxane (PVS) pastes. [45,46]

Non-Newtonian fluids can be classified at least two different ways. In the first way, non-Newtonian fluids are divided into three main classes according to the fluid behavior. The classes are time-independent, time-dependent and viscoelastic fluids. [1,45] The other way is to divide fluids into viscous, viscoelastic and elastic groups. When the fluids are classified in this way, the group of viscous

materials includes all ideally viscous liquids (water and oils). The group of elastic materials includes ideally elastic (rigid) solids (stone and steel). Elastic solids follow the Hooke's law, which is described in more details in Chapter 6.2.3. The fluids, which do not follow the criteria of the groups above, are viscoelastic materials. This kind of fluids is either viscoelastic liquids (glues and shampoos) or viscoelastic solids (pastes, gels, and rubbers). [47] In this thesis, the fluids are classified according to time-independent and time-dependent rheologies.

6.2.1 Time-independent rheology

The viscous properties do not vary as a function of time in time-independent fluids. These fluids can be further subdivided into three types: pseudoplastic, dilatant and viscoplastic (Bingham plastic) fluids. In Figure 17, the behavior of time-independent and Newtonian fluids is shown.

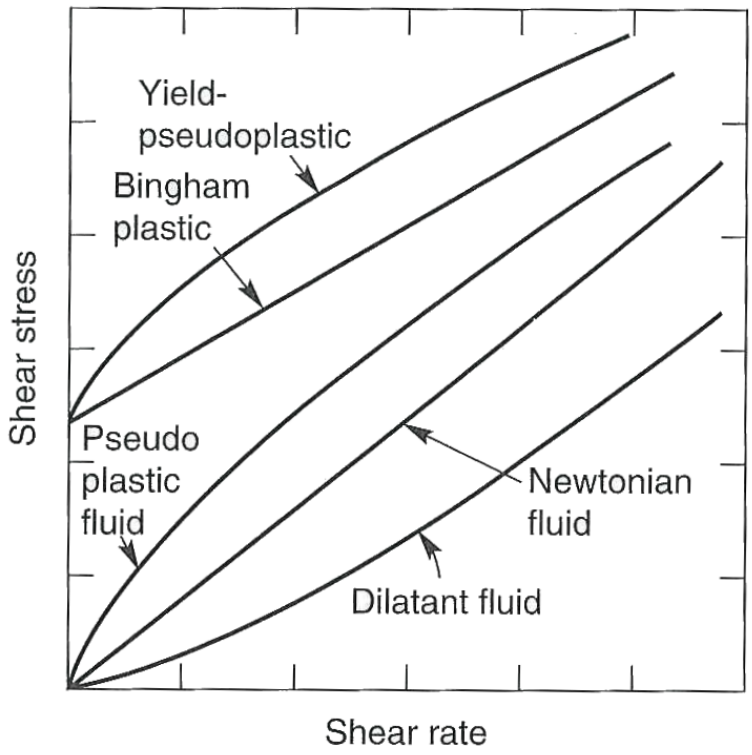

Figure 17. Shear stress of time-independent and Newtonian flows as the function of shear rate [45].

6.2.1.1 Pseudoplastic

Pseudoplastic, also known as shear-thinning, fluids are the most common type of time-independent non-Newtonian fluids. In pseudoplastic fluids, the viscosity decreases when the shear rate increases. [45]

A pseudoplastic fluid can be determined by Power law or Ostwald de Waele model

$$\mu = K\dot{\gamma}^{n-1} \tag{9}$$

where μ dynamic viscosity, Pa·s
K, n index parameters, -
$\dot{\gamma}$ shear rate, 1/s

For pseudoplastic fluids, the index ‘n’ should be between 0 and 1, and the smaller the value n is, the more pseudoplastic behavior occurs [45].

6.2.1.2 Dilatant

Comparing dilatant fluid to the pseudoplastic fluid, the change of viscosity is opposite: the viscosity increases when the shear rate increases. Dilatant fluid is also called shear-thickening. Dilatant behavior of fluid can cause problems in process equipment. In addition, that the shear thickening can damage the equipment, can particles in the fluid agglomerated. These problems can be exploited in the design by controlling the maximum rate of flow. [45,48] In Figure 18, the behavior of dilatant fluid is presented.

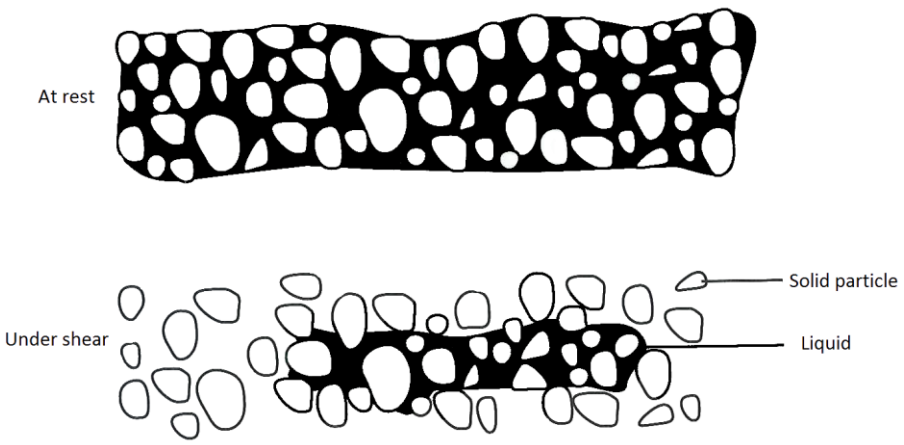

Figure 18. Example of dilatant behavior of fluid at rest and under shear [45].

From the figure can be notices that the shear separates the liquid and solid particles from each other. At rest, the liquid and solid particles are mixed together. At low shear, the liquid anoints each particle so very little stress is resulted. At high shear, the material widens so that there is enough liquid to fill the spaces between solid particles. [45]

The flow behavior of dilatant fluid can be described also by the Power Law-model (Eq. 9). For pseudoplastic fluids the index ‘n’ should be between 0 and 1, but for dilatant fluids the index ‘n’ should be greater than 1. If the index n=1, the fluid shows Newtonian fluid behavior. [45]

6.2.1.3 Viscoplastic

Viscoplastic fluids can resist a small shearing stress. The intensity of shear affects to the movement of the fluid: at high shear stress the fluid moves and at low shear the fluid does not move. Bingham plastic model describes the flow behavior in viscoplastic fluids, which can also be called Bingham plastics. [1,45,49] The Bingham plastic model is represented below:

$$\mu = \frac{\tau - \tau_y}{\dot{\gamma}} \quad \text{for } |\tau| > \tau_y \tag{10}$$

where μ dynamic viscosity, Pa·s
τ shear stress, Pa
τ_y yield stress, Pa
$\dot{\gamma}$ shear rate, 1/s

In addition, the behavior of viscoplastic fluids can be described also by some other models. Next is presented Herschel-Bulkley model. [49]

Herschel-Bulkley model

$$\mu = \frac{\tau_y}{\dot{\gamma}} + K\dot{\gamma}^{n-1} \quad \text{for } |\tau| > \tau_y \tag{11}$$

where K, n index parameters, -

For both models:

$$\dot{\gamma} = 0 \quad \text{for } |\tau| \leq \tau_y \tag{12}$$

6.2.2 Time-dependent rheology

Some non-Newtonian fluid flow behavior cannot be described only by a variation of shear rates. These kinds of fluids are called time-dependent fluids. In time-dependent fluid rheology, the viscosity is a function of time. Time-dependent fluids are for example bentonite-water suspensions, cement pasta, and crude oils. [45]

6.2.2.1 Thixotropic

A fluid is thixotropic when it is sheared at a constant rate and its viscosity decreases with the time of shearing. Some examples of thixotropic fluids are milk, mayonnaise, and greases. Ideally, paints are viscoplastic (Chapter 6.2.1.3) so that they will not drain. However, they are also thixotropic so they will flow more easily under brushing. [45,50]

Thixotropy of the fluid can be measured by so-called hysteresis loop test. In the loop test, the shear rate is linearly increased from zero to a maximum value and then returned it at the same rate to zero. In the test, the sample is stirred for example in a viscometer at a low shear rate a fixed time. During stirring, the torque is measured. After measuring the torque, the speed is increased stepwise and the torque values are measured at different speeds. A plotted curve forms a loop. The shear can be evaluated by measuring the area of the loop. [46,51,52] The behavior (the loop) of thixotropic fluid is shown later in Figure 16.

6.2.2.2 Rheopectic

The rheopectic behavior is an opposite of thixotropic behavior, i.e. the viscosity is the highest when the fluid is longer time under the shear. In rheopectic fluids the structure of the fluid is created by shear and the structure fall apart when the material is resting. Rheopectic fluid can be also called as negative/anti-thixotropic fluids. [45,53] Rheopexy can be also measured by hysteresis loop test. In Figure 19, the loops of both thixotropic and rheopectic fluids are represented.

As can be noticed on Figure 19, the behavior of thixotropic and rheopectic fluids are opposite. The loop of thixotropic fluid shows that the shear stress increases when the shear rate increases. Also can be noticed that shear rate decreases when the shear rate decreases too. The shear stress returns to the start point in lower

level than at the beginning and forms a loop. Instead of, the rheopectic fluid forms a loop, which returns to the start point in higher level than at the beginning.

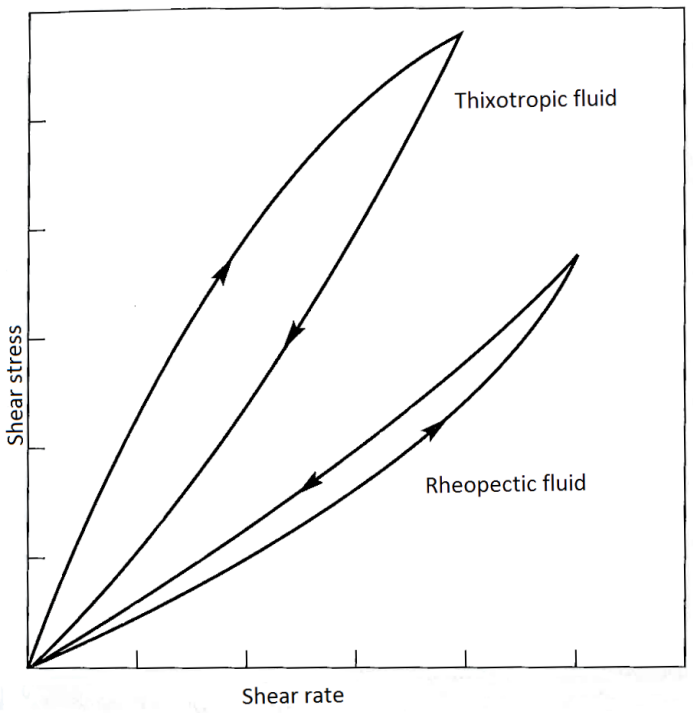

Figure 19. Hysteresis loops of thixotropic and rheopectic fluids. Shear stress is shown as a function of shear rate. [45]

6.2.3 Viscoelasticity

There are materials, which have properties of both solids and liquids in specific flow conditions. These materials are called viscoelastic. For example, highly polymerized liquids such as plastic melts and solutions are viscoelastic [54]. Due to their varying properties, viscoelastic behavior is hard to describe by a mathematical model. In viscoelastic fluids, the time dependence can be described by differential equations in time. The molecular motions in viscoelastic fluids can be described by "spring-dashpot" models. [45,55] The mechanical analogs use Hookean springs, which is represented by equation

$$\tau = G \cdot \gamma \tag{14}$$

where G shear modulus, -

The uncoiling process can be modeled by a Newtonian dashpot

$$\tau = \mu \cdot \dot{\gamma} \tag{15}$$

The behavior of viscoelastic fluid can be described by Maxwell model, which combines the Hookean and Newtonian laws. When λ = μ/G, the Maxwell model is

$$\tau + \lambda\dot{\tau} = \mu\dot{\gamma} \tag{16}$$

where

τ	shear stress, Pa
λ	relaxation time (=μ/G), s
$\dot{\tau}$	time derivative (=dτ/dt), Pa/s
μ	dynamic viscosity, Pa·s
$\dot{\gamma}$	shear rate, 1/s

The Maxwell model is also represented in Figure 20. In Figure, the Hookean spring and Newtonian dashpot is combined.

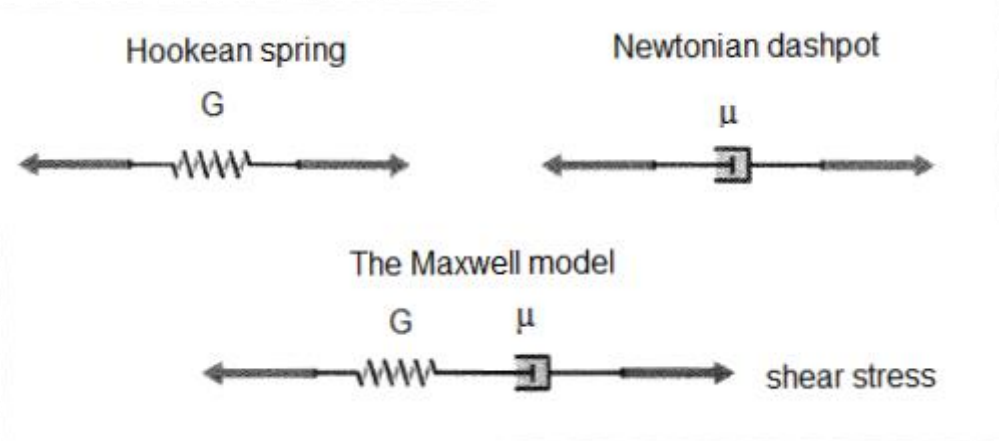

Figure 20. The Hookean spring, the Newtonian dashpot and the Maxwell model. In the Maxwell model Hookean spring and Newtonian dashpot is combined together. [55]

7 VISCOMETER

Viscometer is a device, which measures the viscosity and flow parameters of the fluid. Viscometer works for fluids whose viscosity does not change under varying conditions. The measurement of viscosity is important because exact knowledge fluid's viscosity is needed for the design of industrial processes. In most of viscometers, a spindle is rotated in the measured sample. The resistance to rotational force is measured wherein the viscosity can be determined. [56,57]

The flow of viscous fluid can be described by some models. The simplest model is *Couette flow*, which is generated by the action of boundaries in relative motion. In Couette flow, the fluid is flowing between a stationary plate and a moving plate, which are separated by certain distance. The movement of the fluid is two-dimensional and the velocity gradient has only component which is parallel to the tangent of the plates. The boundaries of Couette flow are shown in Figure 21. [44,50]

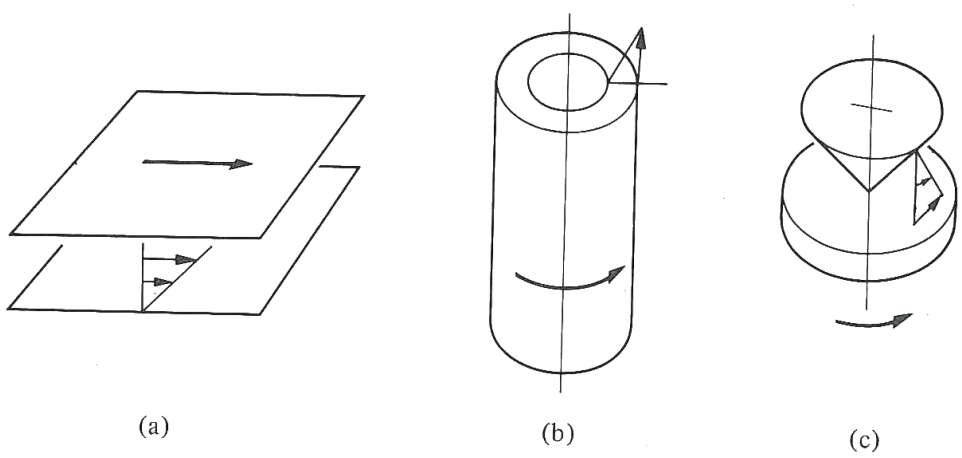

Figure 21. Typical examples of the boundaries in Couette flow a) plane; b) cylindrical; c) spherical [44].

The fluid motion can also be described by *Poiseuille flow* model. In Poiseuille model, the fluid motion is generated by a pressure gradient, which acts parallel to a fixed boundary. It can be used to evaluate the flow through a slit or axial flow through annulus. The boundaries of Poiseuille flow are represented in Figure 22. [44]

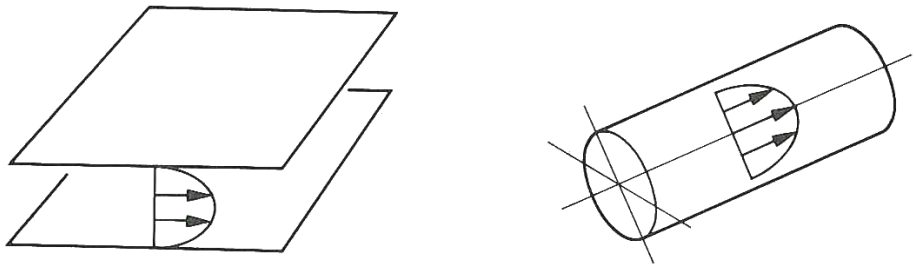

Figure 22. Boundaries for Poiseuille flow a) plane; b) cylindrial [44].

7.1 Viscometer types

The viscometers can be roughly classified into seven categories, which are presented below [56].

Capillary viscometer

Capillary viscometer is the most common type of viscometers. Capillary viscometer consists of capillary tube where the fluid is flowing. In viscosity measurement, fluid volumetric flow rate in capillary is measured. In most cases, the volumetric flow rate is determined by measuring the time that a given volume of fluid takes to move in the tube. [56,58]

Orifice viscometer

The working principle is the same in almost all orifice viscometers. The measured fluid is poured into a cup and the cup is kept at a constant temperature. When the desired temperature is reached, the valve bottom of the cup is opened. When the fluid is flowing out, the time required for a specific volume of fluid through the orifice, is measured. [58]

High temperature high shear rate viscometer

Fluids' viscosities, which are over 1000 poises (= 1000 g/cm·s) can be measured with cylinder-piston type viscometers. The cylinder-piston viscometers consist of a cylinder and the capillary, where the fluid is stored. The cylinder compresses and displaces the fluid. The resulting compressed pressure is proportional to the viscosity of the fluid. The cylinder can use a dead weight, a pneumatic device,

hydraulic pressure, or mechanical device as the power source. High temperature high shear rate viscometer is suitable for the viscous non-Newtonian fluids. [58,59]

Rotational viscometer

In rotational viscometers, the sample is rotated with certain force or torque, and the rotation rate is measured. The rate is measured by spindle, which is immersed in the liquid. When rotational viscometers are compared to the capillary viscometers, rotational viscometers are more comprehensive and less accurate for Newtonian liquids during operation. In addition, the measurements can be done under steady state conditions and several measurements with the same sample can be done at different shear rates in rotational viscometers. There are many different rotational viscometers such as rotating sphere, rotating disc, rotating cylinder etc. [58,60]

Falling ball viscometer

The falling ball viscometer consists of a container (usually circular cylinder) and some liquid in which the container is filled. The measurement is carried out by dropping a solid ball through a measurable viscous medium. The time that the ball takes to drop is measured, and then the viscosity is determined. [58,61]

Vibrational viscometer

In vibrational viscometers, a resonator is embedded in the test liquid and the damping of an oscillating, produced by resonator, is measured. The type of resonator varies but it may be, for example, a cantilever beam, oscillating sphere, or tuning fork. [58]

Ultrasonic viscometer

Ultrasonic viscometers consist of a small sensing element or probe, which is embedded in the fluid. The transducer emits a short ultrasonic pulse and the pulses are reflected back as the echoes. The signals from echoes are processed to obtain the viscosity of the fluid. The speed of reflected signals varies depending on the viscosity of the fluid: the lower the viscosity is the shorter the resulting time. [58,62]

7.2 Rheometer

The rheometer is a device, which is used to determine materials' rheological properties. Comparing rheometer to viscometer, the rheometer has wider range of applications than viscometer. The viscometer measures only fluid viscosity, whereas the rheometer measures viscosity and behavior of the flow. In addition of viscosity, rheometer can measure the elastic properties of the fluid. The elastic properties are researched by oscillatory measurements. [63,64]

There are two types of rheometers: rheometers that control the shear rate and rheometers that control shear stress. In the controlled rate (CR) rheometer, the rotation speed of the analyzed sample is controlled by the motor and the resulting torque is measured. In controlled stress (CS) rheometers, rheometer is connected an electrical current which creates a magnetic field. The magnetic field produces an electrical torque, which rotates the measuring unit. [65]

8 MATERIALS USED IN EXPERIMENTS

Bentonite, starch, and carboxymethyl cellulose (CMC) slurries were used in the experimental part of this thesis. The premise for the experiments was that the rheology-types and viscosities of the slurries would be different. Also, the concentrations of slurries were varied. By using these different materials, it was possible to get broader information about rheological behavior of slurries in pumps. Next are shown some literature review of bentonite, starch, and CMC.

8.1 Bentonite

Bentonite ($Al_2O_2 \cdot 4\ (SiO_2) \cdot H_2O$) is an Aluminium silicate. The content of crystalline silica is normally between 1-60 %, but it could be also less than 1 %. Bentonite is natural clay, which mostly consists of Montmorillonite. Bentonites may include a number of minerals (quartz, feldspar, calcite, and gypsum), which concentrations will affect Bentonite's properties. [65,66,67]

Bentonite adsorbs a lot of water. When bentonite and water are contacted, the volume of solution increases several times. The bentonite and water create a gelatinous and viscous fluid, and at high concentrations, the suspensions are characterized as a gel. [67,68] In water-bentonite suspension, the water molecules are transferred between the bentonite particles, which form hydrogen bridge bonds. When suspension is left still, it will jellify. Whereas the suspension is left under mechanical stress, the hydrogen bonds will partially break allowing the particles to move more. Viscosity of such suspensions is lower under shear than under rest, which makes them thixotropic suspensions. [68]

8.2 Starch

Starch is a polysaccharide consisting of glucose units which are linked together to form long chains. The chemical formula of the starch molecule is $(C_6H_{10}O_5)_n$, and the value of the 'n' varies from five hundred to several hundred. Starch molecule includes two kinds of polysaccharides: amylose and amylopectin. In most of the native starches, the amount of amylose is 20-30 %, and the rest is amylopectin. However, there are starches, which may include only amylopectin or amylose. Starch occurs, for example, in wheat, potatoes, rice, maize, barley, rye, beans, peas, avocados, and so forth. Starch is found in the plants' seeds, fruits, stems,

roots, and tubers. The purpose of starch is to be storage of energy for plants. [69,70]

Several studies are made to research the rheology of starch-water suspensions. Fall *et al.* (2012) and Bischoff White *et al.* (2009) have both researched the rheological properties of the 55 wt-% cornstarch. In both experiments, the rheology of 55 wt-% starch-water suspension was shear-thickening (dilatant) when the shear rate was a high enough. However, in low shear rates the rheology may seek shear-thinning features. [71,72] The starch used in the experiments was cornstarch from Chemigate.

8.3 Carboxymethyl cellulose

Carboxymethyl cellulose (CMC) is a cellulose-based polymer, which have wide range of applications from the food industry to the pharmaceutical industry. CMC is mostly produced as sodium carboxymethyl cellulose, which chemical formula is CH_2COONa. Sodium carboxymethyl cellulose is formed in the reaction of sodium hydroxide and chloroacetic acid. [73] In the reaction, the cellulose swell in aqueous NAOH and in organic solvent, where the etherifying reagent can be either monocholoroacetic acid or its sodium salt [74].

The most important property of CMC is high viscosity in low concentration [75]. Viscosity of CMC solution depends on the etherification rate of CMC. The properties of CMC can be change by varying the molecular weight of the polymer, the carboxyl content, or changing the distribution of carboxyl substituents in the polymer chains. [73] From different CMC solutions have been observed Newtonian, pseudoplastic, thixotropic, and viscoelastic behavior. [76,77] In the experiments, carboxymethyl cellulose was Finnfix30 from CP Kelco.

9 HOSE PUMP EXPERIMENTS

The purpose of the hose pump experiments was to research how the different rheological properties of the slurry affect to pumping. Especially it was researched the effects to the intensity of pressure pulsation. Moreover, it was done some separated experiments in which was researched what kind of impacts the change of pipe material causes. During the experiments were also measured current, voltage, and frequency of the pump. The pressure and the power curves were determined from the obtained results.

9.1 Pumping system and measurement procedure

The pumping system of hose pump experiments is presented in Figure 23. The system consists of the hose pump (Flowrox LPP-T32), the mixing tank, two valves, and the meters. Meters measured temperature, flow rate, and four different pressures. The pressure meters were placed before the pump, after the pump, and then there were two meters in the straight pipe section. The pipelines were steel pipe and the pipe size was NS65, which wall thickness was 3.6 mm. Two Flowrox's pinch valves were used (inner diameters 65 mm) in the pumping system.

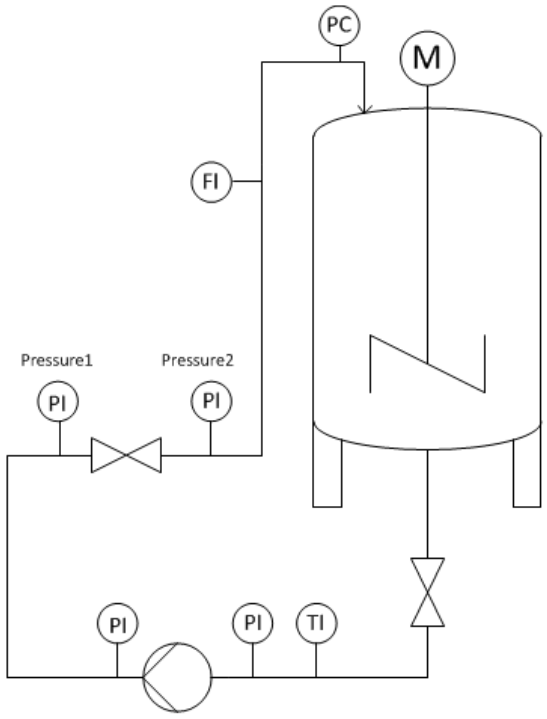

Figure 23. The pumping system of the hose pump. The system consists of the pump, mixing tank, two valves, and meters. Meters measured temperature, flow rate, and pressures in different parts of the system.

The experiments were started by using starch slurries. In the experiments were decided to use five starch slurries, which have different viscosities and concentrations. The first starch slurry was made by adding a certain amount of starch to the mixing tank. The tank was filled with water. The slurry was mixed a while, and then the measurements were started. The experiments were started with the most dilute slurry. The concentration of slurry was increased when the experiments proceed. The experiments were carried out by using three different rotation speeds of the pump and four different counter pressures. By using the counter pressure, the pressure level in the pumping system was possible to change and get higher. Counter pressure was formed by using pressure cylinder, which was installed in the inlet pipe of the slurry tank. Counter pressure was generated by compressed air. Used counter pressures were 0.0, 2.0, 4.0, and 6.0 bar. The used pump rotation speeds were 22, 48, and 78 rpm.

The measurements were carried out by setting 22 rpm rotation speed and 0.0 bar counter pressure to the pumping system. At 22 rpm rotation speed, the slurry was pumped 30 seconds, and after that the speed was increased to 48 rpm. At 48 rpm rotation speed, the slurry was also pumped 30 seconds, and then the speed was increased to 78 rpm. The speed changes were made in five seconds and the total time of measurement was 30+5+30+5+30= 100 seconds. The measurement procedure was repeated in a similar way by using different counter pressures and different slurries. The starch slurry experiments were done in one day.

Bentonite slurries were used after the starch slurry experiments. In experiments were used three different bentonite slurries. The measurements were done in similar way as in starch measurements. The bentonite slurry measurements were also done in one day.

Five different slurries were used in CMC experiments. All CMC slurries were allowed to mix for at least 24 hours, when the solid CMC was added to the water, because CMC needs a lot of time to mix with water. The only exception was the most dilute slurry, which was done first. It was mixed only two hours before the measurements were done because the concentration of the solution was so low that it was assumed to mix in shorter time. The experimental procedure was the

same than in earlier measurements. Three different pump rotation speeds (22, 48, and 78 rpm), and four different counter pressures (0.0, 2.0, 4.0, and 6.0 bar) were used. The measurement time was 100 seconds.

All slurries had measurement data at four different pressure levels and at three different pump rotation speeds.

The remained CMC slurry was pumped to container and recovered when the experiments were done. After slurry removal, the piping was cleaned by pumping pure water in the system.

9.2 Pressure pulsation measurements in hose pump

The intensity of pressure pulsation was determined. In these experiments, only one pressure meter was used in order to get a high frequency data. The used counter pressure was 4.0 bar.

The pulsation experiments were done in the same way as the slurry pumping measurements. Only difference was that the measurements were done at counter pressure 4.0 bar. The measurement time was again 100 seconds and three different pump rotation speeds were used.

It was also studied how different pipe materials and configurations affect to the intensity of pressure pulsation. The used materials were elastic and steel pipes. Also, one prototype of pulsation dampener was used in experiments. The materials were tested by placing them to that part of the pipeline, which was right after the pump. The used pump rotation speeds were 22, 48, and 78 rpm. The used counter pressures were 1.0, 2.0, and 3.0 bars.

10 PROGRESSIVE CAVITY PUMP EXPERIMENTS

The main purpose of the progressive cavity pump experiments was to determine the power, pressure, and $NPSH_R$ curves for Flowrox C10/10 pump. In addition, it was studied how the different viscosity and rheology type of the slurry affect to pump operation.

10.1 Pumping system and measurement procedure

The pumping system was similar to hose pump experiments except that the pump was switched to a PC-pump. The flow sheet of pumping system is shown earlier in Figure 23. The measurement procedure was also similar. Four different counter pressures and three different rotation speeds were used. The counter pressures were the same than in hose pump experiments (0.0, 2.0, 4.0, and 6.0 bars) but the pump rotation speeds were 82, 204, and 326 rpm. In the experiments were used starch and CMC slurries. CMC slurry was the same that was used in hose pump experiments. The experiments were started by transferring CMC slurry back to mixing tank. Slurry was mixed and pumped in the system a while that it would be homogenous. CMC slurry was pumped at three different rotation speeds and at four different counter pressures. The total measurement time of each measurement was 100 seconds. After measurements, the slurry was diluted three times. The same measurements were carried out with all four CMC slurries.

Five different starch slurries were used. The experiments were carried out in a similar way like with CMC slurry.

10.2 $NPSH_R$ determination for progressive cavity pump

The $NPSH_R$ curve was determined for the progressive cavity pump. According to the Hydraulic Institute, the $NPSH_R$ is at the point when the pump loses 3.0 % its volumetric efficiency [11]. In practice, the suction pressure of the pump is reduced until the flow rate decreases. In the experiments, the suction pressure was reduced by throttling the flow. The flow was throttled with a valve. The $NPSH_R$ experiments were done with water.

Water was pumped with nine different pump rotation speeds. The rotation speeds were 82, 122, 163, 204, 245, 286, 326, 367, and 408 rpm. The experiments were started by pumping the water at 82 rpm, and at the same time, the flow was

throttled. When flow rate began to decrease due to throttling and the cavitation noise was occurred, the experiment was ended. After that, rotation speed was increased to 122 rpm and experiment was repeated. The experiments were continued until the experiments were done with each rotation speeds.

11 PROCESSING THE SAMPLES

Starch, bentonite, and carboxymethyl cellulose slurries were used in the experimental part of this thesis. A sample was taken from each of slurry and viscosity and rheology type of slurry was determined. The samples were analyzed with Anton Paar Modular Compact MCR 302 Rheometer.

The viscosity was measured in two ways. In the first way, rotation speed of the rheometer was increased gradually from 0.0 to 150.0 1/s. After that, the speed was decreased similarly from 150.0 to 0.0 1/s. The time-independent rheology was possible to find out with this 'hysteresis loop' test. In the second way, rotation speed was kept at the constant speed all the time. The constant speed was 150.0 1/s. By using this measurement type, the time-dependent rheologies were determined.

The CMC samples were analyzed with a cylinder-type spindle. The starch and the bentonite samples were analyzed with an impeller-type spindle. The impeller-type spindle was used due to possible settling of solids.

The concentration of the slurry was also determined based on weighting the sample before and after evaporation of the liquid. The density of the slurry could be calculated when the densities of the water and solid and the concentration of the slurry were known.

12 PROCESSING THE RESULTS

One part of this thesis was to study pressure pulsation in hose pump system. In the case of hose pump, there occurred problems to define the normal pressure level due to pressure variation in the pumping. The pressure level for each pressure pulsation measurement was determined by calculating the surface area of the pressure spike and then dividing the area by the duration of the spike. The situation is demonstrated in Figure 24. Other methods to treat pressure pulsation data was also tried but the above mentioned method was the best. Other method did not take into account the pressure peak cycle time or the pressure below the peak.

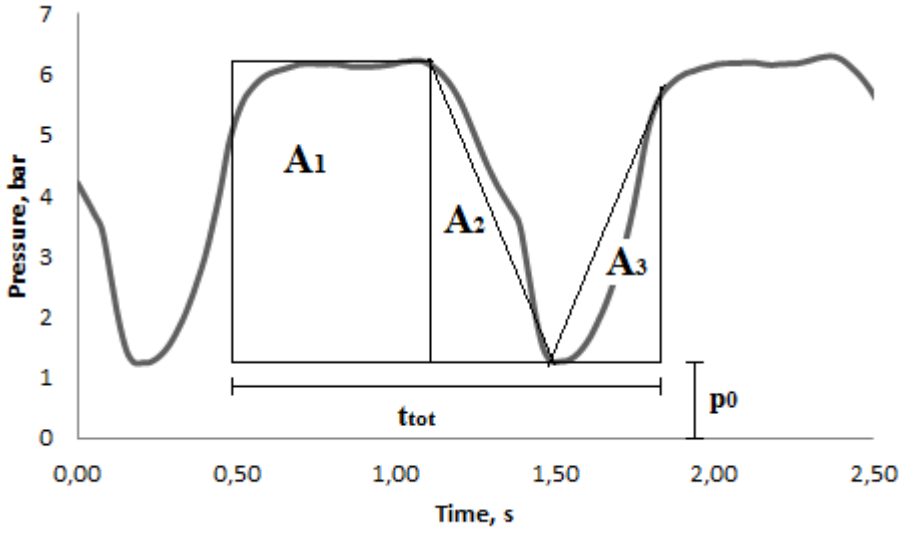

Figure 24. Pressure spike divided into three parts, which surface areas are calculated. In figure A_1, A_2, and A_3 = partial surface areas, p_0 = pressure below the spike, and t_{tot} = pressure peak cycle time.

First, the spike was divided into three parts as presented in Figure 24. The average pressure of the pulsation cycle is calculated according to Equation (17):

$$\bar{p}_A = \frac{1}{t_{tot}} \int_0^{t_{tot}} p(t)dt \approx p_0 + \frac{1}{t_{tot}} \sum_{i=1}^{n} A_i \quad (17)$$

where

$\bar{p}_A$	time averaged pressure in pulsation cycle, bar
t_{tot}	pressure peak cycle time, s
p_0	pressure below the peak, bar
A_i	calculational area, bar·s

The concentration of the slurry was presented as the unit wt-% in the results. In Equation (18) is shown how the concentration was calculated.

$$w = \frac{m}{m_{tot}} \cdot 100\% \tag{18}$$

where
	w	concentration, wt-%
	m	mass of the solid, g
	m_{tot}	mass of the total mixture, g

The average pressures were used when the pressure curves were determined for the pumps. The average pressure was calculated by using Equation (19).

$$\bar{p} = \frac{p_1 + p_2 + \cdots + p_n}{n} \tag{19}$$

where
	$\bar{p}$	average pressure, bar
	p_1, p_2, p_n	pulsation cycle pressures, bar
	n	number of data points, -

The suction pressure and flow rate were measured in PC-pump's $NPSH_R$ curve determination. $NPSH_R$ values were presented as the function of flow rate in $NPSH_R$ curve. The $NPSH_R$ values were calculated from suction pressure value by equation

$$NPSH_R = \frac{p_{sc}}{\rho \cdot g} \tag{20}$$

where
	$NPSH_R$	net positive suction head required, m
	p_{sc}	pump suction pressure, Pa
	ρ_w	density of water, kg/m^3
	g	standard gravity (9.81 m/s^2), m/s^2

According to Severs and Austin (1954), the average fluid shear rate in the pipe can be calculated when the flow velocity and pipe diameter are known. [78]

$$\dot{\gamma} = 8\,\frac{v}{d} \tag{21}$$

where
	$\dot{\gamma}$	shear rate, 1/s
	v	fluid flow velocity, m/s
	d	pipe diameter, m

The slurry viscosity in pipe can be determined by Ostwald de Waele model when the index parameters k and n are known. The viscosity is determined by calculating the values with Ostwald de Waele equation (Eq. (9)), and using the shear rates, which were calculated with Equation (21).

For slurries, which do not follow Ostwald de Waele model, viscosity can be calculated when pressure difference, pipe diameter and length, and fluid flow velocity are known. The distance between pressure meters is shown as 'L4' in Figure 25.

$$\mu = \frac{(p_2 - p_1) \cdot d^2}{128 \cdot l \cdot v} \tag{22}$$

where

μ	dynamic viscosity, Pa·s
p_2	pressure in meter 2, Pa
p_1	pressure in meter 1, Pa
d	pipe diameter, m
l	pipe length/distance between pressure meters, m
v	fluid flow velocity, m/s

The pressure difference, produced by the pump, was needed when was calculated the pump power. The meter, which measured pump discharge pressure, was not used in hose pump experiments. The hose pump discharge pressures were calculated by Bernoulli's equation.

Bernoulli's equation [79]

$$p_d + \frac{\rho \cdot v_d^2}{2} + \rho \cdot g \cdot z_d = p_1 + \frac{\rho \cdot v_1^2}{2} + \rho \cdot g \cdot z_1 + \Delta p_{losses} \tag{23}$$

where

p_d	pump discharge pressure, bar
ρ	density of the fluid, kg/m^3
v_d	velocity of the fluid in discharge, m/s
g	standard gravity (9.81 m/s^2), m/s^2
z_d	discharge height, m
p_1	pressure at point 1, bar
v_1	fluid flow velocity at point 1, m/s
z_1	height at point 1, m
Δp_{losses}	pressure losses, bar

The pressure losses consist of frictional and minor losses [80]:

$$\Delta p_{losses} = \Delta p_{fri} + \Delta p_{minor} \tag{24}$$

The illustration of piping system is shown in Figure 25. The pipe length and diameter were needed, when the frictional losses were calculated. The pipe length was 3.80 m and diameter was 68.9 mm. In Figure 25, the pipe length is L1+L2+L3.

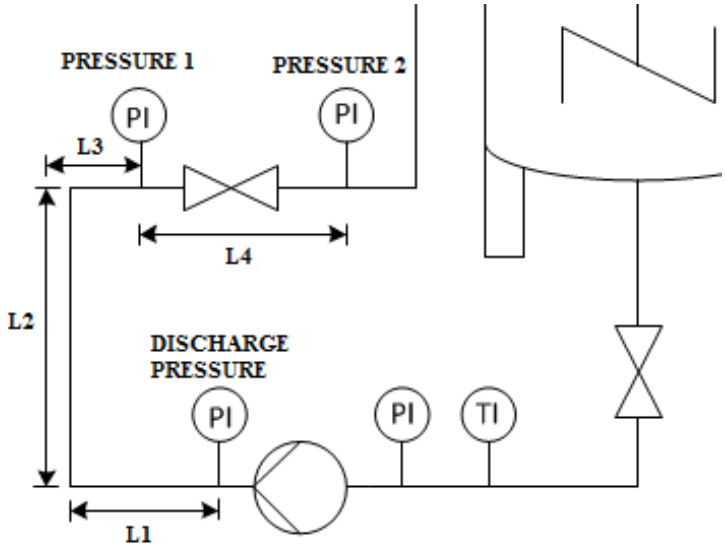

Figure 25. Measurement procedure for calculated viscosity and discharge pressure determinations. Pipe lengths: L1= 1.65 m, L2= 1.05 m, L3= 1.10 m, and L4= 1.10 m. The pipe diameter was 68.9 mm. The figure is not in scale.

Frictional losses can be determined by [79]

$$\Delta p_{fri} = f \cdot \frac{L}{d} \cdot \frac{\rho \cdot v^2}{2} \tag{25}$$

where

Δp_{fri}	frictional loss, Pa
f	friction factor, -
L	pipe length, m

Friction factor can be calculated, when the Reynold's number is known [80]

For laminar flow (Re < 2300)

$$f = \frac{64}{Re} \tag{26}$$

For turbulent flow ($2300 < Re < 10^5$)

$$f = \frac{0.3164}{\sqrt[4]{Re}} \tag{27}$$

where f friction factor, -
Re Reynold's number, -

Reynold's number [79]

$$Re = \frac{\rho \cdot d \cdot v}{\mu} \tag{28}$$

where Re Reynold's number, -
ρ density of the fluid, kg/m^3
d pipe diameter, m
v fluid flow velocity, m/s
μ dynamic viscosity, Pa·s

In addition to the friction losses, in the pipe occur minor losses. Minor losses are due to structure of the piping. For example, the elbows and valves cause minor losses. The minor losses can be calculated by [79]

$$\Delta p_{minor} = \zeta \cdot \frac{\rho \cdot v^2}{2} \tag{29}$$

where Δp_{minor} minor losses, Pa
ζ minor coefficient, -
ρ density of the fluid, kg/m^3
v fluid flow velocity, m/s

Some minor coefficients are shown in Table III. In this case, in the system were two regular 90° elbows. The sum of minor coefficients was 0.6.

Table III Some minor coefficients for pipe components [79].

Component	Coefficient ζ
a. Elbows	
Regular 90º, flanged	0.3
Regular 90º, threaded	1.5
Long radius 90º, flanged	0.2
Long radius 90º, threaded	0.7
Long radius 45º, flanged	0.2
Regular 45º, threaded	0.4
b. 180º return bends	
180º return bend, flanged	0.2
180º return bend, threaded	1.5
c. Tees	
Line flow, flanged	0.2
Line flow, threaded	0.9
Branch flow, flanged	1.0
Branch flow, threaded	2.0

13 RESULTS AND DISCUSSION

The slurry pumping in progressive cavity pump and in hose pump was studied in this thesis. In both cases were pumped different kind of slurries and for the pumps were determined the power and pressure curves. In the case of hose pump, it was also researched pressure pulsation. In addition, the $NPSH_R$ curve was determined for the progressive cavity pump.

13.1 Properties of slurries

Starch, bentonite, and carboxymethyl cellulose (CMC) slurries were used in the experiments. During the experiments, it was taken a sample from the each used slurry. Viscosity and rheology type were determined from the samples with rheometer. In addition, it was determined the weight based concentration and the density of each slurry.

13.1.1 Slurries in hose pump experiments

The rheology types of slurries were Newtonian, pseudoplastic, dilatant, and thixotropic. Starch and CMC slurries followed the Oswald de Waele model, which was presented in Chapters 6.2.1.1 - 6.2.1.2 by Equation (9). According to the equation, the constants K and n were determined for the slurries. It was also determined the regression value, coefficient of determination (R^2), which estimated how the model fit to data. The viscosities, rheology types, and concentrations of starch and CMC slurries are presented in Table IV.

Bentonite slurries did not follow the Ostwald de Waele model and the rheology types were determined by hysteresis loop test (Chapter 6.2.2.1). In Figure 26 are shown the loops of bentonite slurries. When the loops are compared to thixotropic loops in Figure 19, it can be noticed similarities. Firstly, the shear stress increased when the shear rate was increased 0.0-150.0 1/s. The shear rate returned to start point, but in lower level than at the beginning, when the shear rate was decreased 150.0-0.0 1/s. In Table V are shown the viscosities and concentrations of bentonite slurries.

Table IV The properties of starch and CMC slurries in hose pump experiments. Viscosities of slurries follow the Ostwald de Waele model $\mu = K\dot{\gamma}^{n-1}$ therefore the constants K and n are determined. For pseudoplastic fluids 0 < n <1, for dilatant fluids n > 1, and for Newtonian fluid n=1. The value R^2 is regression value.

	Concentration wt-%	Density kg/m^3	Viscosity* Pa·s	Rheology type	K -	n -	R^2
Starch							
Slurry1	20.67	1103.4	0.00158	Slightly non-New.	0.0011	1.0726	0.9983
Slurry2	28.48	1142.4	0.00342	Slightly non-New.	0.0034	1.0011	0.9985
Slurry3	39.89	1199.5	0.00853	Slightly non-New.	0.0100	0.9683	0.9987
Slurry4	47.53	1237.7	0.02170	Slightly non-New.	0.0196	1.0205	0.9942
Slurry5	49.29	1246.5	0.10301	Dilatant	0.0010	1.9250	0.9614
CMC							
Slurry1	2.14	1012.9	0.02486	Slightly non-New.	0.0264	0.988	0.9845
Slurry2	3.87	1023.2	0.13612	Slightly non-New.	0.1697	0.956	0.9448
Slurry3	5.69	1034.2	0.47685	Slightly pseudoplast.	0.8070	0.895	0.9628
Slurry4	7.59	1045.5	1.19194	Slightly pseudoplast.	3.0728	0.811	0.9802
Slurry5	9.57	1057.4	2.53966	Pseudoplastic	10.752	0.712	0.9943

*Viscosities are determined at constant shear rate 150 1/s

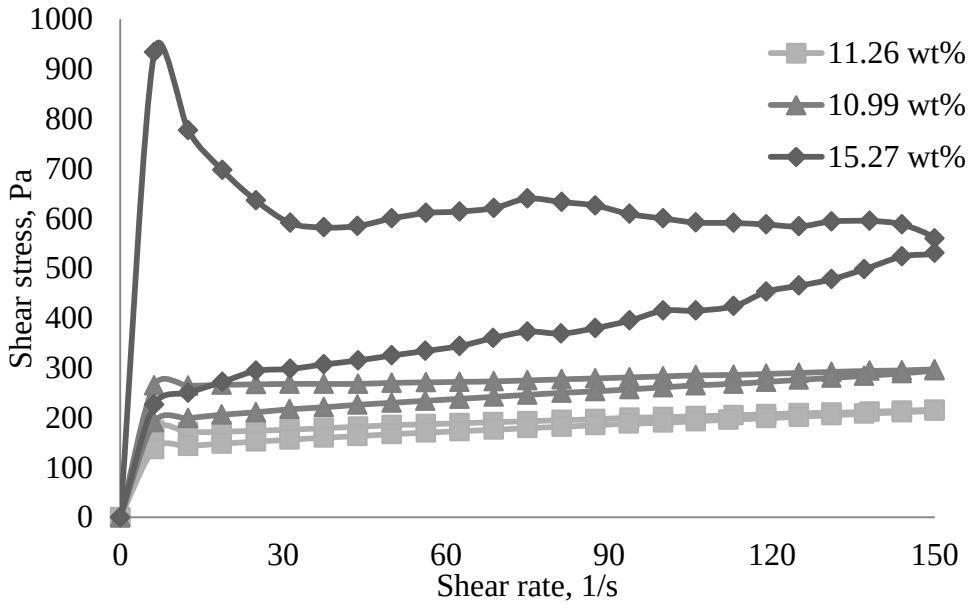

Figure 26. Hysteresis loops of bentonite slurries. At first, the shear rate was increased from zero to 150.0 1/s, and then decreased from 150.0 1/s back to zero. The shear stress forms loops, which upper parts consist of during 0.0-150.0 1/s and the lower parts during 150.0-0.0 1/s.

Table V The properties of bentonite slurries in hose pump experiments.

	Concentration wt-%	Density kg/m^3	Viscosity* Pa·s	Rheology type
Slurry1	10.99	1164.9	1.98	Thixotropic
Slurry2	11.26	1168.9	1.44	Thixotropic
Slurry3	15.27	1229.0	3.74	Thixotropic

*Viscosities are determined at constant shear rate 150 1/s

13.1.2 Slurries in progressive cavity pump experiments

Starch and CMC slurries were used in progressive cavity pump experiments. All the slurries were slightly non-Newtonian, and they followed Ostwald de Waele model. The index parameters K and n, and the regression value R^2 were determined for the fluids. The properties of slurries in PC-pump experiments are presented in Table VI.

Table VI The properties of starch and CMC slurries in progressive cavity pump experiments. Viscosities of slurries follow the Ostwald de Waele model $\mu = \boldsymbol{K\dot{\gamma}^{n-1}}$ therefore the constants K and n are determined. For pseudoplastic fluids 0 < n <1 and for dilatant fluids n > 1. The value R^2 is regression value.

	Concentration wt-%	Density kg/m^3	Viscosity* Pa·s	Rheology type	K -	n -	R^2
Starch							
Slurry1	16.48	1082.4	0.01229	Slightly non-New.	0.0011	1.4817	0.9947
Slurry2	28.44	1142.2	0.00991	Slightly non-New.	0.0492	0.6802	0.9048
Slurry3	36.69	1183.5	0.01563	Slightly non-New.	0.0939	0.6421	0.9235
Slurry4	40.28	1201.4	0.02878	Slightly non-New.	0.0214	1.0591	0.9744
Slurry5	44.38	1221.9	0.03738	Sligthly non-New.	0.0340	1.0184	0.9741
CMC							
Slurry1	6.11	1036.6	0.47076	Sligthly non-New.	0.8023	0.8936	0.9997
Slurry2	5.27	1031.6	0.28081	Sligthly non-New.	0.4284	0.9157	0.9997
Slurry3	4.55	1027.3	0.15177	Sligthly non-New.	0.3964	0.8084	0.9968
Slurry4	3.67	1022.0	0.09227	Sligthly non-New.	0.1136	0.9585	0.9999

*Viscosities are determined at constant shear rate 150 1/s

13.2 Pressure pulsation in hose pump

Pressure pulsation experiments were divided into two parts. In the first part, the effects of viscosity and rheology type of slurry to pumping were examined. In the second part, it was tested how different pipe materials influence the intensity of pressure pulsation.

13.2.1 Slurry tests

One starch, one bentonite, and five CMC slurries were used in pressure pulsation experiments. The slurries followed Ostwald de Waele model, and the index parameters k and n, and the rheology types of slurries are shown in Table VII. The concentration of starch slurry was 49.29 wt-% and the concentration of bentonite slurry was 10.99 wt-%. Concentrations for CMC slurries are presented earlier in Table IV. The experiments were carried out at 4.0 bar counter pressure. The pressure pulsation with starch, bentonite, and CMC slurries are presented in Figure 27. The rheology type of starch slurry was dilatant, bentonite was thixotropic, and CMC was pseudoplastic.

As can be noted in Figure 27, all the slurries behaved differently. Especially can be paid attention to starch slurry, where pressure pulsation attenuated when the pump rotation speed increases. The phenomenon may be explained by the rheological behavior of starch slurry. The viscosity increases as the shear rate increases with shear-thickening starch slurries. In CMC slurry such phenomenon did not occur. Instead, the flow velocity, i.e. velocity gradient, increases the pressure amplitude. Bentonite slurry had the smoothest pressure pulsation, where pulsation did not change as much even when pump rotation speed increased.

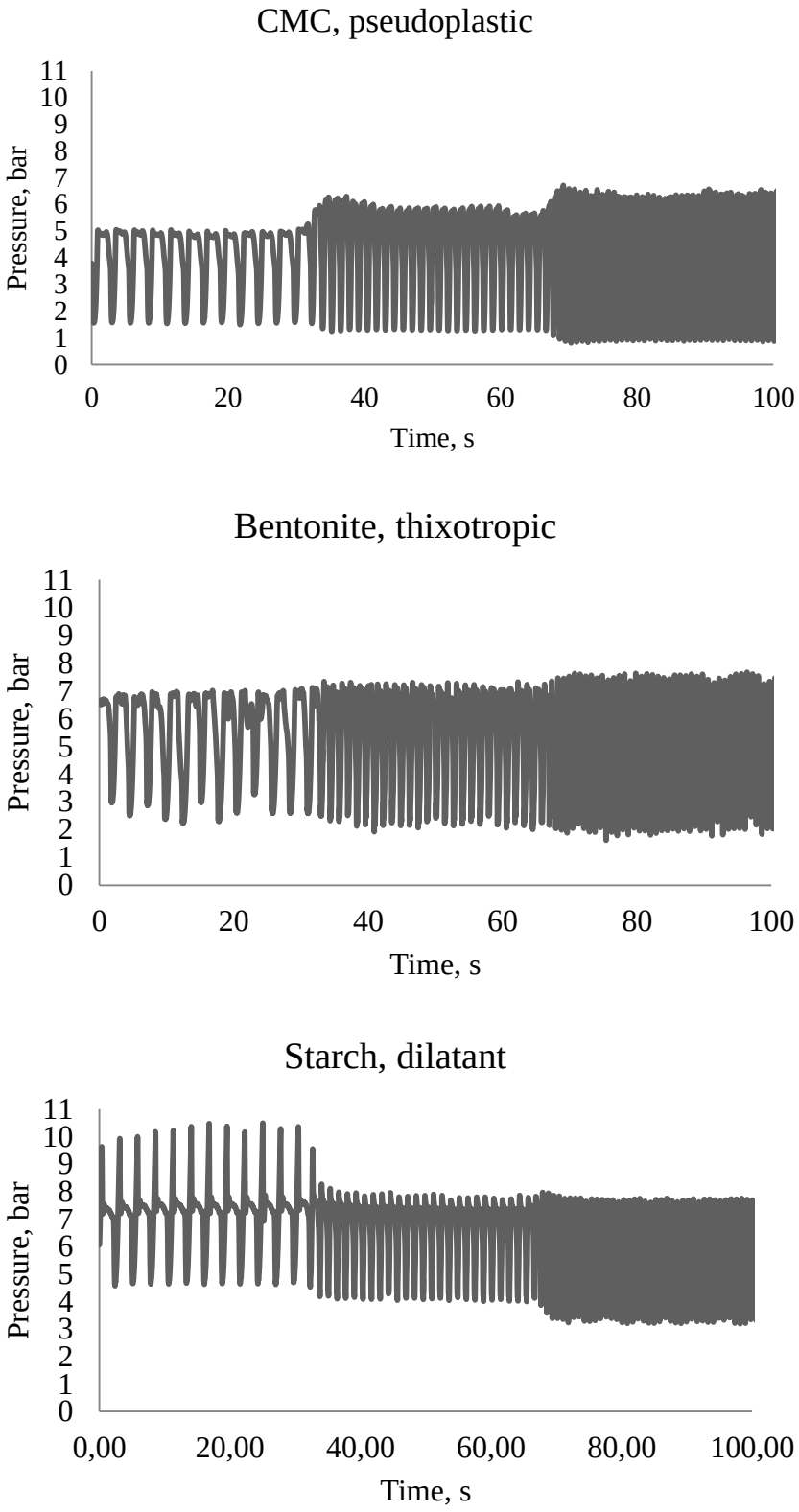

Figure 27. Pressure pulsations in CMC (9.57 wt-%), bentonite (10.99 wt-%), and starch (49.29 wt-%) slurries in hose pump experiments. The pump rotation speeds were 22, 48, and 78 rpm. The counter pressure was 4.0 bar. The total measurement time was 100 s.

Pressure pulsation in different slurries was also compared with the average pressures, which were calculated by using Equation (17). The average pressure values are shown in Table VII. Table VI shows that the pressure pulsation level was higher in starch slurry than in bentonite and in CMC slurries. This can be noticed also from the Figure 27. In starch slurry, the average pressure was 7.25 bar at 22 rpm, when in bentonite and CMC (slurry5) the corresponding values were 5.29 bar and 3.94 bar. In water, the average pressure is 4.35 bar at 22 rpm.

Table VII Average pressures of slurries used in pressure pulsation experiments at different pump's rotation speeds. Counter pressure was 4.0 bar. Average pressures were calculated by using Equation (17). Constants K and n belong to Ostwald de Waele model.

Material	Rheology type	K	n	Average pressure bar		
				22 rpm	48 rpm	78 rpm
Starch 49.29 wt-%	Dilatant	0.0010	1.925	7.25	7.15	6.49
Bentonite 10.99 wt-%	Thixotropic	-	-	5.29	5.96	5.65
CMC						
2.14 wt-%	Slightly non-New.	0.0264	0.988	5.47	5.64	5.72
3.87 wt-%	Slightly non-New.	0.1697	0.956	5.61	5.88	5.81
5.69 wt-%	Slightly pseudop.	0.8070	0.895	4.96	5.43	5.95
7.59 wt-%	Slightly pseudop.	3.0728	0.811	4.75	5.17	5.50
9.57 wt-%	Pseudoplastic	10.752	0.712	3.94	4.73	4.88

Table VII shows also that the average pressures of CMC slurries decreased little by little when the thickness of slurry increased. For example, the average pressure in slurry1 (the most dilute CMC slurry) at 22 rpm was 5.47 bar and in slurry5 (the thickest CMC slurry) the same value was only 3.94 bar. The pressure pulsation in CMC slurries 1 and 5 can be noted also in Figure 28.

Figure 28 shows that pulsation was smoother in dilute CMC slurry compared to thick slurry. In thick slurry, pulsation was temporarily higher when the pump rotation speeds increased. This can be noticed as the small knolls in pulsation data. When rotation speeds stayed constant, pulsation stabilized at a certain level, until it increased again when speed was increased. The higher fluid velocity

caused higher shear rate, which affected to the fluid. In pseudoplastic fluids, the viscosity increases when the velocity gradient (shear rate) decreases. During the change of pump speed, velocity gradient decreases. It can be found that pseudoplastic slurry raises temporarily the pressure to a higher level.

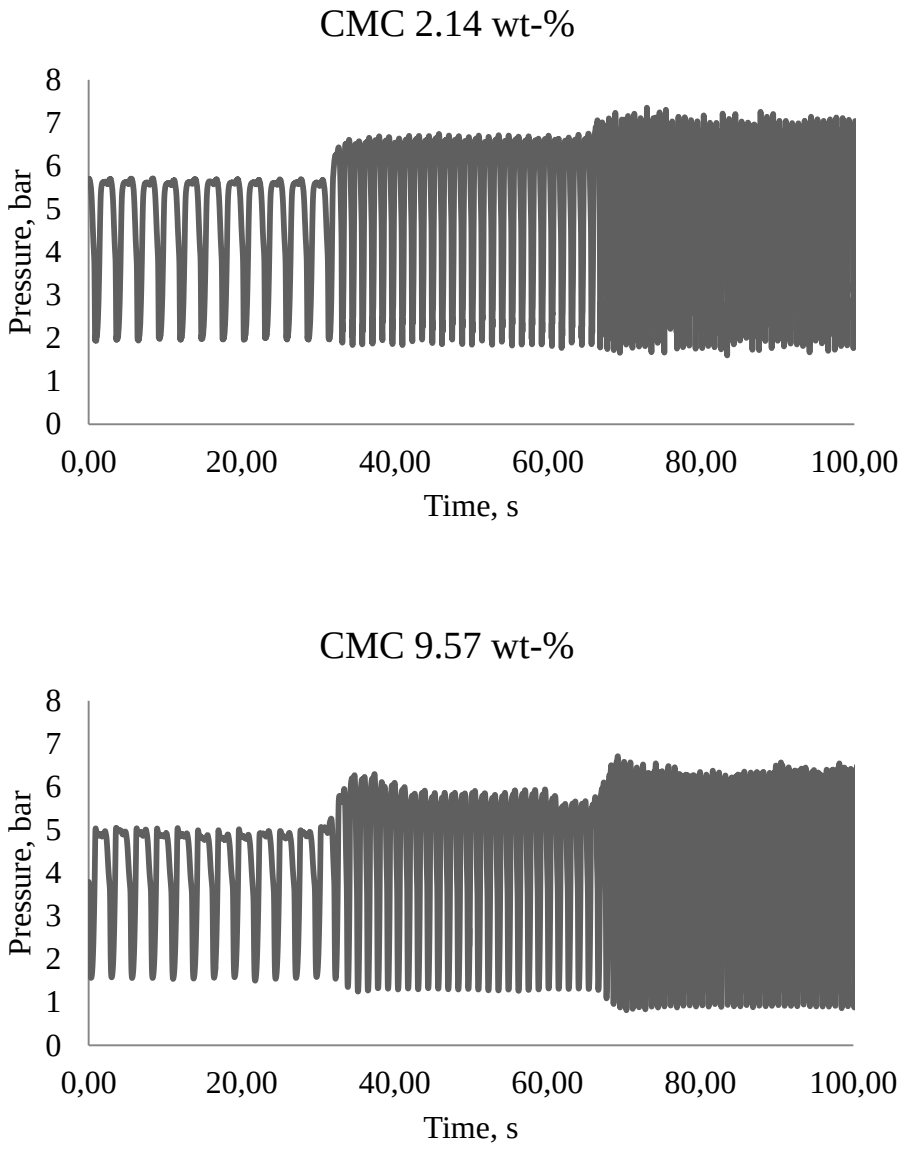

Figure 28. Pressure pulsations in 2.14 and in 9.57 wt-% CMC slurries in hose pump experiments. The pump's rotation speeds were 22, 48, and 78 rpm. The counter pressure was 4.0 bar. The total measurement time was 100 s.

13.2.2 Pipe material tests with water

Steel and elastic pipes and a prototype of pulsation dampener were used in material test of pressure pulsation. The used counter pressures were 1.0, 2.0, and 3.0 bar and used pump rotation speeds were 22, 48, and 78 rpm. The average pressures and standard variations were determined from the results, and they are presented in Table VIII.

Table VIII Pressure values in different pipe material in hose pump experiments. In table $\bar{p}$ = average pressure, Δp = variation between minimum and maximum pressures divided by two, and σ = standard variation in pressure data.

Counter pressure bar	Pump speed rpm	Flow rate m^3/h	Steel pipe $\bar{p} \pm \Delta p$ bar	σ bar	Elastic pipe $\bar{p} \pm \Delta p$ bar	σ bar	Dampener $\bar{p} + \pm\Delta p$ bar	σ bar
1.0								
	22	0.795	0.48 ± 0.33	0.23	0.36 ± 0.04	0.02	0.40 ± 0.06	0.03
	48	1.740	2.08 ± 1.69	1.20	1.82 ± 0.39	0.21	1.68 ± 0.39	0.22
	78	2.746	1.55 ± 1.70	0.97	1.68 ± 0.42	0.26	1.35 ± 0.44	0.24
2.0								
	22	0.813	3.79 ± 3.42	2.04	3.01 ± 1.06	0.68	2.08 ± 0.65	0.43
	48	1.720	4.35 ± 3.53	2.27	4.43 ± 2.53	1.53	5.04 ± 2.48	1.65
	78	2.738	3.81 ± 3.58	1.81	4.15 ± 2.75	1.48	4.45 ± 2.46	1.60
3.0								
	22	0.788	7.98 ± 5.25	3.85	7.14 ± 3.93	3.07	7.81 ± 4.54	3.07
	48	1.705	7.19 ± 5.44	3.45	7.40 ± 4.61	3.22	7.19 ± 4.92	2.91
	78	2.667	6.93 ± 5.67	3.15	6.79 ± 4.94	2.76	7.25 ± 5.30	2.76

Pulsation experiments when the counter pressure was 1.0 bar and the pump rotation speed was 22 rpm are shown in Figure 29. As can be noted, the pulsation amplitude was significantly greater in the case of a steel pipe compared to others. The average pressure was 0.48 ± 0.33 bar and the standard variation was 0.23 bar. In the case of elastic pipe and the pulsation dampener, the average pressures were 0.36 ± 0.06 bar and 0.40 ± 0.04 bar. In addition, the standard variation values

were 0.02 bar in the elastic pipe, and 0.03 bar when a pulsation dampener was used. In this case, the elastic pipe and the pulsation dampener absorbed pulsation much better than the steel pipe. The ability to absorb pulsation was due to flexible properties of elastic pipe and dampener.

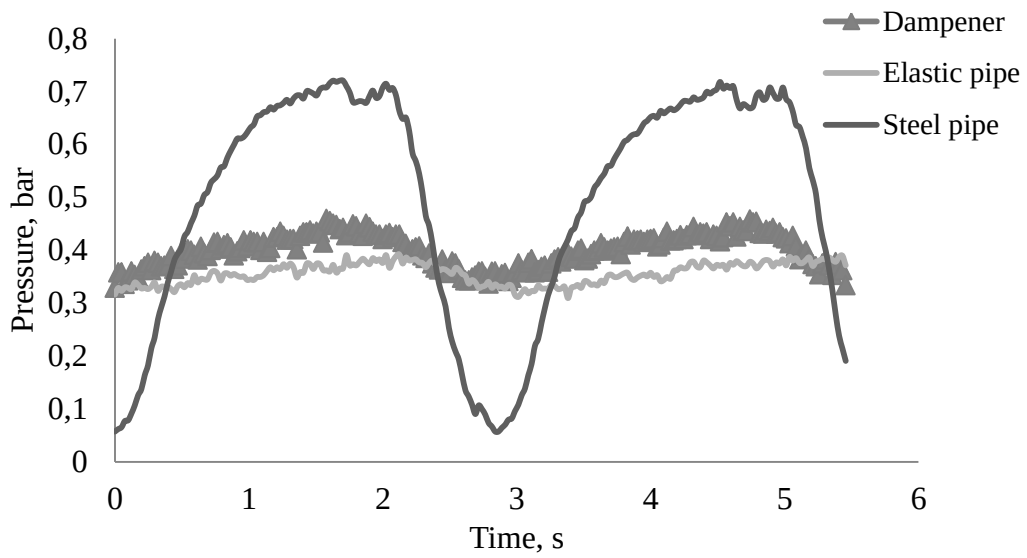

Figure 29. The pressure pulsations in hose pump using different pipe materials. The rotation speed of the pump was 22 rpm, the counter pressure was 1.0 bar, and the pumped fluid was water.

When the rotation speed was increased, the differences between the steel pipe and the two other components increased also. This can be noticed in Figure 30 where pressure pulsation in three components is presented, when the rotation speed was increased to 78 rpm but the counter pressures was kept 1.0 bar. The average pressure in steel pipe was 1.55 ± 1.70 bar, when in the elastic pipe and in the dampener the average pressures were 1.68 ± 0.42 bar and 1.35 ± 0.44 bar. The standard variation values were 0.97 bar in the steel pipe, 0.26 bar in the elastic pipe, and 0.24 bar for the dampener. As can be noticed, the standard variation and the variation between minimum and maximum pressure values were much higher in a steel pipe than in other materials. At 1.0 bar pressure level and at 78 rpm, the maximum pressures were almost 4.0 bar in steel pipe and about 2.0 bar in other components.

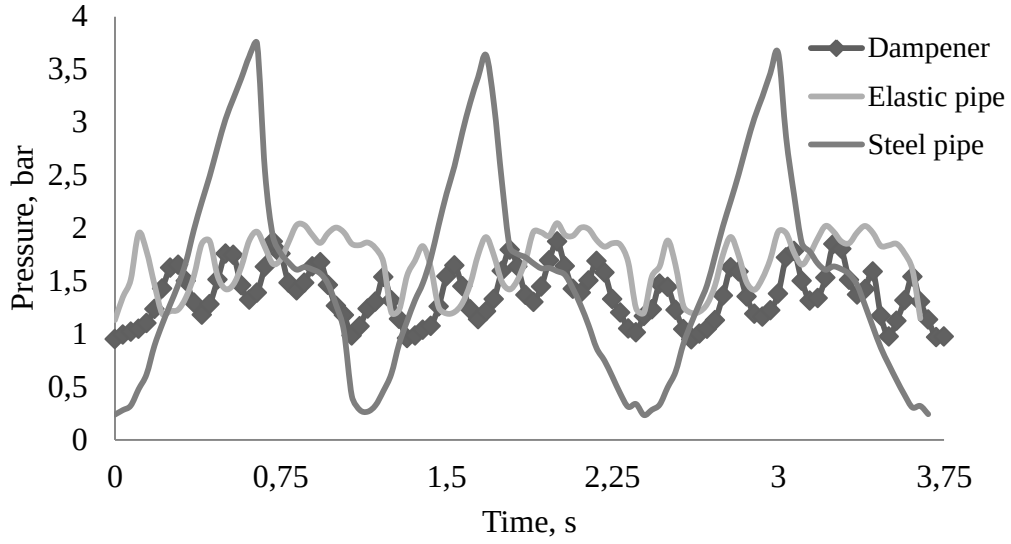

Figure 30. The pressure pulsations in hose pump. The used pipe materials were elastic and steel, and pulsation dampener. The rotation speed of the pump was 78 rpm, the counter pressure was 1.0 bar, and the pumped fluid was water.

When the counter pressure was increased, the differences between different components were stabilized. In Figure 31 is presented pressure pulsation when the speed was 78 rpm and the counter pressure was 3.0 bar. It can be noticed that the shape of the pressure spike was same in every component. The average pressure was 6.96 ± 5.67 bar for the steel pipe, 6.79 ± 4.94 bar for the elastic pipe, and 7.25 ± 5.30 bar for the dampener.

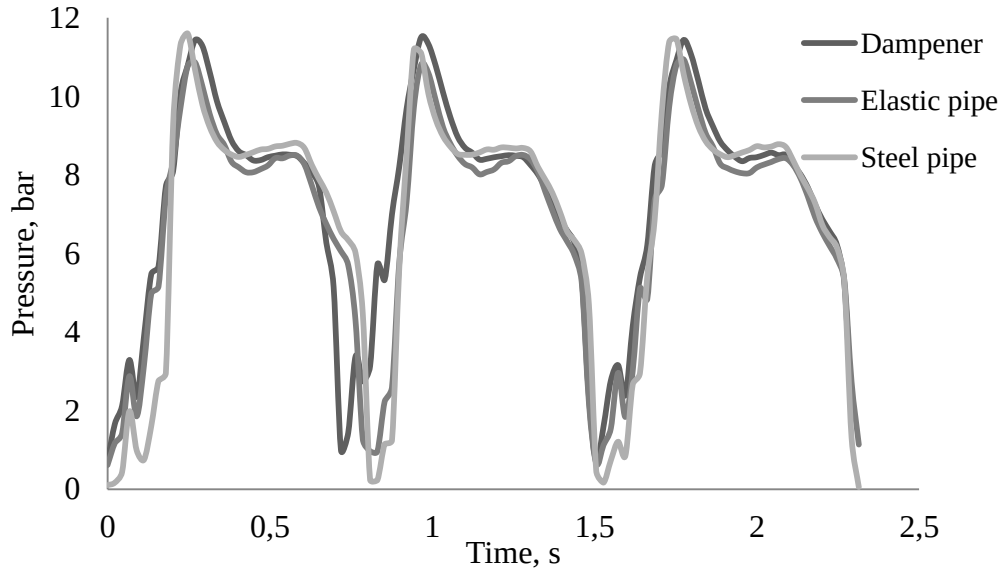

Figure 31. The pressure pulsations in hose pump using different pipe materials. The rotation speed of the pump was 78 rpm, the counter pressure was 3.0 bar and the pumped fluid was water.

13.3 Other graphs of the results

In Figure 32 and 33 are shown the behavior of viscosities of some fluids in hose pump experiments. Fluids were pumped at three different pump rotations speeds. The higher the rotation speeds was, the higher was also the shear rate. The shear rate was calculated by using Equation (21), and Equation (9) was used to determine the viscosities. Viscosity of bentonite slurry was calculated with Equation (22). The properties of fluids were shown in Table VII.

According to the measurements, which were done with rheometer, it was known that the rheology type of CMC was shear-thinning (=pseudoplastic). This can be also noticed from Figure 32, where the viscosity of CMC and bentonite slurries decreased when shear rate increased. The thixotropic behavior of bentonite slurry cannot be observed in Figure 32 even though in viscosity measurements it was observed. According to Figure 32, the bentonite slurry behaved such as CMC slurry but the viscosity was lower.

Figure 33 shows that the viscosity of dilute CMC slurry (2.14 wt-%) stayed nearly constant even the shear rate in the pipe increased. This was noticed also in viscosity measurements where the rheology type of dilute CMC slurry was slightly non-Newtonian. Figure 33 shows also the viscosity of starch slurry increased when shear rate increased too. It can be stated that 49.29 wt-% starch slurry behaved such as shear-thickening (=dilatant) fluid in the pipe as was noted in rheology measurements also.

In progressive cavity pump experiments, starch and CMC slurries behaved almost like Newtonian fluids.

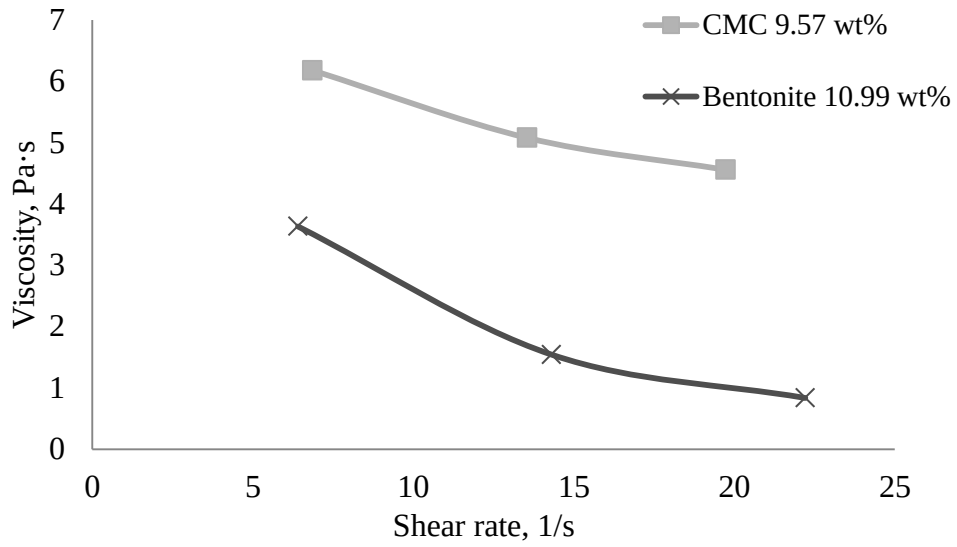

Figure 32. Viscosities of 9.57 wt-% CMC slurry and 10.99 wt-% bentonite slurry in the pipe in hose pump experiments.

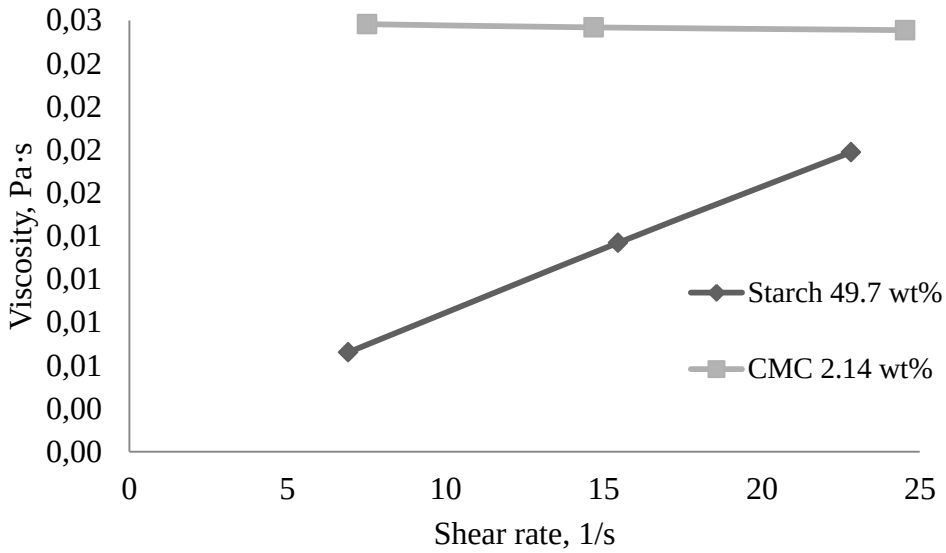

Figure 33. Viscosities of 49.7 wt-% starch slurry and 2.14 wt-% CMC slurry in the pipe in hose pump experiments.

13.4 Power curves

The power curves are presented as the efficiency curves. The efficiencies were calculated by using Equation (4). The power curves for the hose pump and PC-pump are presented in Figures 34 and 35 where the starch slurry concentrations were 39.89 wt-% and 40.28 wt-% respectively. The power curves were chosen in order to compare the power curves of almost similar slurries in different pumps. The power curves of other slurries are presented in Appendices. The power curves of hose pump are in Appendix I, and the power curves of PC-pump are in Appendix II. In addition, the calculated discharge pressures of hose pump are shown in Appendix III.

The pump efficiency increases as the pressure increases in both pumps. It can be also noticed that the efficiencies were higher in PC-pump compared to hose pump. For example, in hose pump the highest efficiency was about 50 %, while in PC-pump the highest efficiency was over 70 %. Figures 34 and 35 show also that the efficiency increases as a function of flow rate in PC-pump, while in the hose pump the efficiency reaches the constant value. In some power curves of hose pump, the efficiency began to decrease, which means that the best efficiency point was achieved already (Appendix I).

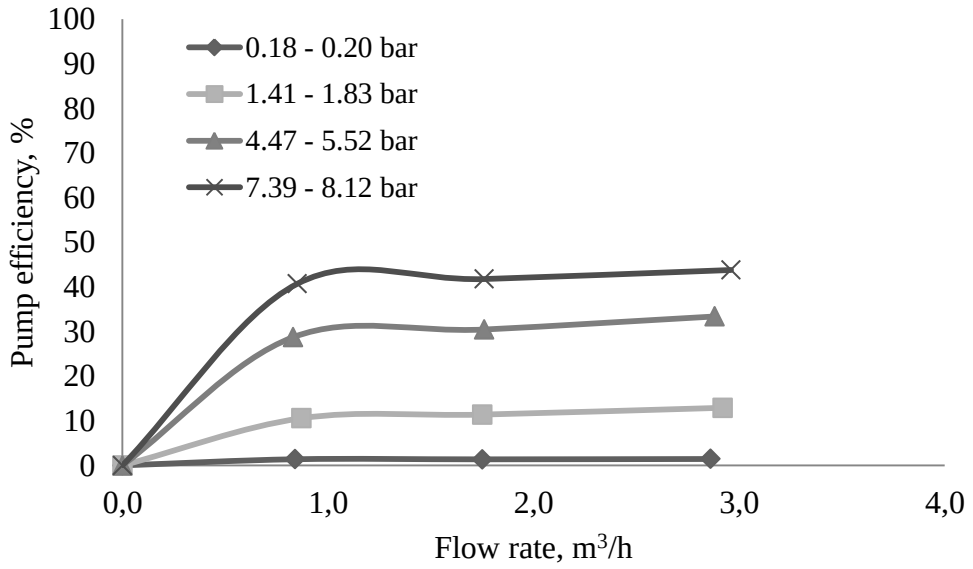

Figure 34. Power curves of 39.89 wt-% starch slurry in hose pump experiments. The used counter pressures were 0.0, 2.0, 4.0, and 6.0 bar. The pump rotation speeds were 22, 48, and 78 rpm.

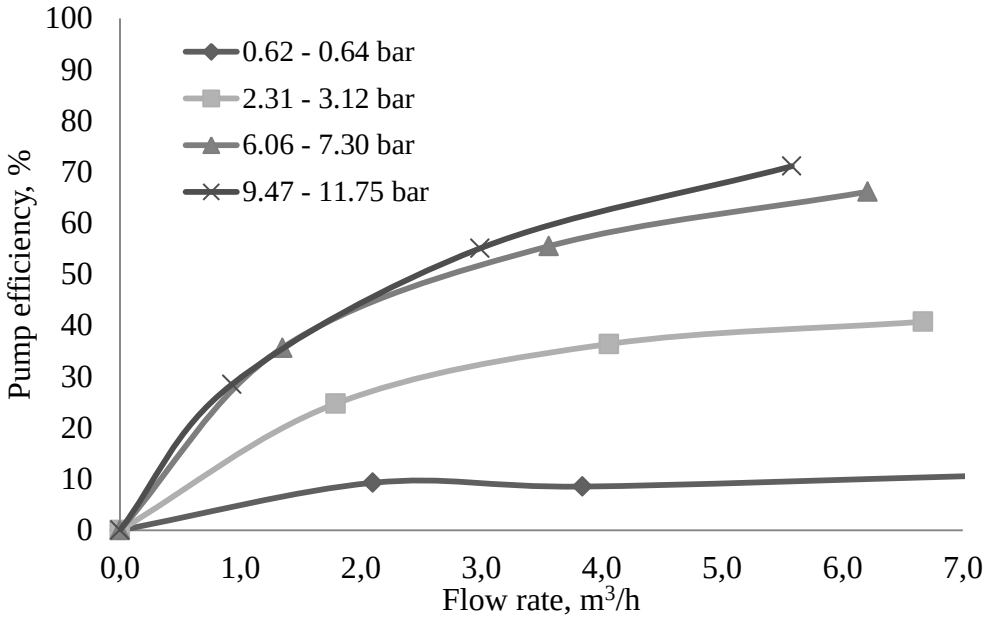

Figure 35. Power curves of 40.28 wt-% starch slurry in progressive cavity pump experiments. The used counter pressures were 0.0, 2.0, 4.0, and 6.0 bar. The pump rotation speeds were 82, 204, and 326 rpm.

The bentonite slurries were pumped only with the hose pump. With the most thickest bentonite slurry (15.26 wt-%), pumping was not successful. In addition, the slurry could not pumped using 6.0 bar counter pressure because the flow rate was almost zero. Pumping without any flow could have broken the pump, so the measurement was not carried out at 6.0 bar counter pressure.

In Figure 36, the efficiency points of 15.26 wt-% bentonite slurry at different counter pressures are shown. Figure 36 shows that in all used counter pressures the pump efficiencies were below 5.0 %. The most likely, the pump was broken or did not work properly in this experiment. Also, the slurry may have included lumps, which blocked the pipe partially and caused variation in flow rate. The failure in pump caused low flow rate and consequently a low pump power.

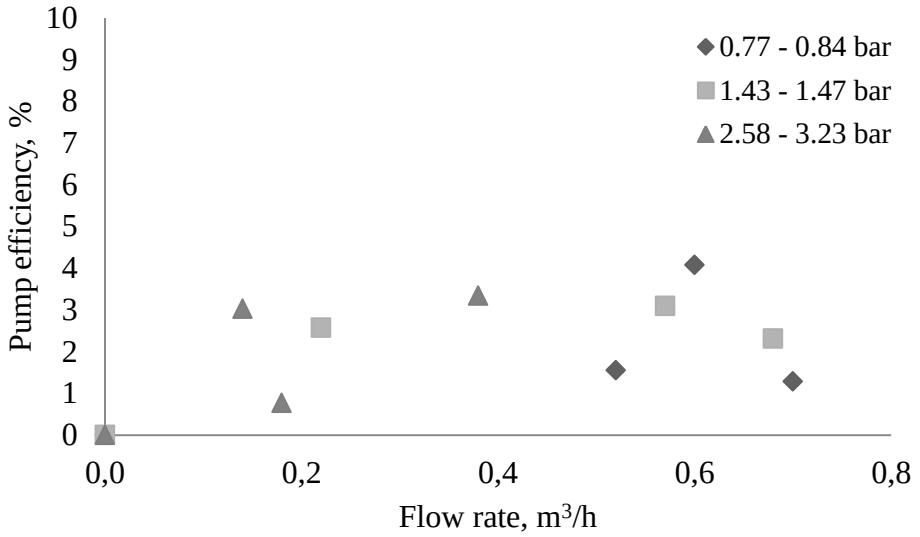

Figure 36. The efficiency points of 15.26 wt-% bentonite slurry in hose pump. Pump rotation speeds were 22, 48, and 78 rpm. The used counter pressures were 0.0, 2.0, and 4.0 bar.

13.5 Pressure curves

The pressure curves were determined for all slurries and for both pumps. In Figures 37 and 38 are presented the pressure curves of 39.89 w-t% starch slurry for hose pump and 40.28 wt-% starch slurry for PC-pump experiments. The power curves of the same slurries were presented earlier in Figures 34 and 35. The pressure curves of other slurries are presented in Appendices IV and V.

As can be noticed from the Figures 37 and 38, in the case of hose pump, the flow rate was almost constant even when the pressure varied. In the case of PC-pump, the flow rate decreased when the pressure increased. The difference was due to the different pump configurations. There is a high possibility of backflow with PC-pump, see Figure 11. In some PC-pump cases, the system pressures increased nearly to 11.0 bar at 10.0 bar counter pressure and at 326 rpm rotation speed. In hose pump, the maximum pressures were less than 10.0 bar at 10.0 counter pressure and 78 rpm.

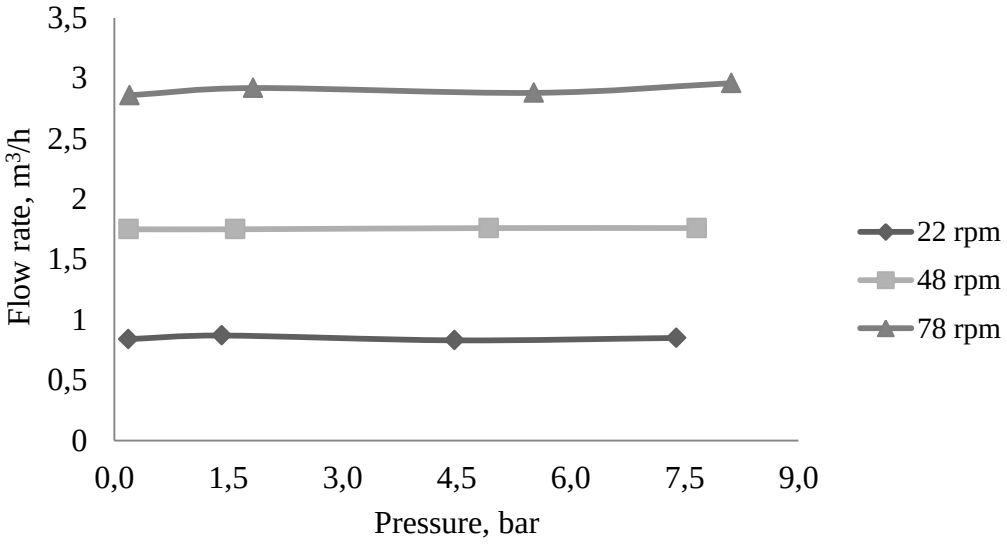

Figure 37. Pressure curves of 39.89 wt-% starch slurry in hose pump experiments. The used counter pressures were 0.0, 2.0, 4.0, and 6.0 bar. The pump's rotation speeds were 22, 48, and 78 rpm.

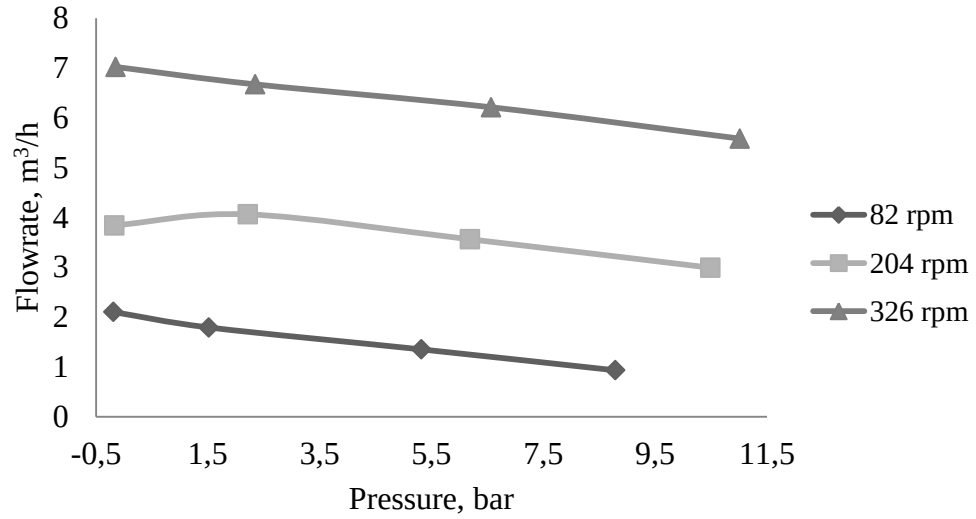

Figure 38. Pressure curves of 40.28 wt-% starch slurry in progressive cavity pump experiments. The used counter pressures were 0.0, 2.0, 4.0, and 6.0 bar. The pump's rotation speeds were 82, 204, and 326 rpm.

The thick (15.26 wt-%) bentonite slurry caused problems also in pressure curve determination. The problems were due to the same reason than in power curve determination, i.e. the slurry included lumps, which blocked the pipe partially causing uneven flow rate or the pump was broken. Additionally, some problems occurred when thick (9.57 wt-%) CMC slurry was pumped. For some reason at 22 rpm, the maximum pressure was only 2.50 bar, even when the counter pressure was 6.0 bar. In other rotation speeds, the pumping was normal in all counter

pressures. The reasons for this may be also the lumps in slurry, or some technical failure in pressure meter.

13.6 $NPSH_R$ curve for PC-pump

The $NPSH_R$ curve was determined for the used progressive cavity pump (Flowrox C10/10). The $NPSH_R$ values were calculated from the suction pressure values by using Equation (20). First, the average pump head was calculated. Next, it was determined the pump head value, which was 3.0 % lower than the average pump head. The $NPSH_R$ value was obtained, when the pump head was permanently 3.0% or more lower than the average pump head. In Figure 39, the $NPSH_R$ curve for the PC-pump is shown.

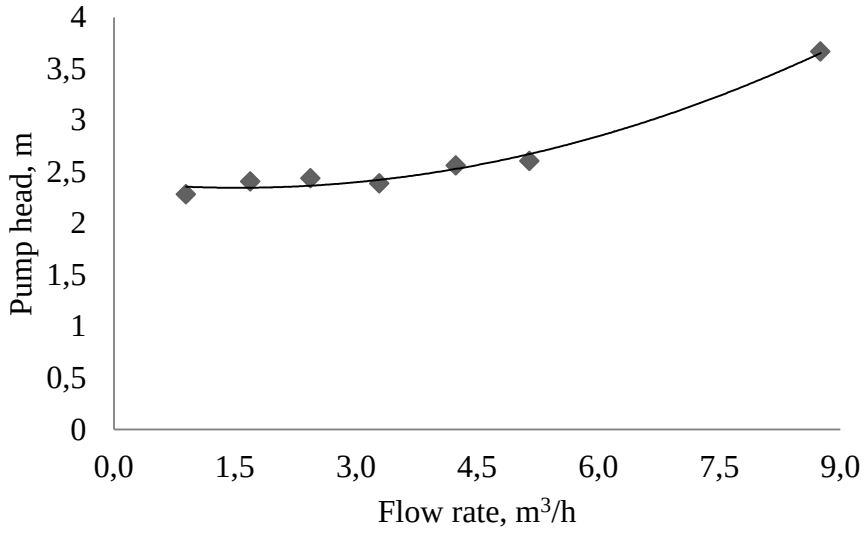

Figure 39. $NPSH_R$ curve for Flowrox C10/10 progressive cavity pump. The used pump's rotation speeds were 82, 122, 163, 204, 245, 286, 326, 367, and 408 rpm. Pumped fluid was water. The experiments were done at room temperature.

Figure 39 shows that $NPSH_R$ curve has the shape of lazy "U" as was expected based on Chapter 5.3 in Figure 13. The $NPSH_R$ values at rotation speeds 326 and 367 rpm are ignored because values differ from other values being too low due to possible errors in measurements. Most likely, the errors were due to too rapid throttling of the suction, and the measurement system could not keep up. Other sources for errors may be technical failure in measurement system or some problems in pump operation, which caused uneven flow.

14 CONCLUSIONS

The aim of this thesis was to study how viscosity and rheology type of slurry affect to slurry pumping. The experiments were carried out by pumping starch, carboxymethyl cellulose, and bentonite slurries with two different pumps. The pumps were progressive cavity pump (Flowrox C10/10) and eccentric hose pump (Flowrox LP-32). Pressure and power curves were determined from the obtained results, of which the rheological effects could be examined. In addition, the $NPSH_R$ curve was determined for the PC-pump. The operation of hose pump caused pressure pulsation in the piping system, so also that phenomenon was investigated. Pulsation was examined by pumping variety of different kinds of slurries, and using different pulsation damping systems in piping system.

The pipe material affected to the intensity of pressure pulsation at low counter pressures. At 1.0 bar counter pressure and at 22 rpm pump rotation speed, the pulsation dampener and elastic pipe attenuated the pulsation much better than steel pipe. In the case of a pulsation dampener or an elastic pipe, the pressure was about 0.3-0.4 bar. In steel pipe, pressure was about 0.1-0.7 bar. When the pump rotation speed was increased to 78 rpm and counter pressure was kept the same (1.0 bar), the dampener, and the elastic pipe worked still better than the steel pipe. The differences between different materials disappeared completely at 3.0 bar counter pressure and at 78 rpm rotation speed. The pressures varied between 0.0 and 12.0 bar.

Pressure pulsation was also examined by pumping different starch, bentonite, and CMC slurries with hose pump at 4.0 bar counter pressure. When pressure pulsation was compared with thick slurries, it was found that the pulsation was different depending on the rheology of slurry. For example, the rheology type of thick starch slurry was shear-thickening. When starch slurry was pumped, the pressure amplitude was the most powerful at 22 rpm being about 4.5-10.0 bar. The pulsation attenuated when the rotation speed increased being 4.0-8.0 bar at 78 rpm. In the case of bentonite slurry, the pressure pulsation was similar at all rotation speeds. In thick CMC slurry, the pressure pulsation increased smoothly with increasing rotation speed.

In both pumps, the efficiencies increased with higher used counter pressures, so the best efficiencies were achieved at 6.0 bar counter pressure. In the case of hose pump, the best efficiencies were 39.7-45.9 % in dilute starch and CMC slurries. Only exception was 3.87 wt-% CMC slurry, where the best efficiency was little higher (51.2 %) than in other dilute slurries. In the thickest starch slurry, the best efficiency was 71.6 %, but in the thickest CMC slurry only 25.3 %. The best efficiencies were 86.6 % in 10.99 wt-% bentonite slurry and 51.1 % in 11.26 wt-% bentonite slurry. In the thickest bentonite slurry, the efficiencies were only between 1.3 and 3.3 % at 0.0-4.0 bar counter pressures. The thickest bentonite slurry could not be pumped at 6.0 bar counter pressure, because the flow rate was then zero and the pump could be broken. According to this research, the rheology of slurry had not impacts to hose pump efficiency or power consumption. It can only be stated that pumping of too thick slurries considerably decreases the efficiency.

In the case of progressive cavity pump, the efficiencies were higher than in hose pump, and the best efficiencies were 64.03-72.54 %. The best efficiencies were also achieved at the highest rotation speed and 6.0 bar counter pressure. In the case of hose pump, the best efficiencies were achieved also at 6.0 bar but the rotation speed varied. In the case of hose pump, the efficiencies were below 3.0 % but in progressive cavity pump, the efficiencies were about 15-17 % in CMC slurries and 8-10 % in starch slurries.

The pressure curves did not provide much new information about slurry pumping. In the case of hose pump, the flow rate varied very little even though the pressure level rises. In the case of progressive cavity pump, the flow rate decreased significantly when pressure increased. The configuration of a PC-pump may be the reason for decreasing flow rates at high counter pressures. The rollers in a hose pump squeezes the hose tightly and with PC-pump the backflow may occur between the stator and rotor spacing.

REFERENCES

1. Abulencia, J.P., Theodore, L., *Fluid flow for the practicing chemical engineering*, 1st ed., John Wiley & Sons, 2009, p. 4, 211.

2. Karassik, I.J., Krutzsch, W.C., Fraser, W.H., Messina, J.P., *Pump Handbook*, 1st ed., McGraw-Hill, 1976, p. 1-1; 1-3; 3-49.

3. SFS 4874. Finnish Standards Association. Standard confirmed 31.12.1982.

4. Parker, D.P., Positive displacement pumps – Performance and application, Warren Pumps Incorporated, 1994.

5. Aalto University. The material of the course: Chemical Engineering I: Part 2 Fluid mechanics.

6. Volk, M., *Pump characteristics and applications*, 3rd ed., CRC Press, 2013, p. 12-13.

7. Waterworld, http://www.waterworld.com/articles/print/volume-27/issue-12/departments/pump-tips-techniques/alternate-pump-types-positive-displacement-rotary-reciprocating.html (21.1.2014)

8. Tawil, E., Centrifugal and positive displacement pumps. https://www.cedengineering.com/upload/Centrifugal%20and%20Positive%20Displacement%20Pumps.pdf (17.2.2014)

9. Pessoa, P.A.S., Paladino, E.E., de Lima, J.A., A simplified model for the flow in a progressive cavity pump, 20th International Congress of Mechanical Engineering, Brazil, 2009.

10. Flowrox material. Progressive cavity pump. 2012.

11. Hydraulic institute, *Hydraulic institute standards for centrifugal, rotary and reciprocating pumps*, 14th ed., 1983, p. 152, 235.

12. Vetter, G., Wirth, W., Understand progressing cavity pumps characteriristics and avoid abrasive wear, University of Erlangen-Nuremberg, Erlangen, Germany.

13. Flowrox material. Hose pumps. 2012.

14. Flowrox, http://www.flowrox.com/fin/ (22.1.2014)

15. Trinity construction, http://www.foamed.com.cn/cpzsshow.asp?id=19 (22.1.2014)

16. Flowrox. Sales manual (Selection instructions) for Flowrox progressive cavity pumps. 2013.

17. Flowrox progressive cavity pump brochure. 2011.

18. Flowrox. LPP-pumps sales manual. 2012.

19. Flowrox peristaltic hose pumps brochure. 2011.

20. Progressive cavity series of success, *World pumps: water & wastewater*, September 2013.

21. Driedger, W., Controlling positive displacement pumps, *Hydrocarbon Processing*, 1996. http://www.driedger.ca/ce2_pdp/CE2_PDP.html (22.5.2014)

22. Forsthoffer, W.E., Rotatint equipment handbooks: pumps, Elsevier Science & Technology Books, 2005, p. 167-168. http://www.unionmillwright.com/Forsthoffer%27s%20Rotating%20Equipment%20Handbooks.pdf (22.5.2014)

23. Wnek, T.F., Pressure pulsations generated by centrifugal pumps. http://www.warrenpumps.com/resources/Pressure%20Pulsations%20Generated%20by%20Centrifugal%20Pumps.pdf (3.3.2014)

24. Cheema, J., Pulsation dampeners for smooth flow in pipes. http://www.fecintl.com/resources/pdf/PulsationDampener.pdf (10.2.2014)

25. Larox Flowsys Oy. Theoretical LPP pulsation chart at pump outlet. 2004.

26. Maillard, J., Active control of pressure pulsations in piping systems, Reseach Report, University of Karlskrona, Ronneby, Sweden, 1998.

27. Teknopump, http://www.teknopump.fi/sykkeenvaimentimet.html (10.2.2014)

28. Cole Palmer, http://www.coleparmer.com.cn/en/TECHINFO/techinfo.asp?openlist=A,A3,B,C,D,D1,D5,D6,D7,E,A1&htmlfile=ppumpsreduc_WP.htm&Title=Reducing+Pulsation+in+Peristaltic+Pumping+Systems (26.2.2014)

29. Hermanus, R., Vrielink, H.O., Peristaltic pump, U.S. Patent No. 0258829, November 8, 2007.

30. IHS Global Spec, http://www.globalspec.com/learnmore/flow_transfer_control/pumps/pumps_all_types (12.2.2014)

31. Huhtinen, M., Korhonen, R., Pimiä, T., Urpalainen, S., *Voimalaitostekniikka*, 1st ed., Otavan Kirjapaino Oy, 2008, p. 138-139.

32. Grundfors wastewater, The sewage pumping handbook, http://www.grundfos.com/content/dam/Global%20Site/Industries%20%26%20solutions/waterutility/pdf/sewage-handbook.pdf (17.2.2014)

33. Sprinkler Warehouse, http://www.sprinklerwarehouse.com/DIY-System-Design-with-a-Pump-s/7080.htm (15.9.2014)

34. Jensen Engineered Systems, http://www.jensenengineeredsystems.com/pump-curves/ (15.9.2014)

35. Lappeenranta University of Technology. The handouts of the course: ”Pumps, blowers, fans and compressors”. 2011.

36. Pump School: “Understanding net positive suction head”. http://www.pumpschool.com/applications/NPSH.pdf (8.2.2014)

37. Evans, J., “Net Positive Suction Head: NPSHR and NPSHA”. http://www.pumpsandsystems.com/topics/net-positive-suction-head-npshr-and-npsha?page=2 (29.9.2014)

38. Aalto University. The course material “Pumping technology”. https://noppa.aalto.fi/noppa/...24.../Kul-24_4410_oppikirjan_luku_8.pdf (11.2.2014.)

39. Volk, M., *Pump Characteristics and Applications*, 1st ed., Taylor & Francis Group, 2005, p. 99-100.

40. Narayna Pillai, P.N., NPSH – A DISCUSSION. http://www.plant-maintenance.com/articles/NPSH.pdf (28.8.2014)

41. Henshaw, T., “Performance Curves and NPSH Tests”. http://www.pumpsandsystems.com/topics/pumps/centrifugal-pumps/performance-curves-and-npsh-tests?page=2 (29.9.2014)

42. Karassik, I.J., McGuire, T., *Centrifugal pumps*, 2nd ed., Chapman & Hall, 1998, p. 484.

43. FinnSonic, http://www.finnsonic.com/fi/tuotteet/ultraaeaenikomponentit (28.8.2014)

44. Harris, J., *Rheology and non-Newtonian flow*, 1st ed., Longman Group Limited, 1977, p. 1-12.

45. Chhabra, R.P., Richardson, J.F., *Non-Newtonian Flow and Applied Rheology: Engineering Applications*, 2nd ed., Butterworth-Heinemann, 2008, p. 1-7, 12-27.

46. Brydson, J.A., *Flow properties of polymer melts*, 2nd ed., Butterworth Group, 1981, p. 6, 12-13.

47. Heyer, P., Anton Paar Rheology, 2011.

48. Lee, Y.S., Wagner, N.J., Dynamic properties of shear thickening colloidal suspensions, *Rheol Acta*, **42** (2003), p. 199-208.

49. Mitsoulis, E., Flows of viscoplastic materials: models and computations, *Rheology Reviews*, (2007), p. 135-178.

50. Churchill, S.W., *Viscous flows: The practical use of theory*, 1st ed., Butterworth Publishers, 1988, p. 27.

51. Azikri de Deus, H.P., Dupim, G.S.P., On behavior of the thixotropic fluids, *Physics Letters A*, **377** (2013), 478-485.

52. Barnes, H.A., Thixotropy – a review, *J. Non-Newtonian Fluid Mech.*, **70** (1997), 1-33.

53. Manconi, M., Aparicio, J., Seyler, D., Vila, A.O., Figueruelo, J., Molina, F., Effect of several electrolytes on the rheopectic behavior of concentrated soy lecithin dispersion, *Colloids and Surfaces A: Physicochem. Eng. Aspects*, **270-271** (2005), 102-106.

54. EKATO, *Handbook of Mixing Technology*, 3rd ed., Rünzi GmbH, Schopfheim, Germany, 2000, p. 22.

55. Roylance, D., Engineering viscoelasticity, Department of Material Science and Engineering, Massachusetts Institute of Technology, 2001.

56. Viswanath, D.S., Ghosh, T.K., Prasad, D.H.L., Dutt, N.V.K., Rani, K.Y., *Viscosity of liquids: Theory, estimation, experiment and data*, 1st ed., Springer, 2007, p.

57. Bright Hub Engineering, http://www.brighthubengineering.com/fluid-mechanics-hydraulics/83996-viscosity-measurement-equipment/ (18.2.2014)

58. Wilke, J., Kryk, H., Hartmann, J., Wagner, D., *Theory and praxis of capillary viscometry*. http://www.sianalytics.com/fileadmin/upload/Informationen/Kapillarviskosimetrie/INT/Primer_VISCO_1-MB_PDF-English.pdf (18.2.2014)

59. Karlsruhe Institute of Technology, http://www.mvm.kit.edu/english/697_789.php (20.2.2014)

60. Bakhtiyarov, S.I., Overfelt, R.A., Measurement of liquid metal viscosity by rotational technique, *Acta mater* **17** (1999), 4311-4319.

61. Measurement of viscosity using a falling ball viscometer http://physics.niser.ac.in/labmanuals/sem1/Viscosity.pdf (24.2.2014)

62. Cohen-Tenoudji, F., Ahlberg, L.A., Tittman, B.R., Pardee, W.J., High temperature ultrasonic viscometer, U.S. Patent No. 4779452, October 25, 1988.

63. Carrington, S., Langridge, J., Viscometer or rheometer? Making the decision, *Particle Analysis*. http://www.iesmat.com/iesmat/upload/file/Malvern/Productos-MAL/REO-Viscometer%20or%20Rheometer.%20Making%20the%20decision.pdf (9.10.2014)

64. Franck, A., Measuring structure of flow viscosity fluids in oscillation using rheometers with and without a separate torque transducer, *Annual transactions of the Nordic rheology society* **11** (2003).

65. Läuger, J., A new rheometer platform for extended testing capabilities, *Annual transactions of the Nordic rheology society **21** (2013).*

66. Industrial Minerals (IMA), available: http://www.ima-europe.eu/about-industrial-minerals/industrial-minerals-ima-europe/bentonite (19.3.2014)

67. International Chemical Safety Card of Bentonite. http://www.cdc.gov/niosh/ipcsneng/neng0384.html (13.3.2014)

68. Bentonite, http://www.bentonite.it/bentonite-properties.php. (13.3.2014)

69. Oregon State University, http://food.oregonstate.edu/learn/starch.html (25.4.2014)

70. Robyt, J.F., Starch: Structure, properties, chemistry and enzymology, Laboratory of Carbohydrate Chemistry and Enzymology, Department of Biochemistry, Biophysics and Molecular Biology, Iowa State University, Ames, USA, 2008.

71. Fall, A., Bertrand, F., Ovarlez, G., Bonn, D., Shear thickening of cornstarch suspensions, *Journal of Rheology*, **56** (2012), p. 575-588.

72. Bischoff White, E.E., Chellamuthu, M., Rothstein, J.P., Extensional rheology of a shear-thickening cornstarch and water suspension, *Rheological Acta*, (2009).

73. Biswal, D.R., Singh, R.P., Characterisation of carboxymethyl cellulose and polyacrylamide graft copolymer, *Carbohydrate Polymers* **57** (2004), 379-387.

74. Togrul, H., Arslan, N., Production of carboxymethyl cellulose from sugar beet pulp cellulose and rheological behaviour of carboxymethyl cellulose, *Carbohydrate Polymers* **54** (2003), 73-82.

75. Yang, X.H., Zhu, W.L., Viscosity properties of sodium carboxymethylvellulose solution, *Cellulose* **14** (2007), 409-417.

76. Ghannam, M.T., Esmail, M.N., Rheological properties of Carboxymethyl Cellulose, Department of Chemical Engineering, University of Saskatchewan, Canada, 1996.

77. Benchabane, A., Bekkour, K., Rheological properties of carboxymethyl cellulose (CMC) solutions, *Colloid Polymer Science* **286** (2008), 1173-1180.

78. Severs, E.T., Austin, J.M., Flow properties of vinyl chloride resin plastisols, *Ind. Eng. Chem*., **46** (1954), 2369-2375.

79. Munson, B.R., Young, D.F., Okiishi, T.H., *Fundamentals of fluid mechanics*, 4th ed., 2002, Wiley & Sons, p. 20, 107, 475, 481, 489.

80. Metropolia University of Applied Science. The material of the course: Hydraulic I. 2009.

APPENDICES

Table I Hose pump's electric and pump powers and pump efficiency values for 2.14 wt% CMC slurry.

Counter pressure bar	Flow rate m^3/h	Pressure difference kPa	Pump power W	Pump electric power W	Efficiency %
0	0.83	0.16	3.7	306.0	1.2
	1.78	0.17	8.4	743.6	1.1
	2.90	0.20	16.1	1072.8	1.5
2	0.86	1.26	30.1	314.6	9.6
	1.78	1.57	77.6	689.6	11.3
	2.90	1.77	142.6	1133.8	12.6
4	0.87	4.36	105.4	368.0	28.6
	1.72	5.10	243.7	791.0	30.8
	2.84	5.40	426.0	1309.3	32.5
6	0.83	7.76	178.9	444.1	40.3
	1.62	8.49	382.1	944.2	40.5
	2.59	8.65	622.3	1568.6	39.7

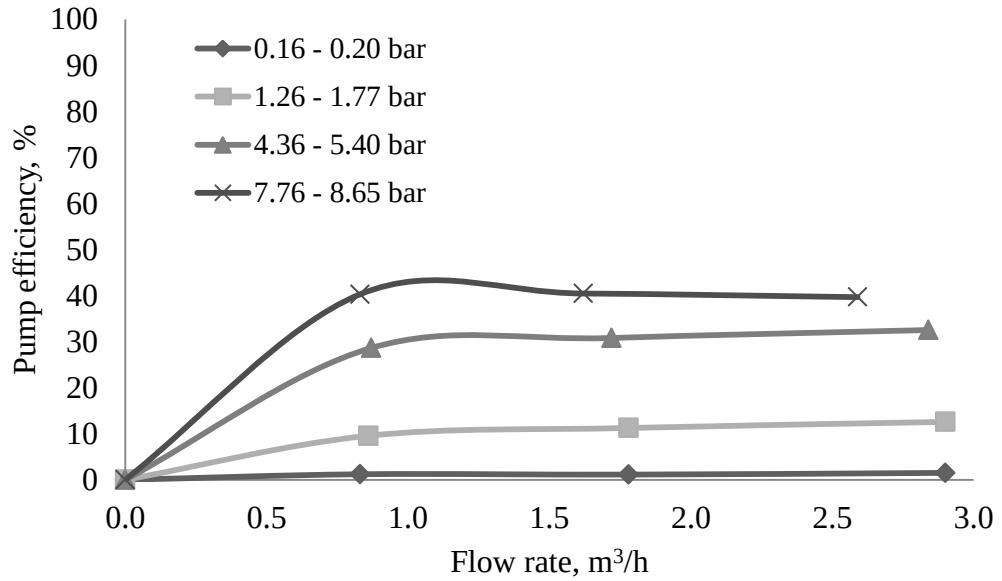

Figure 1. Power curves of 2.14 wt% CMC slurry in hose pump. Control pressures, generated by actuator, were 0.0, 2.0, 4.0, and 6.0 bar.

Table II Hose pump's electric and pump powers and pump efficiency values for 3.87 wt% CMC slurry.

Counter pressure bar	Flow rate m^3/h	Pressure difference kPa	Pump power W	Pump electric power W	Efficiency %
0	0.86	0.17	4.1	327.4	1.2
	1.74	0.17	8.2	714.3	1.2
	2.66	0.18	13.3	1170.2	1.1
2	0.84	1.44	33.6	326.1	10.3
	1.71	1.59	75.5	732.7	10.3
	2.79	1.81	140.3	1233.4	11.4
4	0.87	4.57	110.4	383.6	28.8
	1.90	4.82	254.4	825.3	30.8
	2.87	5.18	413.0	1381.0	29.9
6	0.87	7.60	183.7	453.1	40.5
	2.16	8.41	504.6	985.1	51.2
	2.43	8.97	605.5	1656.7	36.5

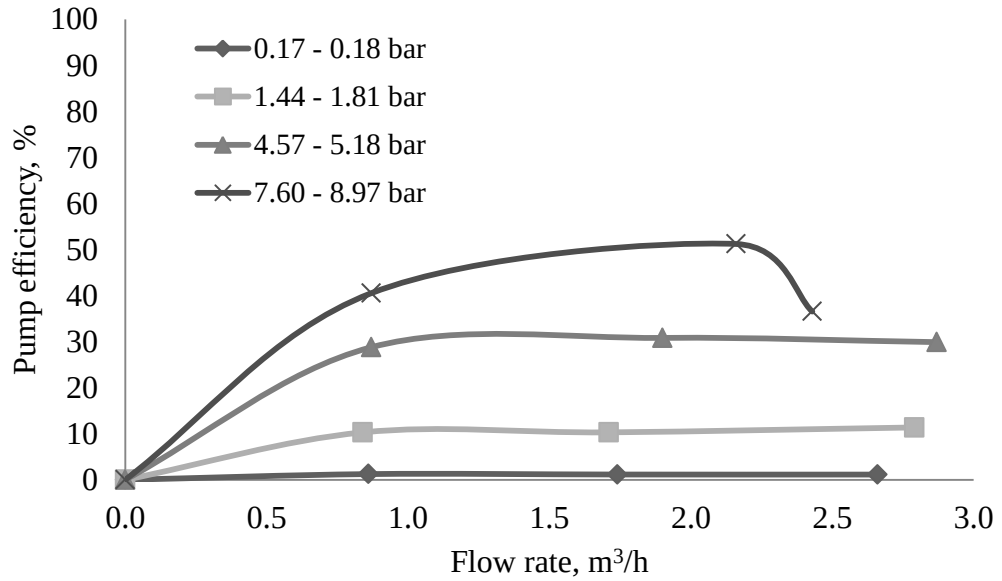

Figure 2. Power curves of 3.87 wt% CMC slurry in hose pump. Control pressures, generated by actuator, were 0.0, 2.0, 4.0, and 6.0 bar.

Table III Hose pump's electric and pump powers and pump efficiency values for 5.69 wt% CMC slurry.

Counter pressure bar	Flow rate m^3/h	Pressure difference kPa	Pump power W	Pump electric power W	Efficiency %
0	0.81	0.19	4.3	311.1	1.4
	1.71	0.21	10.0	721.6	1.4
	2.77	0.24	18.5	1186.1	1.6
2	0.82	1.17	26.7	327.1	8.1
	1.72	1.28	61.2	737.3	8.3
	2.75	1.45	110.8	1244.4	8.9
4	0.82	4.18	95.2	368.8	25.8
	1.65	4.45	204.0	833.4	24.5
	2.82	4.85	379.9	1423.1	26.7
6	0.80	7.22	160.4	440.8	36.4
	1.80	7.96	398.0	1000.4	29.8
	2.87	8.72	695.2	1622.0	42.9

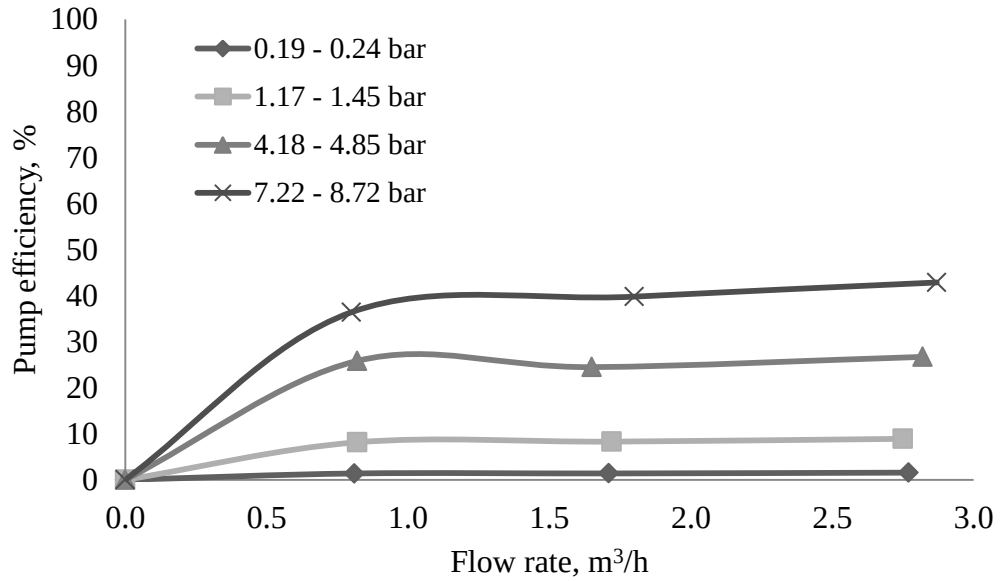

Figure 3. Power curves of 5.69 wt% CMC slurry in hose pump. Control pressures, generated by actuator, were 0.0, 2.0, 4.0, and 6.0 bar.

Table IV Hose pump's electric and pump powers and pump efficiency values for 7.59 wt% CMC slurry.

Counter pressure bar	Flow rate m^3/h	Pressure difference kPa	Pump power W	Pump electric power W	Efficiency %
0	0.82	0.22	5.0	325.2	1.5
	1.71	0.30	14.3	742.2	1.9
	2.68	0.37	27.5	1248.8	2.2
2	0.78	1.30	28.2	319.4	8.8
	1.71	1.55	73.6	765.8	9.6
	2.69	1.71	127.8	1275.3	10.0
4	0.82	3.85	87.7	366.6	23.9
	1.70	1.14	53.8	852.7	6.3
	2.67	4.44	329.3	1417.1	23.2
6	0.90	7.07	176.8	445.1	39.7
	1.66	7.73	356.4	1025.1	34.8
	2.83	8.11	637.5	1681.7	37.9

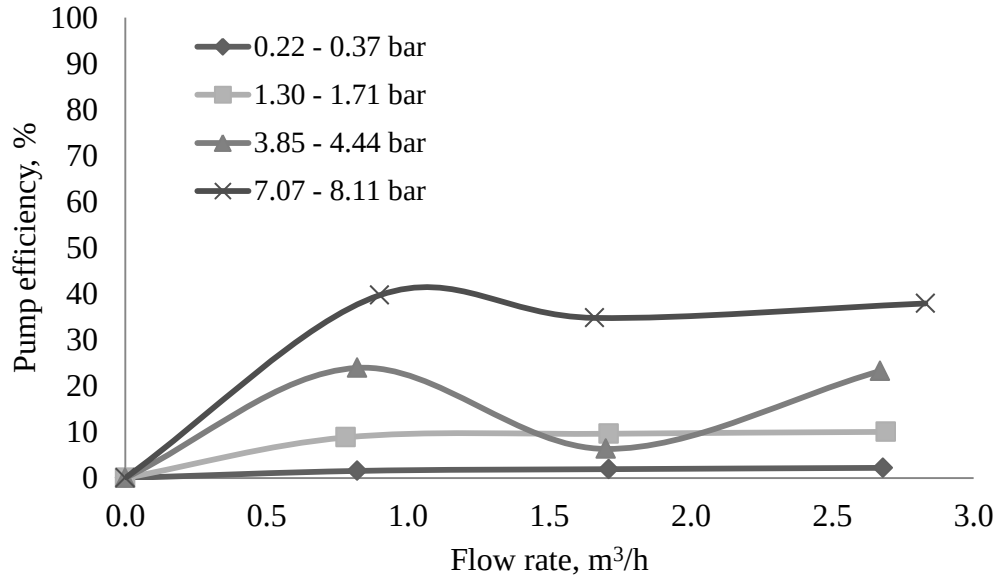

Figure 4. Power curves of 7.59 wt% CMC slurry in hose pump. Control pressures, generated by actuator, were 0.0, 2.0, 4.0, and 6.0 bar.

Table V Hose pump's electric and pump powers and pump efficiency values for 9.57 wt% CMC slurry.

Counter pressure bar	Flow rate m^3/h	Pressure difference kPa	Pump power W	Pump electric power W	Efficiency %
0	0.82	0.33	7.5	345.6	2.2
	1.59	0.49	21.6	776.5	2.8
	2.37	0.60	39.5	1273.0	3.1
2	0.79	1.17	25.7	344.1	7.5
	1.62	1.5	67.5	802.5	8.4
	2.31	1.73	111.0	1345.1	8.3
4	0.79	1.56	34.2	349.0	9.8
	1.32	2.33	85.4	818.3	10.4
	2.14	3.14	186.7	1413.6	13.2
6	0.83	2.56	59.0	358.3	16.5
	1.55	5.38	231.6	968.0	23.9
	2.34	6.39	415.4	1639.3	25.3

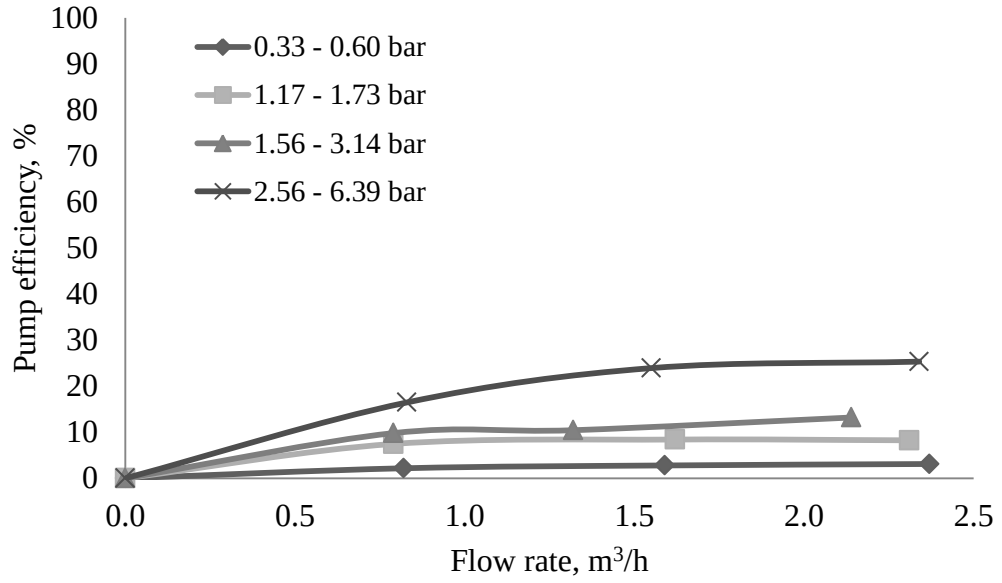

Figure 5. Power curves of 9.57 wt% CMC slurry in hose pump. Control pressures, generated by actuator, were 0.0, 2.0, 4.0, and 6.0 bar.

Table VI Hose pump's electric and pump powers and pump efficiency values for 10.99 wt% bentonite slurry.

Counter pressure bar	Flow rate m^3/h	Pressure difference kPa	Pump power W	Pump electric power W	Efficiency %
0	0.74	0.29	6.0	312.3	1.9
	1.61	0.29	13.0	693.4	1.9
	2.55	0.30	19.8	1102.6	1.8
2	0.79	2.09	45.9	334.4	13.7
	1.58	2.13	93.5	696.4	13.4
	2.55	2.11	149.5	1104.9	13.5
4	0.82	5.43	123.7	331.2	37.3
	1.64	5.53	251.9	697.5	36.1
	2.36	5.40	354.0	1090.5	32.5
6	1.11	9.03	278.4	321.5	86.6
	1.52	9.16	386.8	691.1	56.0
	1.85	9.03	464.0	1105.3	42.0

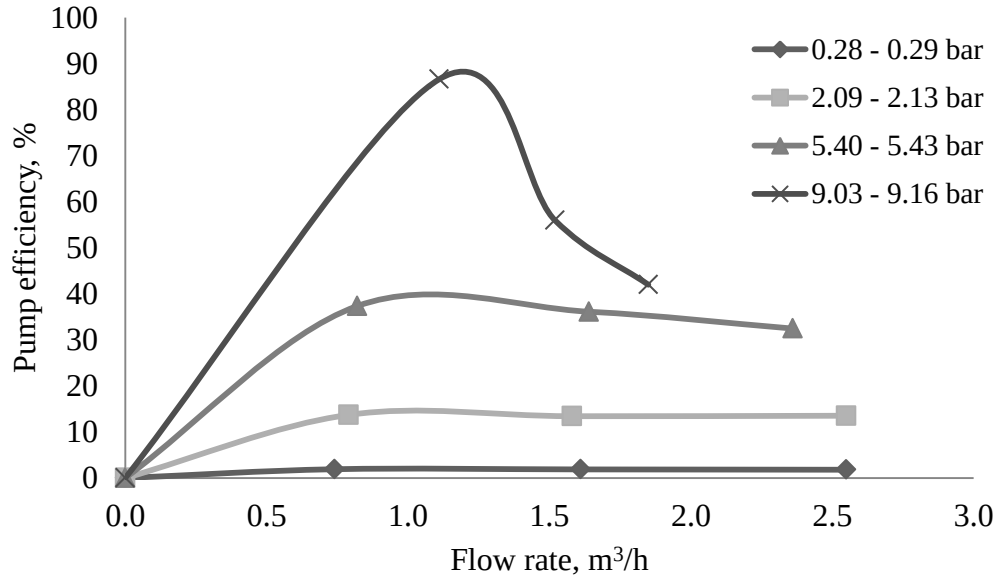

Figure 6. Power curves of 10.99 wt% bentonite slurry in hose pump. Control pressures, generated by actuator, were 0.0, 2.0, 4.0, and 6.0 bar.

Table VII Hose pump's electric and pump powers and pump efficiency values for 11.26 wt% bentonite slurry.

Counter pressure bar	Flow rate m^3/h	Pressure difference kPa	Pump power W	Pump electric power W	Efficiency %
0	-	-	-	-	-
	-	-	-	-	-
	-	-	-	-	-
2	0.82	1.37	31.2	326.6	9.6
	1.72	1.42	67.8	733.3	9.3
	2.39	1.65	109.5	1187.3	9.2
4	0.65	5.93	107.1	394.6	27.1
	1.29	5.96	213.6	877.6	24.3
	3.23	6.01	539.2	1404.7	38.4
6	1.01	9.92	278.3	544.6	51.1
	1.92	9.73	518.9	1070.2	48.5
	2.22	9.53	587.7	1675.0	35.1

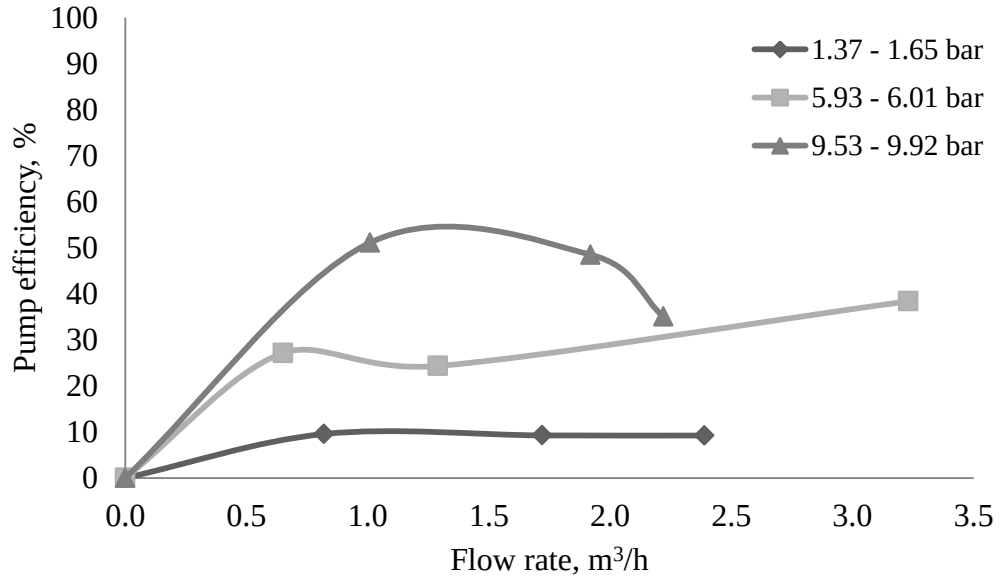

Figure 7. Power curves of 10.99 wt% bentonite slurry in hose pump. Control pressures, generated by actuator, were 0.0, 2.0, 4.0, and 6.0 bar.

Table VIII Hose pump's electric and pump powers and pump efficiency values for 15.26 wt% bentonite slurry.

Counter pressure bar	Flow rate m^3/h	Pressure difference kPa	Pump power W	Pump electric power W	Efficiency %
0	0.60	0.84	14.0	343.1	4.1
	0.52	0.77	11.1	716.4	1.6
	0.70	0.77	15.0	1164.8	1.3
2	0.22	1.43	8.7	339.5	2.6
	0.57	1.43	22.6	731.8	3.1
	0.68	1.47	27.8	1199.6	2.3
4	0.14	3.23	12.6	415.5	3.0
	0.28	2.79	29.5	882.4	3.3
	0.18	2.58	12.9	1669.8	0.8
6	-	-	-	-	-
	-	-	-	-	-
	-	-	-	-	-

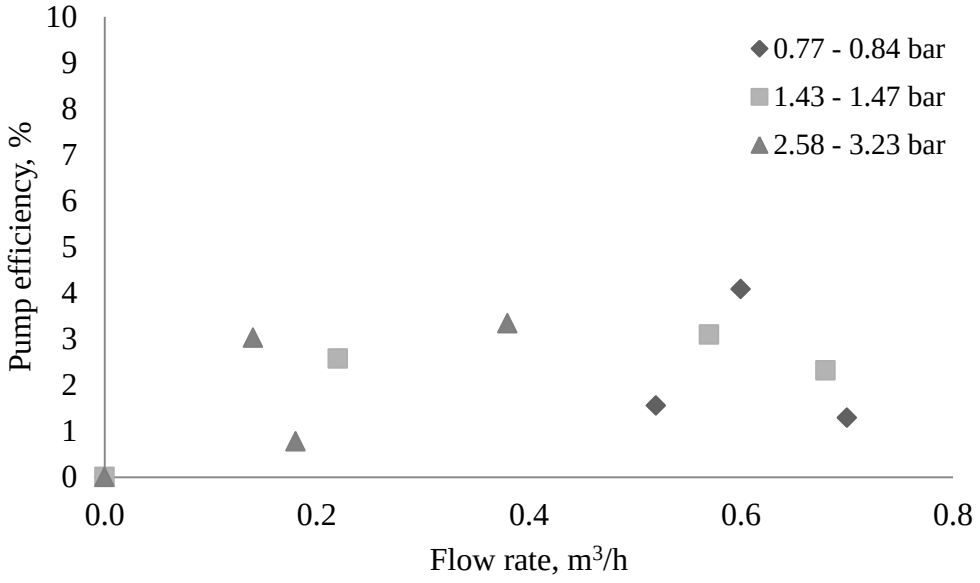

Figure 8. Power curves of 15.26 wt% bentonite slurry in hose pump. Control pressures, generated by actuator, were 0.0, 2.0, 4.0, and 6.0 bar.

Table IX Hose pump's electric and pump powers and pump efficiency values for 20.67 wt% starch slurry.

Counter pressure bar	Flow rate m^3/h	Pressure difference kPa	Pump power W	Pump electric power W	Efficiency %
0	0.82	0.17	3.9	296.1	1.3
	1.71	0.17	8.1	673.0	1.2
	2.85	0.15	11.9	1105.4	1.1
2	0.84	1.75	40.8	323.3	12.6
	1.74	1.98	95.7	711.6	13.4
	2.79	2.33	180.6	1195.4	15.1
4	0.89	4.69	115.9	381.1	30.4
	1.80	5.11	255.5	804.5	31.8
	2.57	5.52	394.1	1366.9	28.8
6	0.82	7.94	180.9	461.4	39.2
	1.92	8.19	436.8	951.0	45.9
	2.72	8.32	8.32	1565.7	40.1

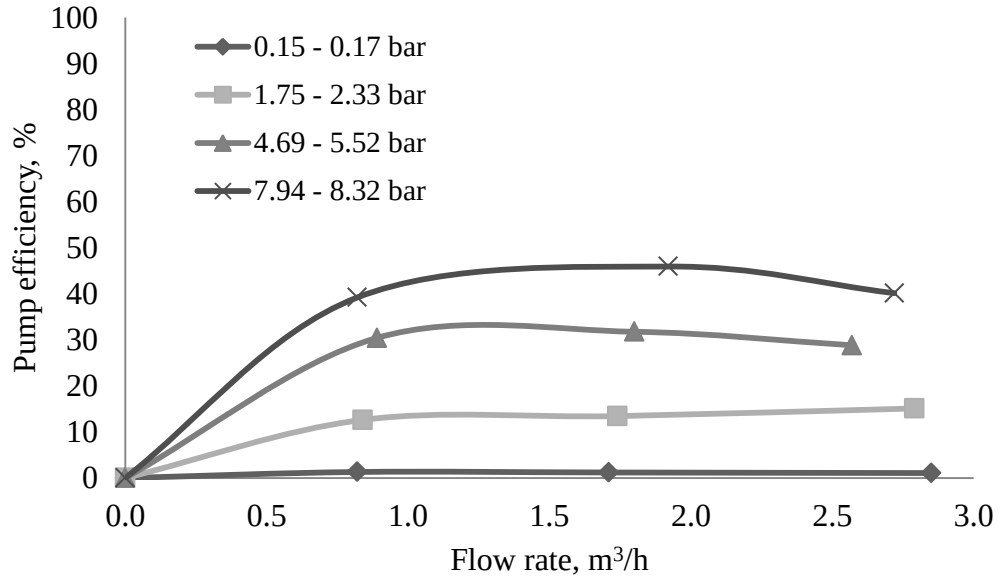

Figure 9. Power curves of 20.67 wt% starch slurry in hose pump. Control pressures, generated by actuator, were 0.0, 2.0, 4.0, and 6.0 bar.

Table X Hose pump's electric and pump powers and pump efficiency values for 28.48 wt% starch slurry

Counter pressure bar	Flow rate m^3/h	Pressure difference kPa	Pump power W	Pump electric power W	Efficiency %
0	0.85	0.18	4.3	309.6	1.4
	1.75	0.18	8.8	674.0	1.3
	2.88	0.19	15.2	1107.9	1.4
2	0.84	1.71	39.9	319.4	12.5
	1.75	1.96	95.3	702.0	13.6
	2.83	2.34	184.0	1184.2	15.5
4	0.83	4.72	108.8	365.4	29.8
	1.34	5.24	195.0	810.3	24.1
	2.98	5.56	460.2	1384.2	33.2
6	0.92	7.97	203.7	457.8	44.5
	1.80	8.32	416-0	956.3	43.5
	2.54	8.62	608.2	1573.1	38.7

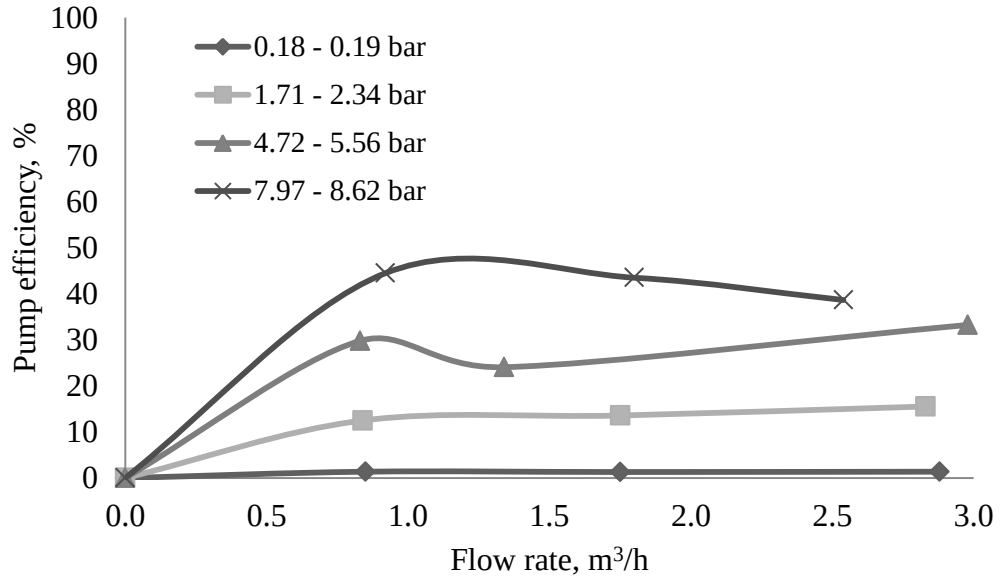

Figure 10. Power curves of 28.48 wt% starch slurry in hose pump. Control pressures, generated by actuator, were 0.0, 2.0, 4.0, and 6.0 bar.

Table XI Hose pump's electric and pump powers and pump efficiency values for 39.89 wt% starch slurry

Counter pressure bar	Flow rate m^3/h	Pressure difference kPa	Pump power W	Pump electric power W	Efficiency %
0	0.84	0.18	4.2	303.5	1.4
	1.75	0.19	9.2	677.3	1.4
	2.86	0.20	15.9	1104.1	1.4
2	0.87	1.41	34.1	322.5	10.6
	1.75	1.59	77.3	678.7	11.4
	2.92	1.83	148.4	1149.6	12.9
4	0.83	4.47	103.1	358.8	28.7
	1.76	4.92	240.5	789.9	30.5
	2.88	5.52	441.6	1323.1	33.4
6	0.85	7.39	174.5	428.8	40.7
	1.76	7.66	374.5	896.7	41.8
	2.96	8.12	667.6	1524.7	43.8

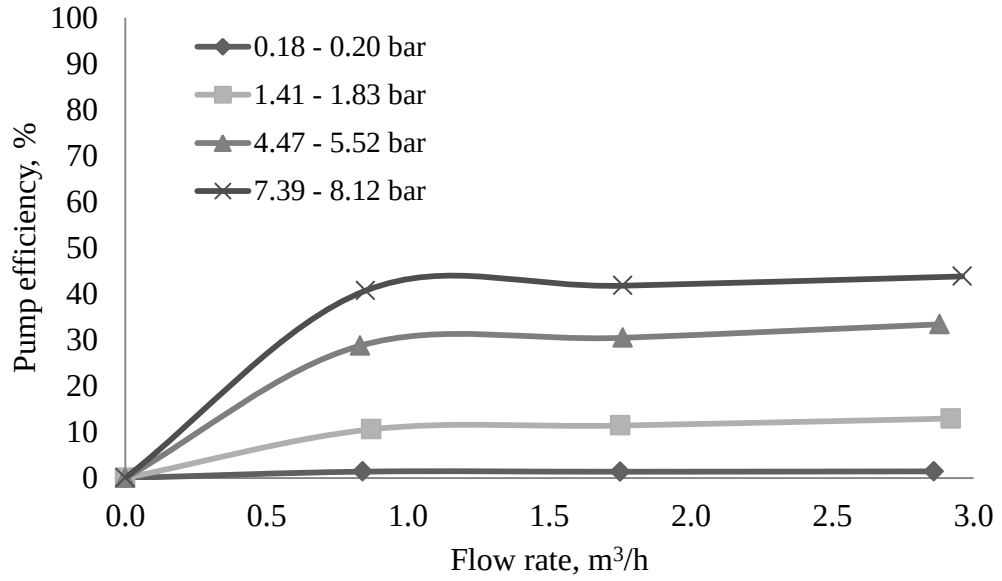

Figure 11. Power curves of 39.89 wt% starch slurry in hose pump. Control pressures, generated by actuator, were 0.0, 2.0, 4.0, and 6.0 bar.

Table XII Hose pump's electric and pump powers and pump efficiency values for 47.53 wt% starch slurry

Counter pressure bar	Flow rate m^3/h	Pressure difference kPa	Pump power W	Pump electric power W	Efficiency %
0	0.84	0.19	4.4	305.2	1.5
	1.78	0.18	8.9	670.9	1.3
	2.86	0.16	12.7	1093.3	1.2
2	0.81	1.39	31.3	301.7	10.4
	1.81	1.49	74.9	698.2	10.7
	1.83	1.58	124.2	1145.4	10.8
4	0.86	3.70	88.4	350.2	25.2
	1.79	4.22	209.8	772.6	27.2
	2.94	4.62	377.3	1286.1	29.3
6	0.88	6.82	166.7	414.7	40.2
	1.55	7.27	313.0	885.2	35.4
	2.84	7.89	622.4	1485.8	41.9

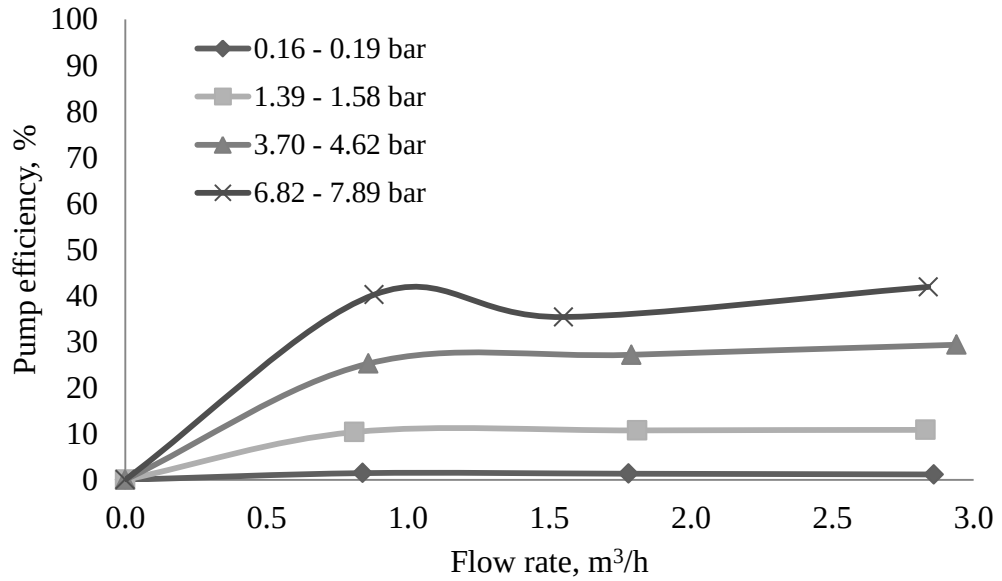

Figure 12. Power curves of 47.53 wt% starch slurry in hose pump. Control pressures, generated by actuator, were 0.0, 2.0, 4.0, and 6.0 bar.

Table XIII Hose pump's electric and pump powers and pump efficiency values for 49.29 wt% starch slurry

Counter pressure bar	Flow rate m^3/h	Pressure difference kPa	Pump power W	Pump electric power W	Efficiency %
0	0.83	0.19	4.4	494.6	0.9
	1.75	0.20	9.7	1021.4	1.0
	2.49	0.21	14.5	1658.8	0.9
2	0.83	2.14	49.3	324.4	15.2
	1.76	2.15	105.1	727.4	14.5
	2.43	2.09	141.1	1230.4	11.5
4	0.80	7.00	155.1	406.8	38.1
	1.79	6.60	328.2	874.1	37.5
	2.64	6.30	459.8	1445.1	31.8
6	0.80	9.85	218.9	305.7	71.6
	1.53	9.74	414.0	684.9	60.4
	2.13	9.05	535.5	1160.0	46.1

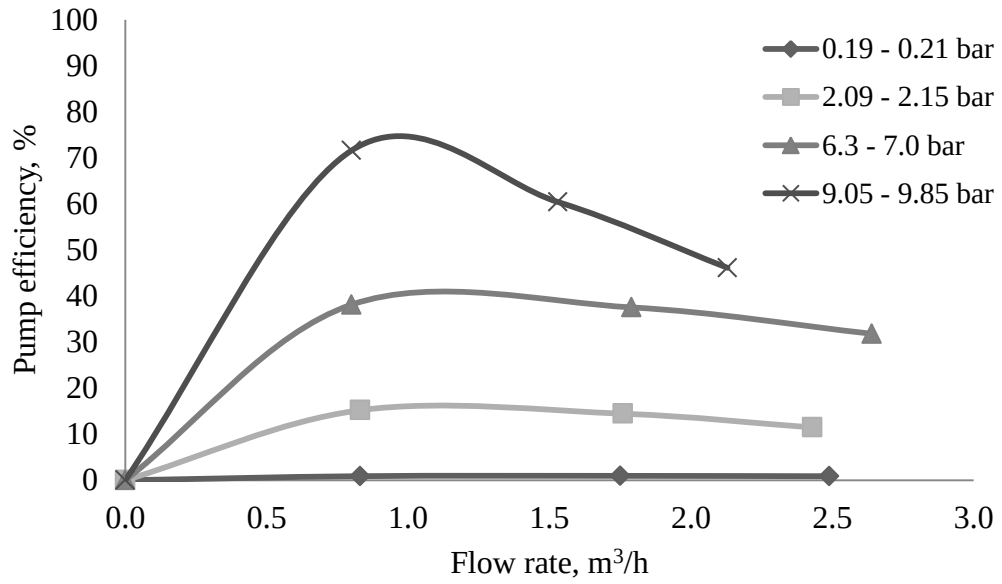

Figure 13. Power curves of 49.29 wt% starch slurry in hose pump. Control pressures, generated by actuator, were 0.0, 2.0, 4.0, and 6.0 bar.

Table I Progressive cavity pump's electric and pump powers and pump efficiency values for 6.11 wt% CMC slurry.

Counter pressure bar	Flow rate m^3/h	Pressure difference kPa	Pump power W	Pump electric power W	Efficiency %
0	1.97	76.0	57.6	340.4	16.9
	4.17	83.0	133.1	728.5	18.3
	6.85	90.0	237.1	1197.8	19.8
2	1.97	194.0	106.2	381.1	27.9
	4.30	214.0	255.6	804.3	31.8
	6.75	251.0	470.6	1319.8	35.7
4	1.65	523.0	239.7	491.1	48.8
	3.88	585.0	630.5	1053.3	69.9
	6.27	693.0	1207.0	1796.5	67.1
6	1.08	932.0	279.6	714.4	39.1
	3.20	107.0	951.1	1538.5	61.8
	5.62	115.0	1795.3	2516.5	71.3

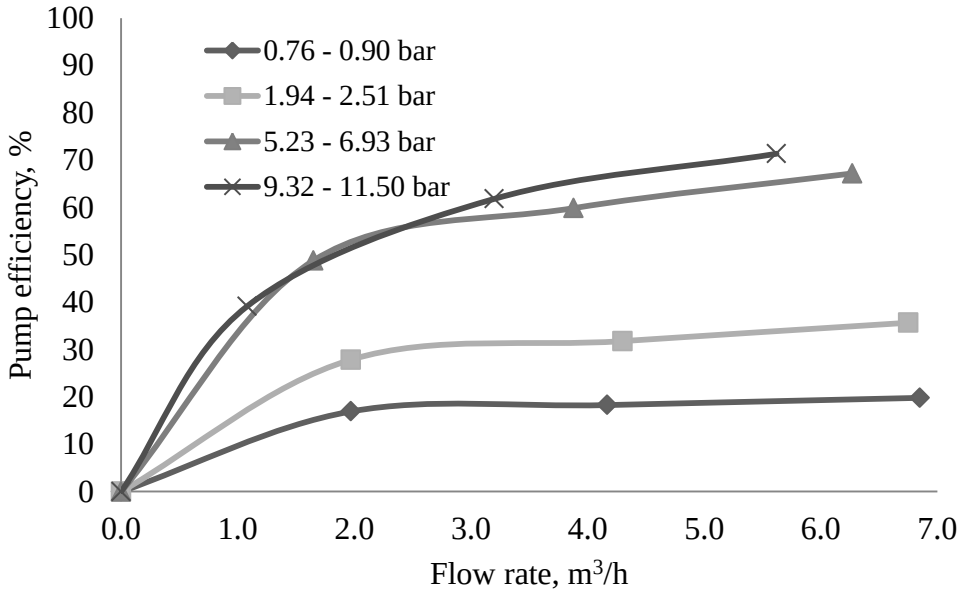

Figure 1. Power curves of 6.11 wt% CMC slurry in progressive cavity pump. Control pressures, generated by actuator, were 0.0, 2.0, 4.0, and 6.0 bar.

Table II Progressive cavity pump's electric and pump powers and pump efficiency values for 5.27 wt% CMC slurry.

Counter pressure bar	Flow rate m^3/h	Pressure difference kPa	Pump power W	Pump electric power W	Efficiency %
0	2.02	0.69	53.6	350.7	15.3
	4.33	0.73	121.6	732.7	16.6
	6.90	0.80	212.3	1172.8	18.10
2	1.96	2.06	112.2	388.1	28.9
	4.26	2.48	293.5	827.4	35.5
	6.75	2.99	560.6	1382.1	40.6
4	1.54	5.56	237.8	515.5	46.14
	3.75	6.52	679.2	1120.1	60.63
	6.24	7.10	1230.7	1806.2	68.14
6	0.83	10.87	250.6	842.8	29.7
	3.10	11.33	975.6	1514.9	64.4
	5.58	11.95	1852.3	2553.5	72.5

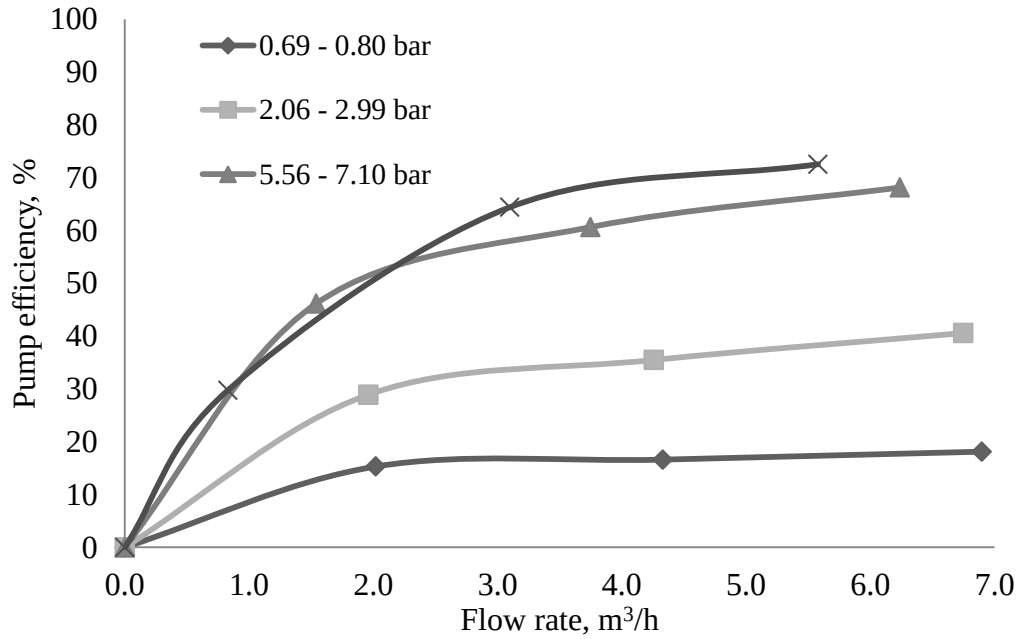

Figure 2. Power curves of 5.27 wt% CMC slurry in progressive cavity pump. Control pressures, generated by actuator, were 0.0, 2.0, 4.0, and 6.0 bar.

Table III Progressive cavity pump's electric and pump powers and pump efficiency values for 4.55 wt% CMC slurry.

Counter pressure bar	Flow rate m^3/h	Pressure difference kPa	Pump power W	Pump electric power W	Efficiency %
0	1.96	0.71	53.5	340.4	15.7
	4.31	0.71	117.7	727.7	16.2
	6.95	0.75	200.5	1175.6	17.1
2	1.85	2.12	108.9	381.2	28.6
	4.13	2.57	294.8	810.6	36.4
	6.76	3.16	593.4	1390.5	42.7
4	1.45	5.70	229.6	530.6	43.3
	3.68	6.66	680.8	1123.2	60.6
	6.25	7.36	1277.8	1833.6	69.7
6	0.92	9.41	240.5	735.3	32.7
	3.06	10.97	932.5	1570.2	59.4
	5.39	11.75	1259.2	2175.0	71.1

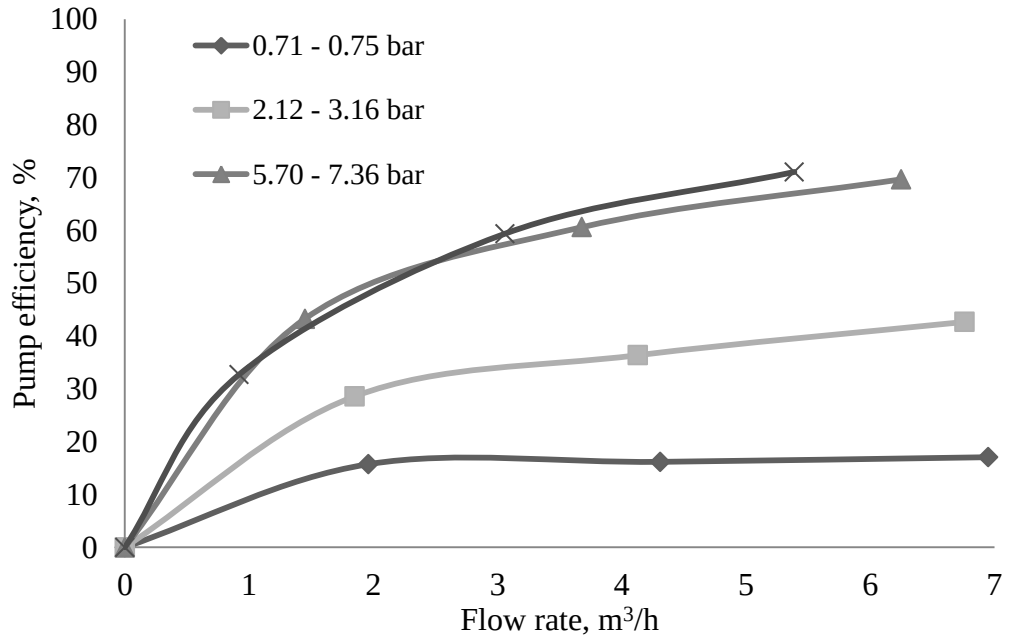

Figure 3. Pressure curves of 4.55 wt% CMC slurry in progressive cavity pump. Control pressures, generated by actuator, were 0.0, 2.0, 4.0, and 6.0 bar.

Table IV Progressive cavity pump's electric and pump powers and pump efficiency values for 3.67 wt% CMC slurry.

Counter pressure bar	Flow rate m^3/h	Pressure difference kPa	Pump power W	Pump electric power W	Efficiency %
0	2.00	0.69	53.1	353.4	15.0
	4.41	0.70	118.7	742.1	16.0
	7.05	0.72	195.2	1164.3	16.8
2	1.89	2.21	116.0	392.7	29.6
	4.10	2.73	310.9	826.2	37.6
	6.64	3.24	597.6	1364.1	43.8
4	1.36	5.22	197.2	500.0	39.4
	3.60	6.48	648.0	1112.4	58.3
	6.23	7.37	1275.4	1822.4	70.0
6	0.65	10.13	182.9	787.6	23.2
	2.88	11.46	916.8	1645.9	55.7
	5.41	12.10	1818.4	2534.6	71.7

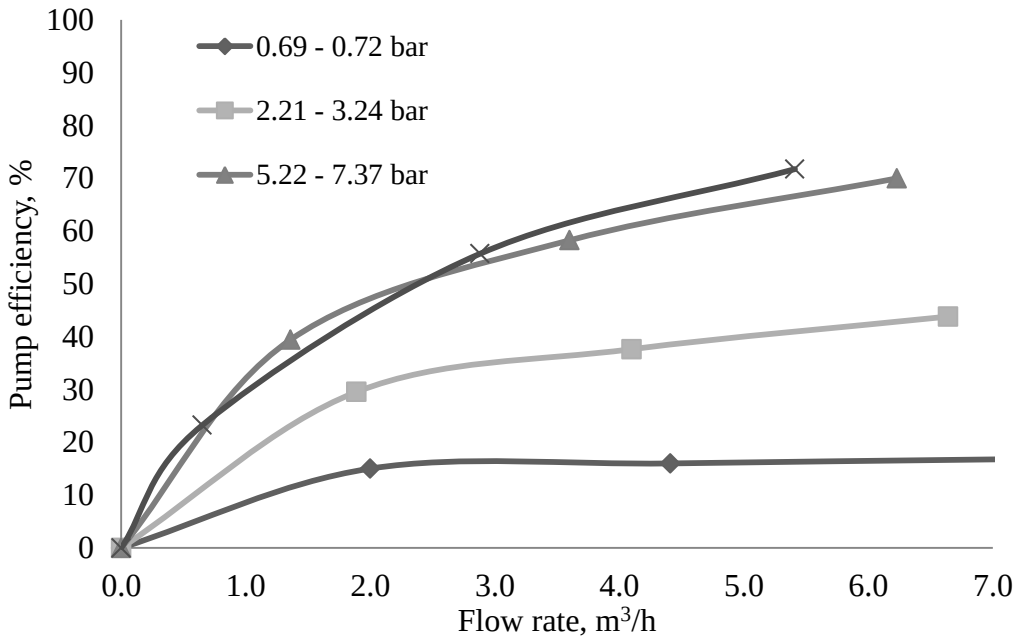

Figure 4. Power curves of 3.67 wt% CMC slurry in progressive cavity pump. Control pressures, generated by actuator, were 0.0, 2.0, 4.0, and 6.0 bar.

Table V Progressive cavity pump's electric and pump powers and pump efficiency values for 16.48 wt% starch slurry.

Counter pressure bar	Flow rate m^3/h	Pressure difference kPa	Pump power W	Pump electric power W	Efficiency %
0	2.06	0.65	37.2	407.3	9.1
	4.36	0.64	77.5	779.3	10.0
	6.95	0.66	127.4	1190.0	10.7
2	1.42	2.61	103.0	475.7	21.6
	3.70	3.24	333.0	951.1	35.0
	6.15	3.59	613.3	1436.5	42.7
4	0.96	5.90	157.3	623.6	25.2
	3.21	7.25	646.5	1276.0	50.7
	5.85	7.79	1265.9	1984.8	63.8
6	0.59	9.17	150.3	843.1	17.8
	2.57	11.21	800.3	1720.8	46.5
	5.07	11.90	1675.9	2617.4	64.0

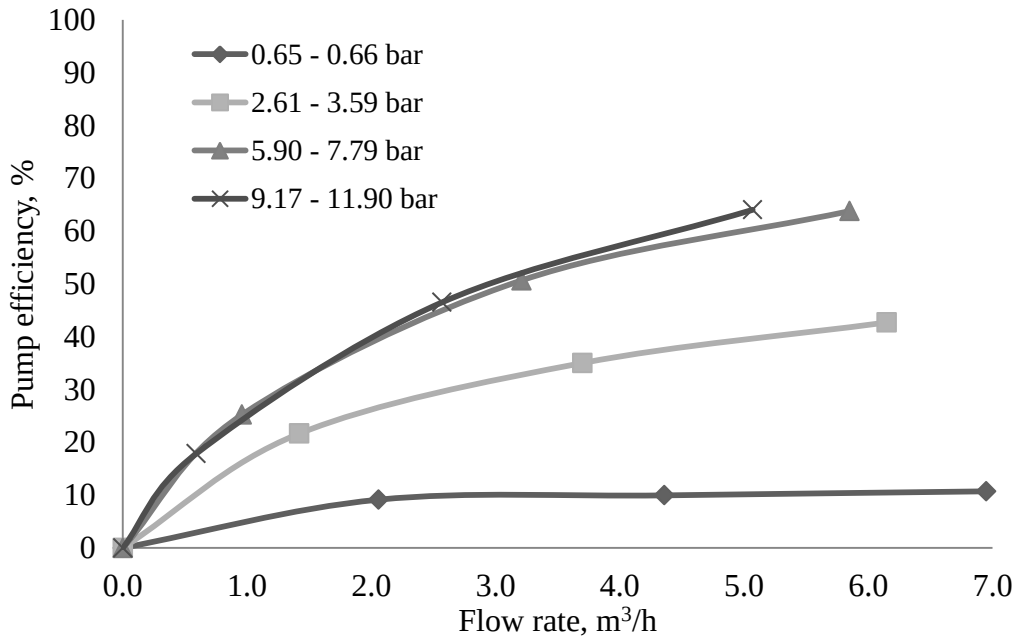

Figure 5. Power curves of 16.48 wt% starch slurry in progressive cavity pump. Control pressures, generated by actuator, were 0.0, 2.0, 4.0, and 6.0 bar..

Table VI Progressive cavity pump's electric and pump powers and pump efficiency values for 28.44 wt% starch slurry.

Counter pressure bar	Flow rate m^3/h	Pressure difference kPa	Pump power W	Pump electric power W	Efficiency %
0	2.09	0.62	36.0	405.0	8.89
	4.41	0.61	74.7	771.2	9.69
	6.92	0.63	121.1	1189.7	10.18
2	1.54	2.33	99.7	461.4	21.6
	3.84	2.96	315.7	913.5	34.6
	6.49	3.05	549.8	1400.2	39.3
4	1.17	6.51	211.6	684.5	30.9
	3.37	6.92	647.8	1244.2	52.1
	5.94	7.42	1224.3	1912.0	64.0
6	0.53	10.14	149.3	928.8	16.1
	2.88	10.80	864.0	1688.9	51.2
	5.30	11.74	1728.4	2593.2	66.7

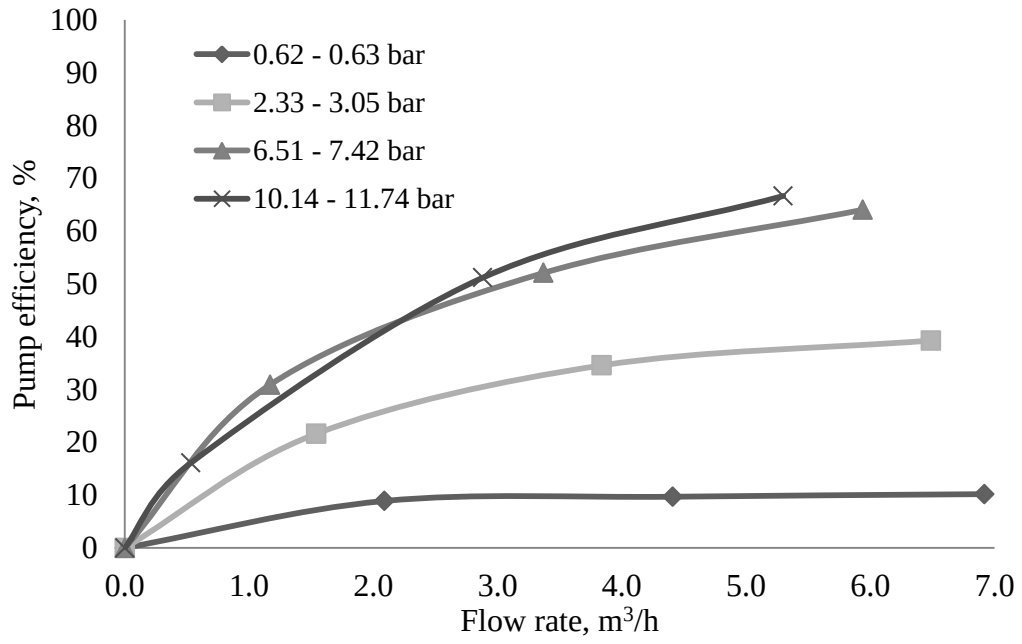

Figure 6. Power curves of 28.44 wt% starch slurry in progressive cavity pump. Control pressures, generated by actuator, were 0.0, 2.0, 4.0, and 6.0 bar.

Table VII Progressive cavity pump's electric and pump powers and pump efficiency values for 36.69 wt% starch slurry.

Counter pressure bar	Flow rate m^3/h	Pressure difference kPa	Pump power W	Pump electric power W	Efficiency %
0	2.03	0.68	38.3	412.0	9.3
	4.45	0.66	81.6	773.6	10.6
	6.89	0.65	124.4	1189.4	10.5
2	1.59	2.25	99.4	438.8	22.7
	4.00	2.87	318.9	922.0	34.6
	6.60	2.88	528.0	1386.6	38.1
4	1.27	5.77	203.6	615.4	33.1
	3.53	6.98	684.4	1251.1	54.7
	6.07	7.66	1291.6	1929.7	66.9
6	0.88	8.99	219.8	821.6	26.8
	2.90	11.30	910.3	1707.2	53.3
	5.41	11.81	1774.8	2588.4	68.6

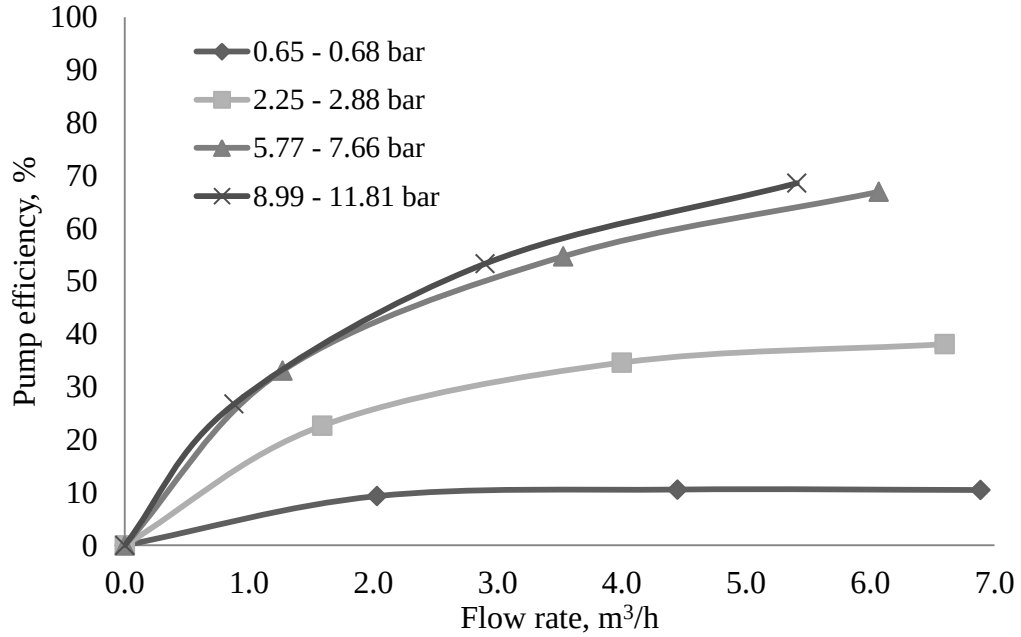

Figure 7. Power curves of 36.69 wt% starch slurry in progressive cavity pump. Control pressures, generated by actuator, were 0.0, 2.0, 4.0, and 6.0 bar..

Table VIII Progressive cavity pump's electric and pump powers and pump efficiency values for 40.28 wt% starch slurry.

Counter pressure bar	Flow rate m^3/h	Pressure difference kPa	Pump power W	Pump electric power W	Efficiency %
0	2.10	0.62	36.2	390.3	9.3
	3.84	0.61	65.1	762.9	8.5
	7.02	0.64	124.8	1182.7	10.6
2	1.79	2.31	114.9	464.9	24.7
	4.06	2.97	335.0	920.5	36.4
	6.67	3.12	578.1	1418.7	40.8
4	1.35	6.06	227.3	637.7	35.6
	3.56	6.90	682.3	1229.7	55.5
	6.21	7.30	1259.3	1903.9	66.1
6	0.93	9.47	244.6	858.5	28.5
	2.99	11.20	930.2	1689.2	55.1
	5.58	11.75	1821.3	2560.7	71.1

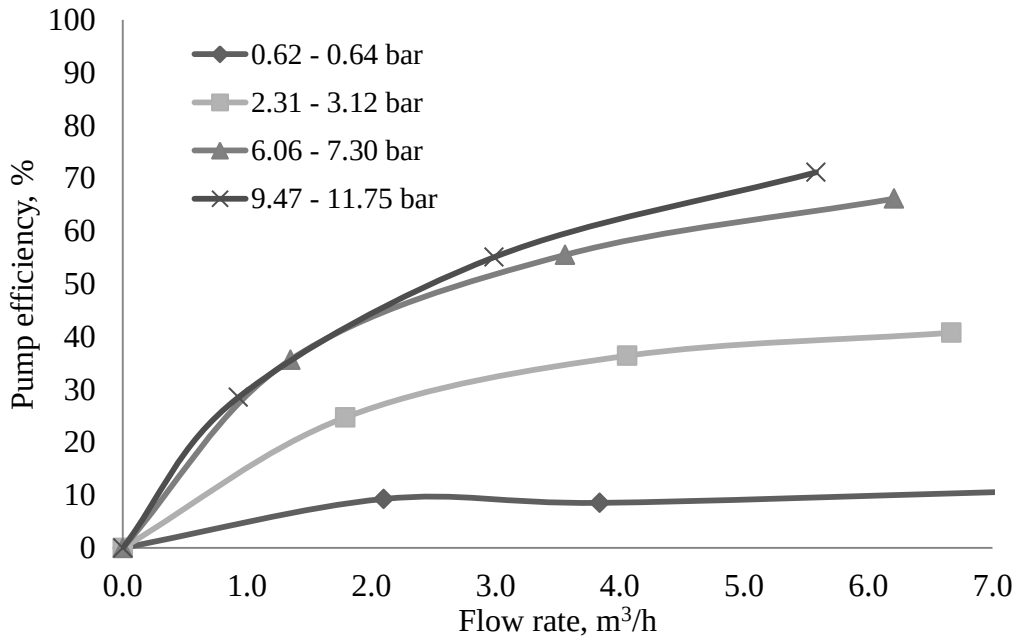

Figure 8. Power curves of 40.28 wt% CMC slurry in progressive cavity pump. Control pressures, generated by actuator, were 0.0, 2.0, 4.0, and 6.0 bar.

Table IX Progressive cavity pump's electric and pump powers and pump efficiency values for 44.38 wt% starch slurry.

Counter pressure bar	Flow rate m^3/h	Pressure difference kPa	Pump power W	Pump electric power W	Efficiency %
0	2.17	0.67	40.4	412.7	9.8
	4.32	0.66	79.2	770.2	10.3
	6.90	0.67	128.4	1200.2	10.7
2	1.86	2.21	114.2	445.7	25.6
	4.20	2.62	305.7	900.1	34.0
	6.67	3.21	594.7	1427.5	41.7
4	1.54	5.36	229.3	582.3	39.4
	3.80	6.61	697.7	1215.8	57.4
	6.32	7.55	1325.4	1952.0	67.9
6	1.09	9.72	294.3	860.9	34.2
	3.30	10.80	990.0	1668.0	59.4
	5.72	11.52	1830.4	2544.4	71.9

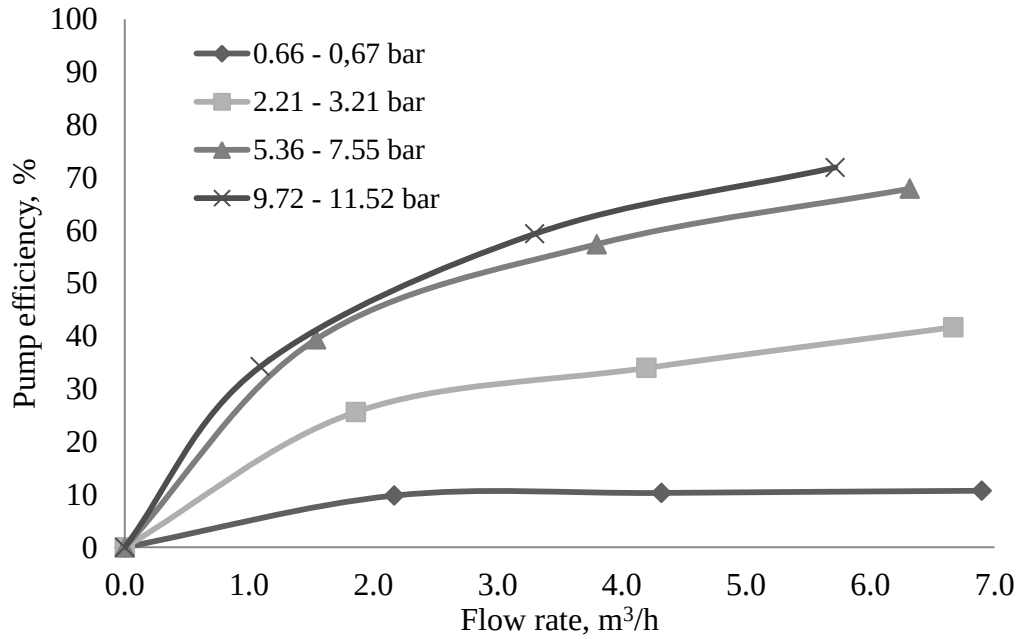

Figure 9. Power curve of 44.38 wt% starch slurry in progressive cavity pump. Control pressures, generated by actuator, were 0.0, 2.0, 4.0, and 6.0 bar.

Table I Values for CMC slurries' discharge pressure calculations in hose pump experiments. Pipe length was 3.80 m and diameter was 68.9 mm. Total minor loss coefficient was 0.60.

Density	Flow	Viscosity	Reynold's number	Friction factor	Friction losses	Minor losses	Suction pressure	Discharge pressure
kg/m^3	m/s	Pa·s	-	-	Pa	Pa	bar	bar
1013	0.062	0.02578	168	0.38	40.90	1.17	0.16	0.16
1013	0.132	0.02555	362	0.18	86.04	5.29	0.17	0.17
1013	0.216	0.02540	594	0.11	140.41	14.18	0.20	0.20
1013	0.062	0.02578	168	0.38	40.90	1.17	1.26	1.26
1013	0.132	0.02555	360	0.18	86.52	5.29	1.57	1.57
1013	0.211	0.02541	579	0.11	137.46	13.53	1.77	1.77
1013	0.065	0.02577	175	0.37	43.16	1.28	4.36	4.36
1013	0.126	0.02557	345	0.19	82.26	4.82	5.10	5.10
1013	0.211	0.02541	578	0.11	137.69	13.53	5.40	5.40
1013	0.062	0.02579	167	0.38	41.15	1.17	7.76	7.76
1013	0.120	0.02560	329	0.19	78.24	4.38	8.49	8.49
1013	0.193	0.02544	529	0.12	125.88	11.32	8.64	8.65
1023	0.064	0.15540	29	2.21	255.06	1.26	0.17	0.17
1023	0.130	0.15061	61	1.05	500.30	5.19	0.17	0.17
1023	0.198	0.14785	94	0.68	753.14	12.03	0.17	0.18
1023	0.063	0.15551	28	2.29	255.98	1.22	1.43	1.44
1023	0.128	0.15072	60	1.07	493.11	5.03	1.58	1.59
1023	0.208	0.14753	99	0.65	789.16	13.28	1.80	1.81
1023	0.064	0.15529	29	2.21	255.06	1.26	4.57	4.57
1023	0.142	0.15004	67	0.96	543.47	6.19	4.82	4.82
1023	0.214	0.14735	102	0.63	810.78	14.06	5.17	5.18
1023	0.065	0.15538	30	2.13	254.32	1.30	7.60	7.60
1023	0.161	0.14939	76	0.84	615.90	7.96	8.40	8.41
1023	0.181	0.14855	86	0.74	687.91	10.06	8.96	8.97
1034	0.060	0.65821	7	9.14	938.69	1.12	0.18	0.19
1034	0.128	0.60806	15	4.27	1993.64	5.08	0.19	0.21
1034	0.207	0.57813	25	2.56	3128.38	13.29	0.21	0.24

1034	0.061	0.65681	7	9.14	970.24	1.15	1.16	1.17
1034	0.128	0.60784	15	4.27	1993.64	5.08	1.26	1.28
1034	0.205	0.57869	25	2.56	3068.22	13.04	1.42	1.45
1034	0.061	0.65739	7	9.14	970.24	1.15	4.17	4.18
1034	0.123	0.61081	14	4.57	1972.43	4.69	4.43	4.45
1034	0.210	0.57722	26	2.46	3095.88	13.68	4.81	4.85
1034	0.060	0.65977	6	10.67	1095.14	1.12	7.21	7.22
1034	0.134	0.60537	16	4.00	2048.37	5.57	7.94	7.96
1034	0.214	0.57931	26	2.46	3214.94	14.21	8.69	8.72
1046	0.061	2.12439	2	32.00	3432.95	1.17	0.19	0.22
1046	0.128	1.84702	5	12.80	6046.28	5.14	0.24	0.30
1046	0.200	1.69629	8	8.00	9225.89	12.55	0.28	0.37
1046	0.058	2.14029	2	32.00	3103.59	1.06	1.26	1.30
1046	0.128	1.84643	5	12.80	6046.28	5.14	1.49	1.55
1046	0.200	1.69571	9	7.11	8200.79	12.55	1.63	1.71
1046	0.061	2.12233	2	32.00	3432.95	1.17	3.82	3.85
1046	0.126	1.84987	5	12.80	5858.81	4.98	4.08	4.14
1046	0.199	1.69963	8	8.00	9133.86	12.42	4.35	4.44
1046	0.067	2.08697	2	32.00	4141.50	1.41	7.03	7.07
1046	0.124	1.86053	5	12.80	5674.29	4.82	7.67	7.73
1046	0.211	1.68624	9	7.11	9127.69	13.96	8.02	8.11
1057	0.061	6.11760	1	64.00	6944.06	1.18	0.26	0.33
1057	0.119	5.05332	2	32.00	13213.49	4.49	0.36	0.49
1057	0.176	4.50740	3	21.33	19268.94	9.83	0.41	0.60
1057	0.059	6.18715	1	64.00	6496.17	1.10	1.10	1.17
1057	0.120	5.03088	2	32.00	13436.50	4.57	1.37	1.50
1057	0.172	4.53689	3	21.33	18403.03	9.38	1.54	1.73
1057	0.059	6.17862	1	64.00	6496.17	1.10	1.49	1.55
1057	0.117	5.07807	2	32.00	12773.07	4.34	2.21	2.33
1057	0.170	4.55689	3	21.33	17977.54	9.17	2.96	3.14
1057	0.056	6.26952	1	64.00	5852.34	0.99	2.50	2.56
1057	0.116	5.09364	2	32.00	12555.66	4.27	5.26	5.38
1057	0.169	4.58008	3	21.33	17766.66	9.06	6.22	6.39

Table II Values for starch slurries' discharge pressure calculations in hose pump experiments. Pipe length was 3.80 m and diameter was 68.9 mm. Total minor loss coefficient was 0.60.

Density	Flow	Viscosity	Reynold's number	Friction factor	Friction losses	Minor losses	Suction pressure	Discharge pressure
kg/m3	m/s	Pa·s	-	-	Pa	Pa	bar	bar
1103	0.061	0.00127	3653	0.04	4.61	1.23	0.17	0.17
1103	0.128	0.00134	7247	0.03	17.10	5.42	0.17	0.17
1103	0.213	0.00139	11643	0.03	42.05	15.02	0.15	0.15
1103	0.063	0.00127	3763	0.04	4.88	1.31	1.75	1.75
1103	0.130	0.00134	7375	0.03	17.56	5.59	1.98	1.98
1103	0.208	0.00139	11390	0.03	40.32	14.32	2.33	2.33
1103	0.067	0.00128	3970	0.04	5.44	1.49	4.69	4.69
1103	0.134	0.00134	7597	0.03	18.52	5.94	5.11	5.11
1103	0.192	0.00138	10588	0.03	34.99	12.20	5.52	5.52
1103	0.061	0.00127	3663	0.04	4.60	1.23	7.94	7.94
1103	0.143	0.00134	8114	0.03	20.74	6.77	8.19	8.19
1103	0.202	0.00138	11153	0.03	38.23	13.51	8.32	8.32
1142	0.063	0.00341	1461	0.04	5.48	1.36	0.18	0.18
1142	0.130	0.00341	3005	0.04	22.75	5.79	0.18	0.18
1142	0.215	0.00341	4953	0.04	54.92	15.84	0.19	0.19
1142	0.062	0.00341	1440	0.04	5.38	1.32	1.71	1.71
1142	0.130	0.00341	3011	0.04	22.74	5.79	1.96	1.96
1142	0.211	0.00341	4860	0.04	53.15	15.26	2.34	2.34
1142	0.062	0.00341	1428	0.04	5.43	1.32	4.72	4.72
1142	0.100	0.00341	2300	0.03	8.77	3.43	5.24	5.24
1142	0.222	0.00341	5121	0.04	58.07	16.89	5.56	5.56
1142	0.069	0.00341	1585	0.04	6.06	1.63	7.97	7.97
1142	0.134	0.00341	3091	0.04	24.00	6.15	8.32	8.32
1142	0.189	0.00341	4361	0.04	43.81	12.24	8.62	8.62
1200	0.062	0.00939	548	0.12	14.85	1.38	0.18	0.18
1200	0.130	0.00918	1173	0.05	30.50	6.08	0.19	0.19
1200	0.213	0.00903	1948	0.03	49.30	16.33	0.20	0.20
1200	0.065	0.00938	572	0.11	15.64	1.52	1.41	1.41

1200	0.130	0.00918	1174	0.05	30.47	6.08	1.59	1.59
1200	0.218	0.00903	1993	0.03	50.48	17.10	1.82	1.82
1200	0.062	0.00940	546	0.12	14.90	1.38	4.47	4.47
1200	0.131	0.00918	1178	0.05	30.84	6.18	4.92	4.92
1200	0.215	0.00903	1963	0.03	49.85	16.63	5.52	5.52
1200	0.063	0.00939	554	0.12	15.17	1.43	7.39	7.39
1200	0.131	0.00919	1182	0.05	30.74	6.18	7.66	7.66
1200	0.221	0.00903	2019	0.03	51.21	17.58	8.12	8.12
1238	0.062	0.02041	260	0.25	32.30	1.43	0.19	0.19
1238	0.133	0.02073	546	0.12	70.77	6.57	0.18	0.18
1238	0.213	0.02093	868	0.07	114.17	16.85	0.16	0.16
1238	0.061	0.02040	254	0.25	32.00	1.38	1.39	1.39
1238	0.135	0.02074	554	0.12	71.86	6.77	1.49	1.49
1238	0.211	0.02093	858	0.07	113.35	16.53	1.58	1.58
1238	0.064	0.02042	266	0.24	33.64	1.52	3.70	3.70
1238	0.133	0.02073	548	0.12	70.51	6.57	4.22	4.22
1238	0.219	0.02094	892	0.07	117.45	17.81	4.63	4.63
1238	0.065	0.02043	272	0.24	33.93	1.57	6.82	6.82
1238	0.116	0.02066	478	0.13	61.49	5.00	7.27	7.27
1238	0.211	0.02930	862	0.07	112.82	16.53	7.89	7.89
1247	0.062	0.00617	857	0.07	9.87	1.44	0.19	0.19
1247	0.130	0.01233	907	0.07	40.99	6.32	0.20	0.20
1247	0.185	0.01709	931	0.07	80.87	12.80	0.21	0.21
1247	0.062	0.00621	858	0.07	9.86	1.44	2.14	2.14
1247	0.131	0.01244	907	0.07	41.62	6.42	2.15	2.15
1247	0.181	0.01672	930	0.07	77.50	12.25	2.09	2.09
1247	0.060	0.00598	856	0.07	9.25	1.35	6.98	6.98
1247	0.133	0.01259	908	0.07	42.86	6.61	6.60	6.60
1247	0.197	0.01805	935	0.07	91.31	14.51	6.27	6.27
1247	0.059	0.00594	858	0.07	8.93	1.30	9.85	9.85
1247	0.114	0.01089	900	0.07	31.77	4.86	9.74	9.74
1247	0.159	0.01478	922	0.07	60.32	9.45	9.05	9.05

Table III Values for bentonite slurries' discharge pressure calculations in hose pump experiments. Pipe length was 3.80 m and diameter was 68.9 mm. Total minor loss coefficient was 0.60.

Density	Flow	Flow	Viscosity	Δp	Reynold's number	Friction factor	Friction losses	Minor losses	Suction pressure	Discharge pressure
kg/m^3	m^3/h	m/s	Pa·s	Pa	-	-	Pa	Pa	bar	bar
1165	0.74	0.055	3.61681	5900	1	52.44	5095.45	2.41	0.24	0.29
1165	1.61	0.120	1.57341	5600	6	10.46	4288.58	4.46	0.25	0.29
1165	2.55	0.190	0.79854	4500	19	3.35	2050.19	6.66	0.26	0.28
1165	0.79	0.059	3.31445	5800	1	44.80	5009.09	1.22	2.04	2.09
1165	1.58	0.118	1.60008	5600	6	10.81	4836.36	4.87	2.08	2.13
1165	2.55	0.190	0.90501	5100	17	3.80	4404.55	12.62	2.07	2.11
1165	0.82	0.061	1.98980	3600	2	26.01	3109.09	1.30	5.40	5.43
1165	1.64	0.122	0.85672	3100	11	5.60	2677.27	5.20	5.50	5.53
1165	2.36	0.176	3.44823	18000	4	15.62	15545.45	10.83	5.25	5.40
1165	1.11	0.083	2.23419	5500	3	21.46	4750.00	2.41	8.99	9.03
1165	1.52	0.113	0.47739	1600	19	3.37	1381.82	4.46	9.15	9.16
1165	1.85	0.138	-0.21989	-900	-50	-1.27	-777.27	6.66	9.04	9.03
1169	0.91	0.068	3.32202	6700	2	38.82	5786.36	1.62	0.22	0.28
1169	1.54	0.115	1.90569	6500	5	13.17	5613.64	4.64	0.23	0.28
1169	2.93	0.218	0.61864	4000	28	2.26	3454.55	16.67	0.27	0.30
1169	0.70	0.052	4.08482	6300	1	62.42	5440.91	0.95	1.32	1.37
1169	1.40	0.104	2.33418	7200	4	17.84	6218.18	3.79	1.36	1.42
1169	2.93	0.218	0.78877	5100	22	2.88	4404.55	16.67	1.60	1.65
1169	0.64	0.048	2.31797	3300	2	38.38	2850.00	0.81	5.90	5.93
1169	1.28	0.095	1.34864	3800	6	11.28	3281.82	3.16	5.93	5.96
1169	3.22	0.240	1.29245	9200	15	4.28	7945.45	20.20	5.93	6.01
1169	1.01	0.075	3.86610	8600	2	40.96	7427.27	1.97	9.84	9.92
1169	1.92	0.143	1.57970	6700	7	8.78	5786.36	7.17	9.67	9.73
1169	2.23	0.166	1.50300	7400	9	7.20	6390.91	9.66	9.47	9.53
1229	0.59	0.044	-0.84290	-1100	-4	-14.48	-950.00	0.71	0.85	0.84
1229	0.52	0.039	0.51871	600	6	10.05	518.18	0.56	0.76	0.77
1229	0.70	0.052	2.65838	4100	2	38.64	3540.91	1.00	0.74	0.77

1229	0.21	0.016	9.48262	4500	0	447.94	3886.36	0.09	1.39	1.43
1229	0.58	0.043	3.05796	3900	1	53.75	3368.18	0.68	1.40	1.43
1229	0.70	0.052	6.80803	10500	1	98.95	9068.18	1.00	1.38	1.47
1229	0.59	0.044	0.38314	500	10	6.58	431.82	0.71	3.22	3.23
1229	0.68	0.051	3.78309	5700	1	56.28	4922.73	0.95	2.74	2.79
1229	1.22	0.091	9.04033	24400	1	75.08	21072.73	3.05	2.37	2.58

Table I Flow rates and piping pressures of 2.14 wt% CMC slurry in hose pump experiments. The used pump rotation speeds were 22, 48, and 78 rpm. Piping pressures were generated by control pressures of the actuator. Control pressures were 0.0, 2.0, 4.0, and 6.0 bar.

Pump rotation speed rpm	Flow rate m^3/h	Control pressure bar	Piping pressure bar
22	0.83	0.0	0.16
	0.83	2.0	1.26
	0,87	4.0	4.36
	0.83	6.0	7.76
48	1.78	0.0	0.17
	1.77	2.0	1.57
	1.70	4.0	5.10
	1.62	6.0	8.49
78	2.90	0.0	0.20
	2.83	2.0	1.77
	2.83	4.0	5.40
	2.59	6.0	8.64

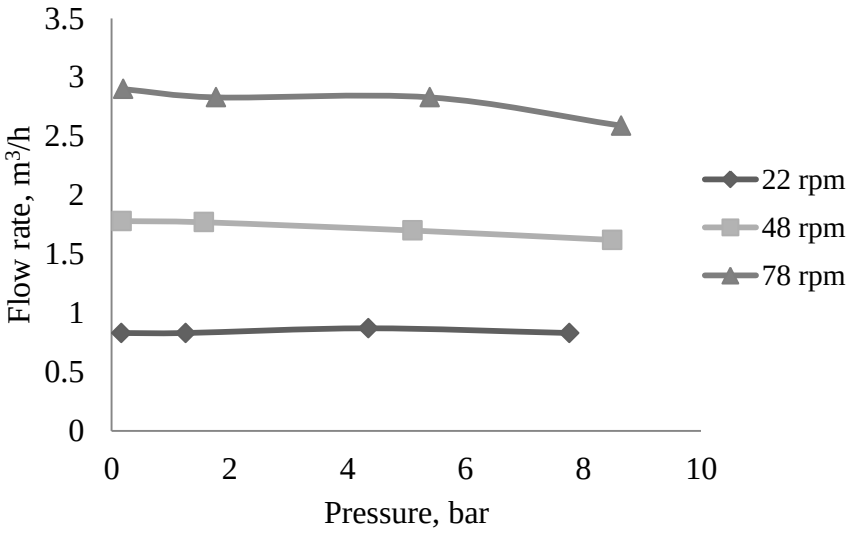

Figure 1. Pressure curves of 2.14 wt% CMC slurry in hose pump. The used pump rotation speeds were 22, 48, and 78 rpm.

Table II Flow rates and piping pressures of 3.87 wt% CMC slurry in hose pump experiments. The used pump rotation speeds were 22, 48, and 78 rpm. Piping pressures were generated by control pressures of the actuator. Control pressures were 0.0, 2.0, 4.0, and 6.0 bar.

Pump rotation speed rpm	Flow rate m^3/h	Control pressure bar	Piping pressure bar
22	0.86	0.0	0.17
	0.84	2.0	1.43
	0.87	4.0	4.57
	0.88	6.0	7.60
48	1.74	0.0	0.17
	1.72	2.0	1.58
	1.90	4.0	4.82
	2.16	6.0	8.40
78	2.66	0.0	0.17
	2.80	2.0	1.80
	2.87	4.0	5.17
	2.43	6.0	8.96

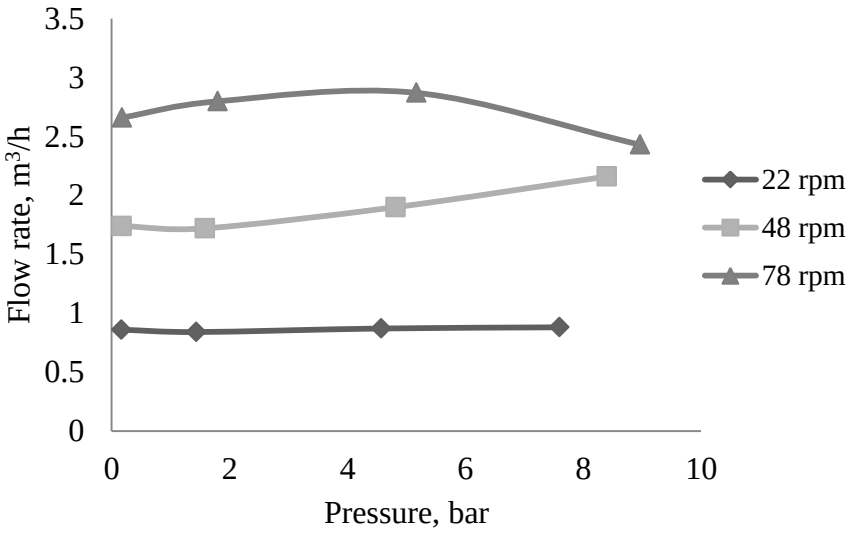

Figure 2. Pressure curves of 3.87 wt% CMC slurry in hose pump. The used pump rotation speeds were 22, 48, and 78 rpm

Table III Flow rates and piping pressures of 5.69 wt% CMC slurry in hose pump experiments. The used pump rotation speeds were 22, 48, and 78 rpm. Piping pressures were generated by control pressures of the actuator. Control pressures were 0.0, 2.0, 4.0, and 6.0 bar.

Pump rotation speed rpm	Flow rate m^3/h	Control pressure bar	Piping pressure bar
22	0.81	0.0	0.18
	0.82	2.0	1.16
	0.82	4.0	4.17
	0.80	6.0	7.31
48	1.72	0.0	0.19
	1.72	2.0	1.26
	1.65	4.0	4.43
	1.80	6.0	7.94
78	2.77	0.0	0.21
	2.75	2.0	1.42
	2.82	4.0	4.81
	2.87	6.0	8.69

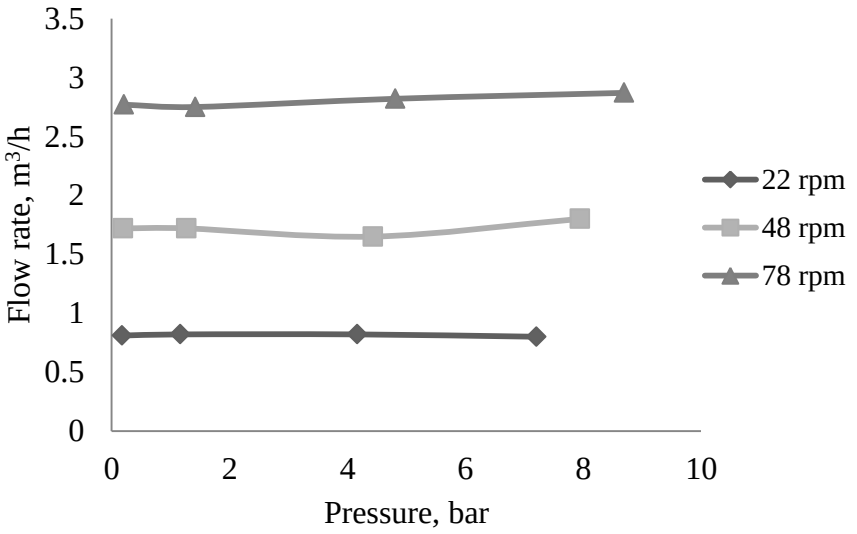

Figure 3. Pressure curves of 5.69 wt% CMC slurry in hose pump. The used pump rotation speeds were 22, 48, and 78 rpm

Table IV Flow rates and piping pressures of 7.59 wt% CMC slurry in hose pump experiments. The used pump rotation speeds were 22, 48, and 78 rpm. Piping pressures were generated by control pressures of the actuator. Control pressures were 0.0, 2.0, 4.0, and 6.0 bar.

Pump rotation speed rpm	Flow rate m^3/h	Control pressure bar	Piping pressure bar
22	0.82	0.0	0.19
	0.79	2.0	1.26
	0.82	4.0	3.82
	0.90	6.0	7.03
48	1.71	0.0	0.24
	1.71	2.0	1.49
	1.70	4.0	4.08
	1.66	6.0	7.67
78	2.68	0.0	0.28
	2.67	2.0	1.63
	2.67	4.0	4.35
	2.83	6.0	8.02

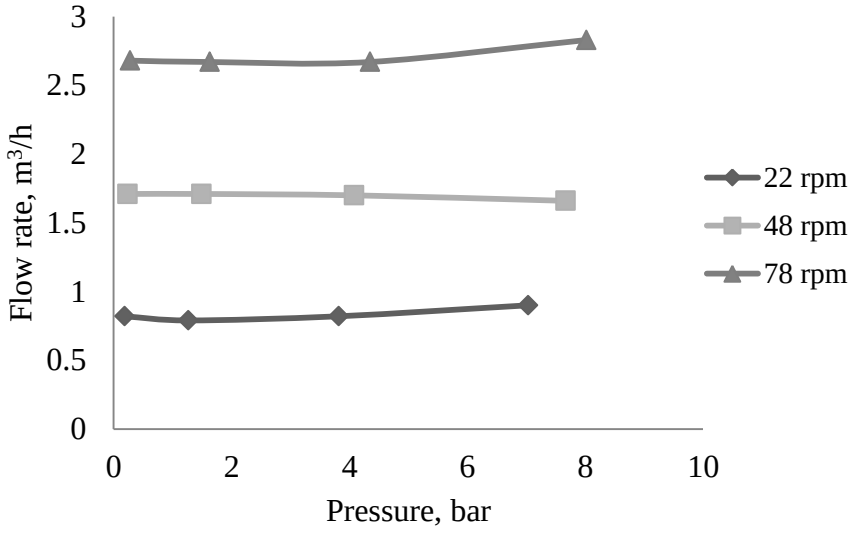

Figure 4. Pressure curves of 7.59 wt% CMC slurry in hose pump. The used pump rotation speeds were 22, 48, and 78 rpm

Table V Flow rates and piping pressures of 9.57 wt% CMC slurry in hose pump experiments. The used pump rotation speeds were 22, 48, and 78 rpm. Piping pressures were generated by control pressures of the actuator. Control pressures were 0.0, 2.0, 4.0, and 6.0 bar.

Pump rotation speed rpm	Flow rate m^3/h	Control pressure bar	Piping pressure bar
22	0.82	0.0	0.26
	0.79	2.0	1.10
	0.79	4.0	1.49
	0.75	6.0	2.5
48	1.59	0.0	0.36
	1.62	2.0	1.37
	1.57	4.0	2.21
	1.56	6.0	5.26
78	2.37	0.0	0.41
	2.31	2.0	1.54
	2.28	4.0	2.96
	2.27	6.0	6.22

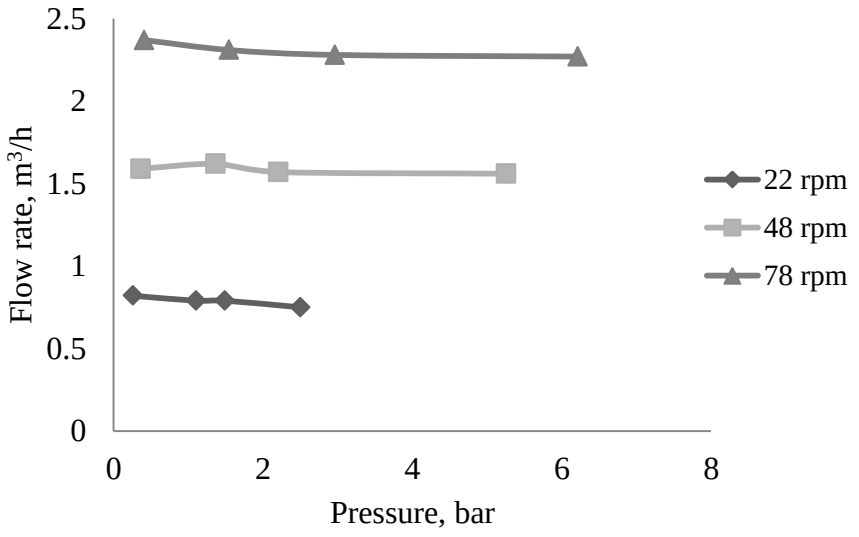

Figure 5. Pressure curves of 9.57 wt% CMC slurry in hose pump. The used pump rotation speeds were 22, 48, and 78 rpm

Table VI Flow rates and piping pressures of 10.99 wt% bentonite slurry in hose pump experiments. The used pump rotation speeds were 22, 48, and 78 rpm. Piping pressures were generated by control pressures of the actuator. Control pressures were 0.0, 2.0, 4.0, and 6.0 bar.

Pump rotation speed rpm	Flow rate m^3/h	Control pressure bar	Piping pressure bar
22	0.74	0.0	0.24
	0.80	2.0	2.04
	0.81	4.0	5.40
	1.11	6.0	8.99
48	1.65	0.0	0.25
	1.58	2.0	2.08
	1.63	4.0	5.50
	1.51	6.0	9.15
78	2.56	0.0	0.26
	2.55	2.0	2.07
	2.36	4.0	5.25
	1.85	6.0	9.04

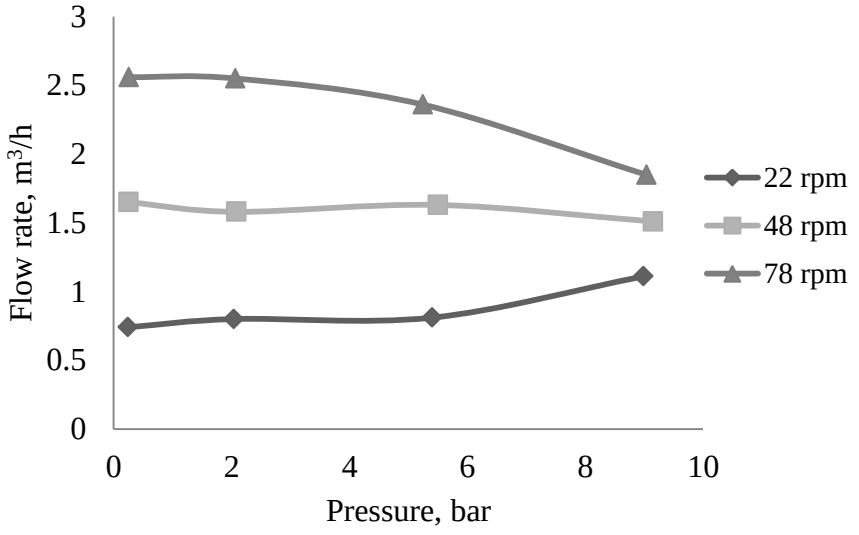

Figure 6. Pressure curves of 10.99 wt% bentonite slurry in hose pump. The used pump rotation speeds were 22, 48, and 78 rpm

Table VII Flow rates and piping pressures of 11.26 wt% bentonite slurry in hose pump experiments. The used pump rotation speeds were 22, 48, and 78 rpm. Piping pressures were generated by control pressures of the actuator. Control pressures were 0.0, 2.0, 4.0, and 6.0 bar.

Pump rotation speed rpm	Flow rate m^3/h	Control pressure bar	Piping pressure bar
22	0.91	0.0	0.22
	0.70	2.0	1.32
	0.65	4.0	5.90
	1.00	6.0	9.84
48	1.55	0.0	0.23
	1.40	2.0	1.36
	1.28	4.0	5.93
	1.92	6.0	9.67
78	2.92	0.0	0.27
	2.92	2.0	1.60
	3.22	4.0	5.93
	2.23	6.0	9.47

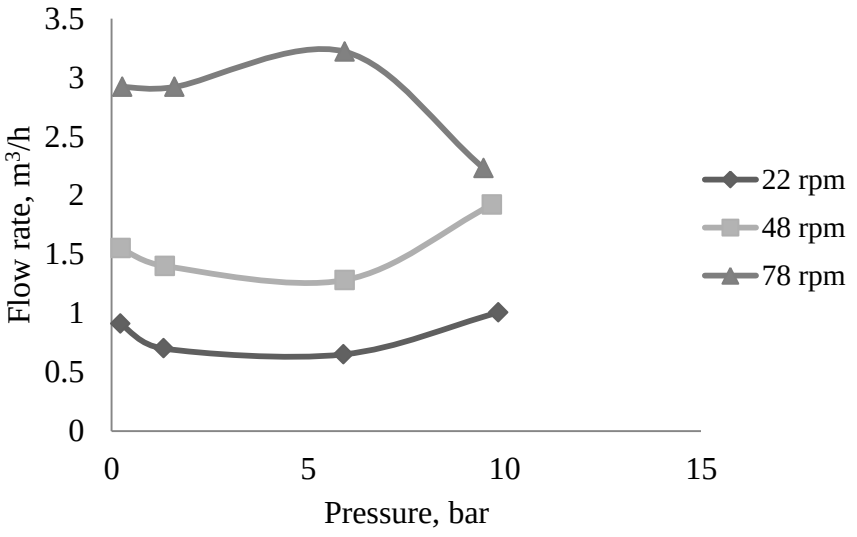

Figure 7. Pressure curves of 11.26 wt% bentonite slurry in hose pump. The used pump rotation speeds were 22, 48, and 78 rpm

Table VIII Flow rates and piping pressures of 15.27 wt% bentonite slurry in hose pump experiments. The used pump rotation speeds were 22, 48, and 78 rpm. Piping pressures were generated by control pressures of the actuator. Control pressures were 0.0, 2.0, 4.0, and 6.0 bar.

Pump rotation speed rpm	Flow rate m^3/h	Control pressure bar	Piping pressure bar
22	0.60	0.0	0.85
	0.21	2.0	1.39
	0.59	4.0	3.23
48	0.53	0.0	0.76
	0.57	2.0	1.40
	0.64	4.0	2.74
78	0.70	0.0	0.74
	0.70	2.0	1.38
	1.22	4.0	2.37

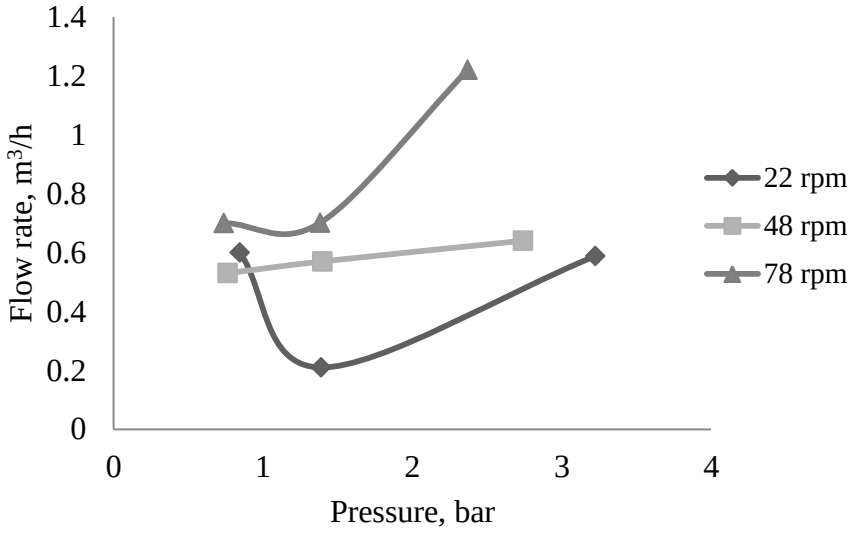

Figure 8. Pressure curves of 15.27 wt% bentonite slurry in hose pump. The used pump rotation speeds were 22, 48, and 78 rpm

Table IX Flow rates and piping pressures of 20.67 wt% starch slurry in hose pump experiments. The used pump rotation speeds were 22, 48, and 78 rpm. Piping pressures were generated by control pressures of the actuator. Control pressures were 0.0, 2.0, 4.0, and 6.0 bar.

Pump rotation speed rpm	Flow rate m^3/h	Control pressure bar	Piping pressure bar
22	0.82	0.0	0.17
	0.84	2.0	1.75
	0.89	4.0	4.69
	0.82	6.0	7.94
48	1.71	0.0	0.17
	1.74	2.0	1.98
	1.80	4.0	5.11
	1.93	6.0	8.19
78	2.85	0.0	0.15
	2.79	2.0	2.33
	2.57	4.0	5.52
	2.72	6.0	8.32

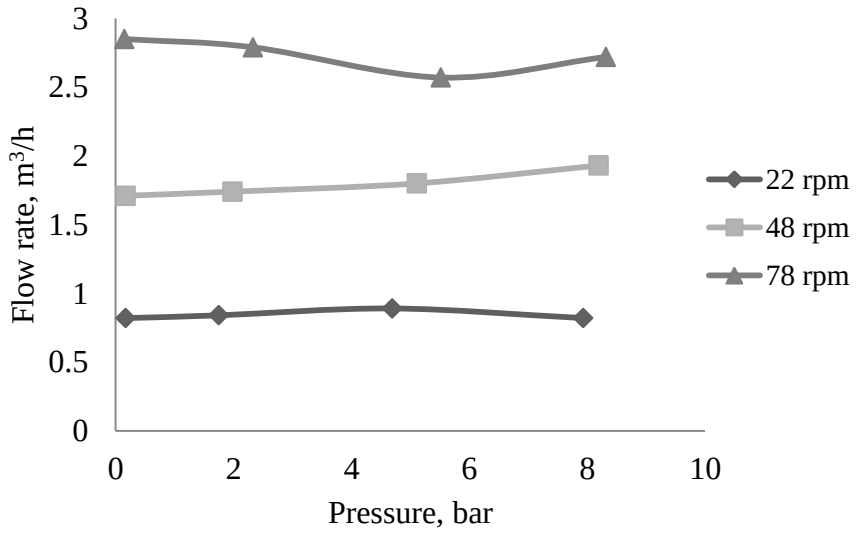

Figure 9. Pressure curves of 20.67 wt% starch slurry in hose pump. The used pump rotation speeds were 22, 48, and 78 rpm

Table X Flow rates and piping pressures of 28.48 wt% starch slurry in hose pump experiments. The used pump rotation speeds were 22, 48, and 78 rpm. Piping pressures were generated by control pressures of the actuator. Control pressures were 0.0, 2.0, 4.0, and 6.0 bar.

Pump rotation speed rpm	Flow rate m^3/h	Control pressure bar	Piping pressure bar
22	0.85	0.0	0.18
	0.84	2.0	1.71
	0.83	4.0	4.72
	0.92	6.0	7.97
48	1.75	0.0	0.18
	1.75	2.0	1.96
	1.34	4.0	5.24
	1.80	6.0	8.32
78	2.88	0.0	1.19
	2.83	2.0	2.34
	2.98	4.0	5.56
	2.54	6.0	8.62

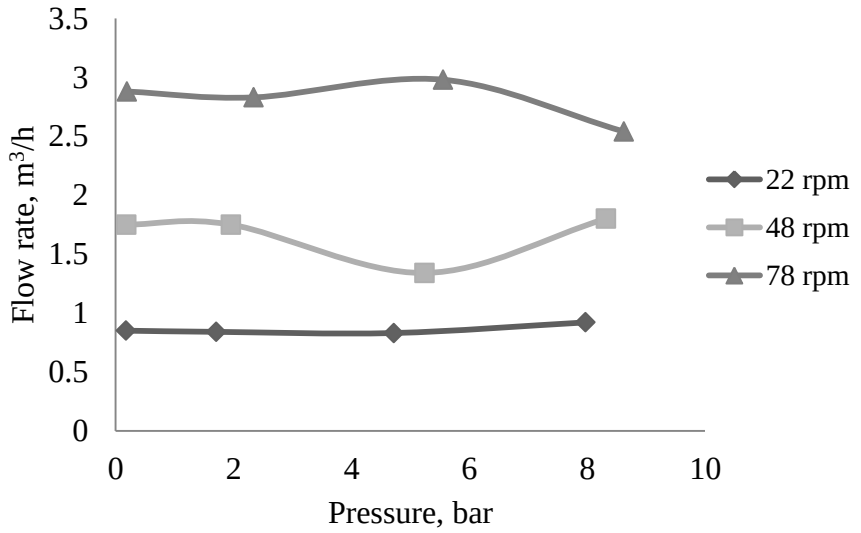

Figure 10. Pressure curves of 28.48 wt% starch slurry in hose pump. The used pump rotation speeds were 22, 48, and 78 rpm

Table XI Flow rates and piping pressures of 38.89 wt% starch slurry in hose pump experiments. The used pump rotation speeds were 22, 48, and 78 rpm. Piping pressures were generated by control pressures of the actuator. Control pressures were 0.0, 2.0, 4.0, and 6.0 bar.

Pump rotation speed rpm	Flow rate m^3/h	Control pressure bar	Piping pressure bar
22	0.84	0.0	0.18
	0.87	2.0	1.41
	0.83	4.0	4.47
	0.85	6.0	7.39
48	1.75	0.0	0.19
	1.75	2.0	1.59
	1.76	4.0	4.92
	1.76	6.0	7.66
78	2.86	0.0	0.20
	2.92	2.0	1.82
	2.88	4.0	5.52
	2.96	6.0	8.12

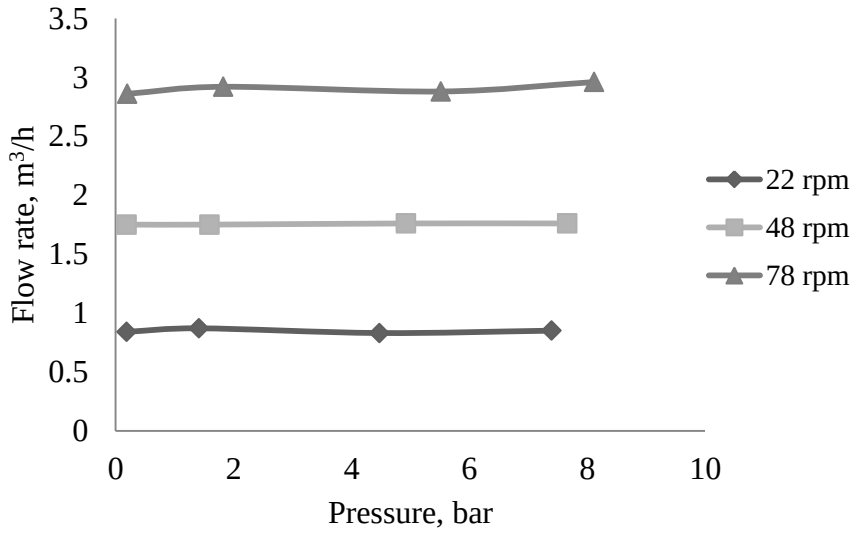

Figure 11. Pressure curves of 38.89 wt% starch slurry in hose pump. The used pump rotation speeds were 22, 48, and 78 rpm

Table XII Flow rates and piping pressures of 47.53 wt% starch slurry in hose pump experiments. The used pump rotation speeds were 22, 48, and 78 rpm. Piping pressures were generated by control pressures of the actuator. Control pressures were 0.0, 2.0, 4.0, and 6.0 bar.

Pump rotation speed rpm	Flow rate m^3/h	Control pressure bar	Piping pressure bar
22	0.84	0.0	1.88
	0.82	2.0	1.39
	0.86	4.0	3.70
	0.88	6.0	6.82
48	1.78	0.0	0.18
	1.81	2.0	1.49
	1.79	4.0	4.22
	1.55	6.0	7.27
78	2.86	0.0	0.16
	2.83	2.0	1.58
	2.94	4.0	4.63
	2.84	6.0	7.89

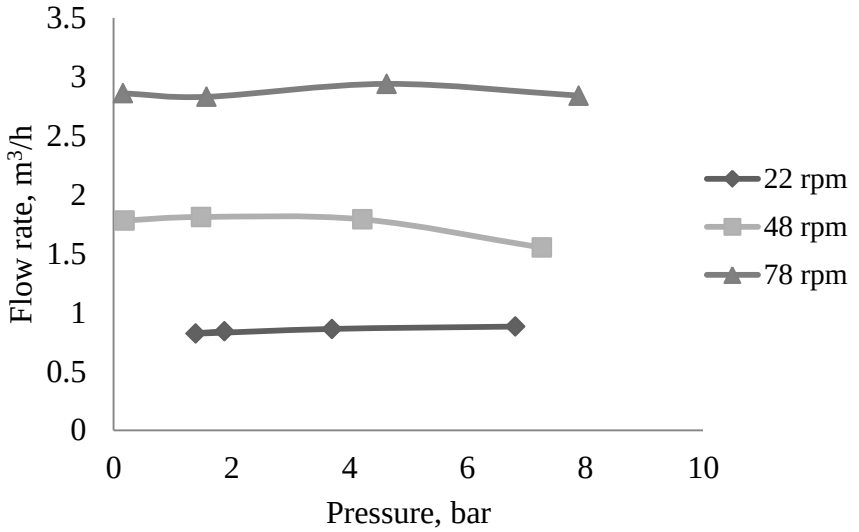

Figure 12. Pressure curves of 47.53 wt% starch slurry in hose pump. The used pump rotation speeds were 22, 48, and 78 rpm

Table XIII Flow rates and piping pressures of 49.29 wt% starch slurry in hose pump experiments. The used pump rotation speeds were 22, 48, and 78 rpm. Piping pressures were generated by control pressures of the actuator. Control pressures were 0.0, 2.0, 4.0, and 6.0 bar.

Pump rotation speed rpm	Flow rate m^3/h	Control pressure bar	Piping pressure bar
22	0.83	0.0	0.19
	0.83	2.0	2.14
	0.80	4.0	6.98
	0.80	6.0	9.85
48	1.75	0.0	0.20
	1.77	2.0	2.15
	1.79	4.0	6.60
	1.53	6.0	9.74
78	2.45	0.0	0.21
	2.43	2.0	2.09
	2.64	4.0	6.27
	2.13	6.0	9.05

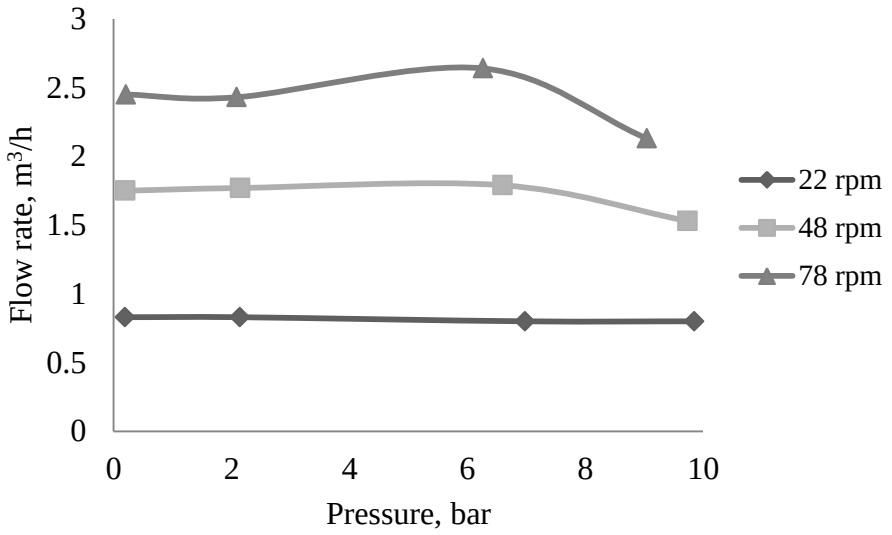

Figure 13. Pressure curves of 49.29 wt% starch slurry in hose pump. The used pump rotation speeds were 22, 48, and 78 rpm

Table I Flow rates and piping pressures of 6.11 wt% CMC slurry in progressive cavity pump experiments. The used pump rotation speeds were 82, 204, and 326 rpm. Piping pressures were generated by control pressures of the actuator. Control pressures were 0.0, 2.0, 4.0, and 6.0 bar.

Pump rotation speed rpm	Flow rate m^3/h	Control pressure bar	Piping pressure bar
82	1.97	0.0	0.02
	1.97	2.0	1.24
	1.65	4.0	4.62
	1.08	6.0	8.79
204	4.17	0.0	0.09
	4.31	2.0	1.43
	3.88	4.0	5.22
	3.20	6.0	10.14
326	6.85	0.0	0.14
	6.86	2.0	1.77
	6.27	4.0	6.28
	5.62	6.0	10.89

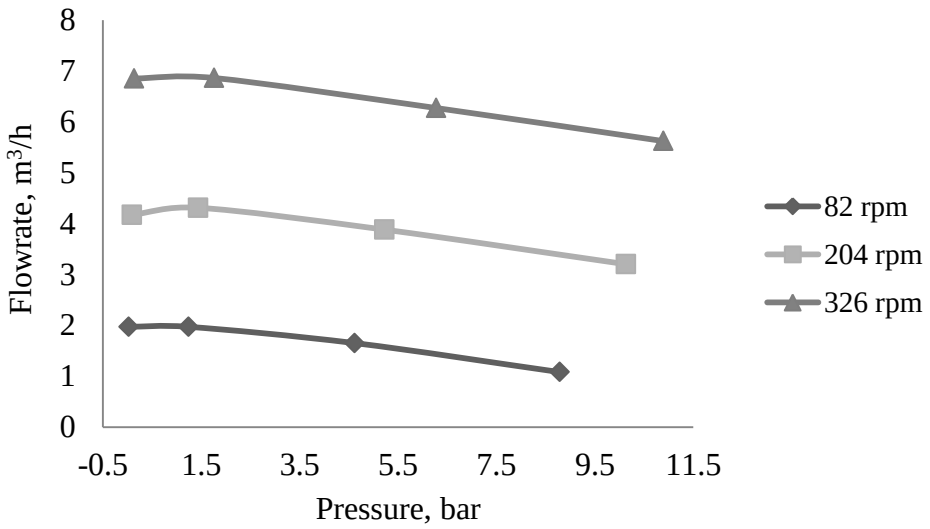

Figure 1. Pressure curves of 6.11 wt% CMC slurry in progressive cavity pump. The used pump rotation speeds were 82, 204, and 326 rpm.

Table II Flow rates and piping pressures of 5.27 wt% CMC slurry in progressive cavity pump experiments. The used pump rotation speeds were 82, 204, and 326 rpm. Piping pressures were generated by control pressures of the actuator. Control pressures were 0.0, 2.0, 4.0, and 6.0 bar.

Pump rotation speed rpm	Flow rate m^3/h	Counter pressure bar	Piping pressure bar
82	2.01	0.0	-0.03
	1.96	2.0	1.38
	1.54	4.0	4.97
	0.83	6.0	10.31
204	4.33	0.0	0.03
	4.26	2.0	1.82
	3.75	4.0	5.94
	3.10	6.0	10.80
326	6.90	0.0	0.08
	6.75	2.0	2.31
	6.24	4.0	6.49
	5.58	6.0	11.38

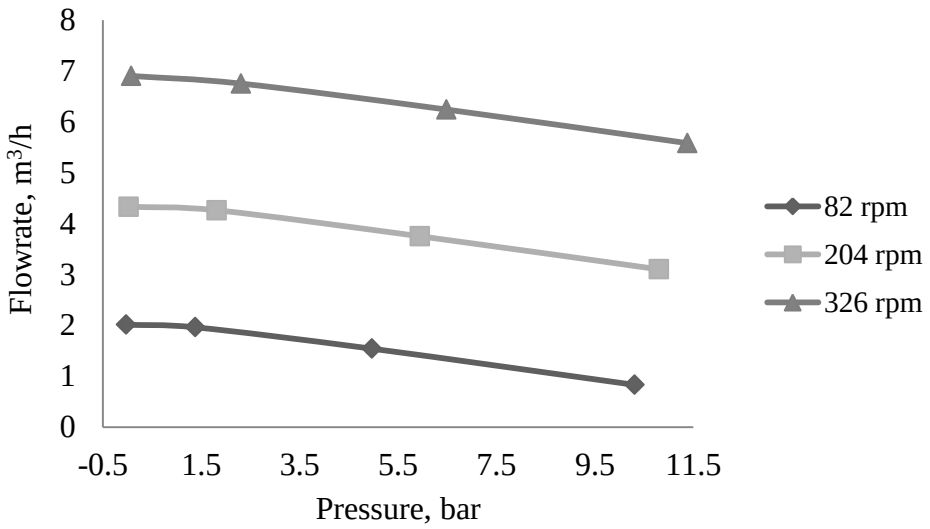

Figure 2. Pressure curves of 5.27 wt% CMC slurry in progressive cavity pump. The pump rotation speeds were 82, 204, and 326 rpm.

Table III Flow rates and piping pressures of 4.55 wt% CMC slurry in progressive cavity pump experiments. The used pump rotation speeds were 82, 204, and 326 rpm. Piping pressures were generated by control pressures of the actuator. Control pressures were 0.0, 2.0, 4.0, and 6.0 bar.

Pump rotation speed rpm	Flow rate m^3/h	Counter pressure bar	Piping pressure bar
82	1.96	0.0	0.00
	1.85	2.0	1.45
	1.45	4.0	5.13
	0.92	6.0	8.88
204	4.31	0.0	0.02
	4.13	2.0	1.92
	3.68	4.0	6.11
	3.06	6.0	10.45
326	6.95	0.0	0.04
	6.76	2.0	2.51
	6.25	4.0	6.77
	5.39	6.0	11.19

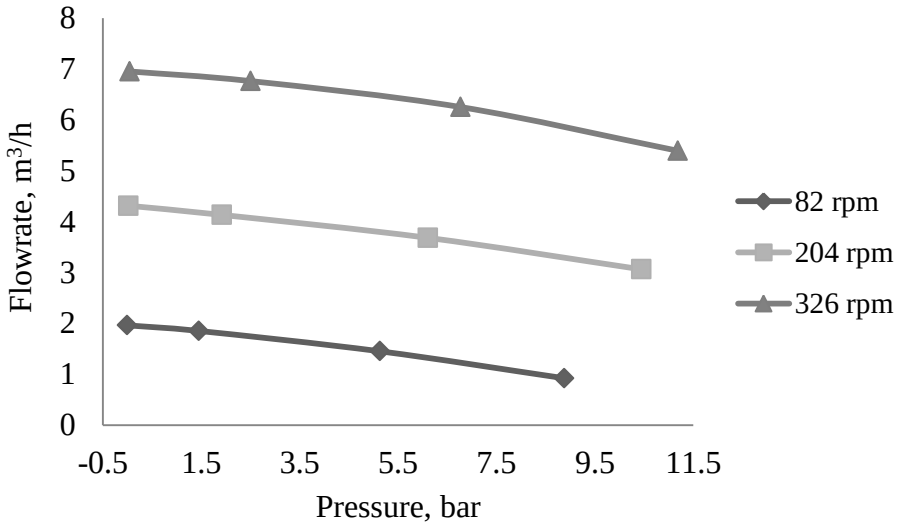

Figure 3. Pressure curves of 4.55 wt% CMC slurry in progressive cavity pump. The pump rotation speeds were 82, 204, and 326 rpm.

Table IV Flow rates and piping pressures of 3.67 wt% CMC slurry in progressive cavity pump experiments. The used pump rotation speeds were 82, 204, and 326 rpm. Piping pressures were generated by control pressures of the actuator. Control pressures were 0.0, 2.0, 4.0, and 6.0 bar.

Pump rotation speed rpm	Flow rate m^3/h	Counter pressure bar	Piping pressure bar
82	2.00	0.0	0.00
	1.89	2.0	1.55
	1.36	4.0	4.65
	0.65	6.0	9.61
204	4.41	0.0	0.02
	4.10	2.0	2.09
	3.60	4.0	5.93
	2.88	6.0	10.98
326	7.05	0.0	0.03
	6.64	2.0	2.60
	6.23	4.0	6.79
	5.41	6.0	11.55

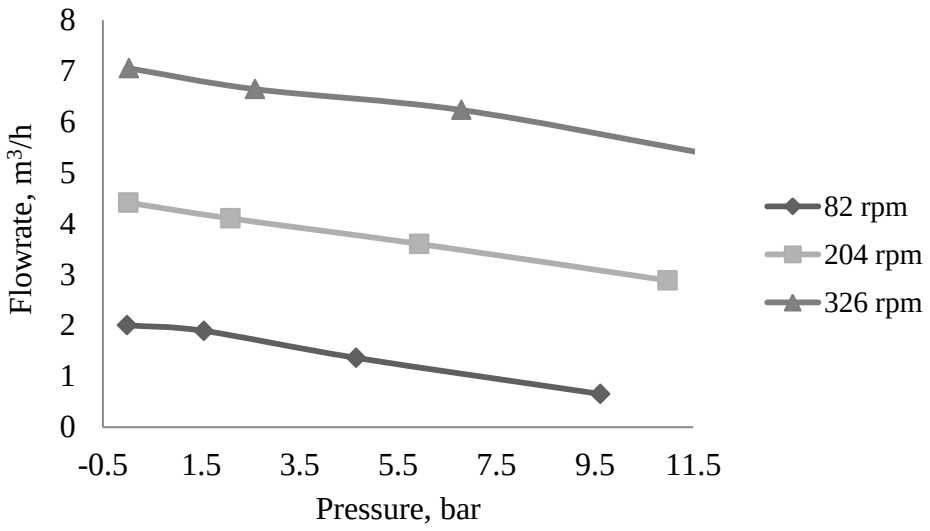

Figure 4. Pressure curves of 3.67 wt% CMC slurry in progressive cavity pump. The used pump rotation speeds were 82, 204, and 326 rpm.

Table V Flow rates and piping pressures of 16.48 wt% starch slurry in progressive cavity pump experiments. The used pump rotation speeds were 82, 204, and 326 rpm. Piping pressures were generated by control pressures of the actuator. Control pressures were 0.0, 2.0, 4.0, and 6.0 bar.

Pump rotation speed rpm	Flow rate m^3/h	Counter pressure bar	Piping pressure bar
82	2.06	0.0	-0.09
	1.43	2.0	1.93
	0.96	4.0	5.30
	0.59	6.0	8.57
204	4.36	0.0	-0.06
	3.70	2.0	2.61
	3.21	4.0	6.70
	2.57	6.0	10.72
326	6.95	0.0	-0.04
	6.15	2.0	2.96
	5.85	4.0	7.21
	5.07	6.0	11.36

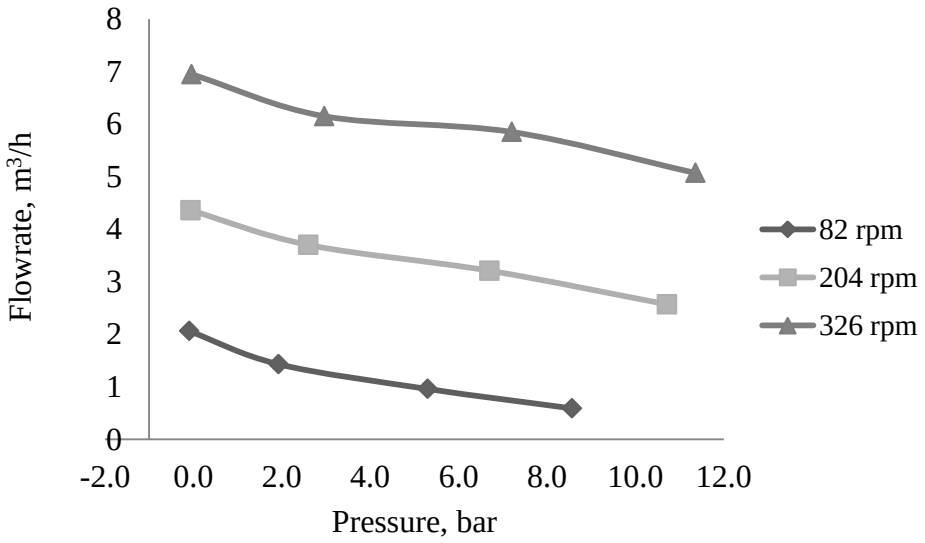

Figure 5. Pressure curves of 16.48 wt% starch slurry in progressive cavity pump. The pump rotation speeds were 82, 204, and 326 rpm.

Table VI Flow rates and piping pressures of 28.44 wt% starch slurry in progressive cavity pump experiments. The used pump rotation speeds were 82, 204, and 326 rpm. Piping pressures were generated by control pressures of the actuator. Control pressures were 0.0, 2.0, 4.0, and 6.0 bar.

Pump rotation speed rpm	Flow rate m^3/h	Counter pressure bar	Piping pressure bar
82	2.09	0.0	0.09
	1.54	2.0	1.66
	1.17	4.0	5.91
	0.53	6.0	9.60
204	4.41	0.0	-0.07
	3.84	2.0	2.32
	3.37	4.0	6.38
	2.88	6.0	10.30
326	6.92	0.0	-0.06
	6.49	2.0	2.39
	5.94	4.0	6.86
	5.30	6.0	11.21

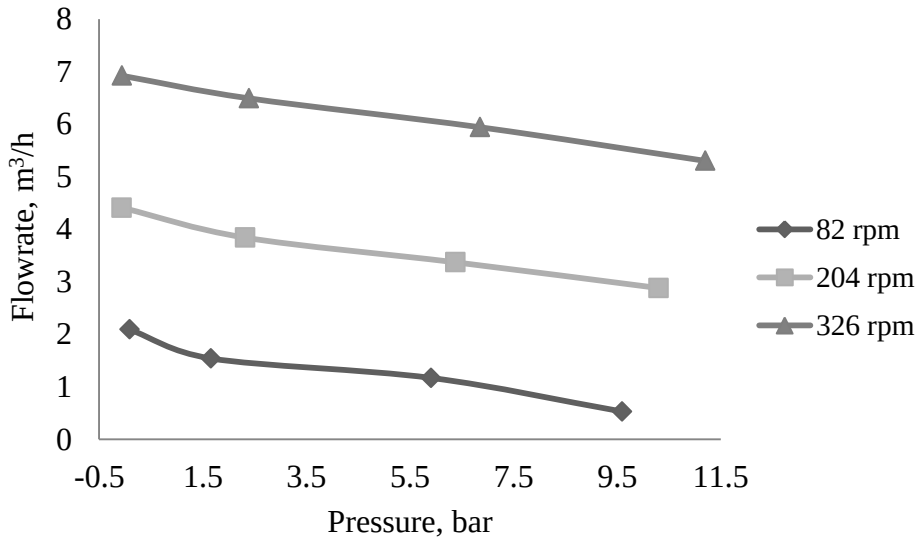

Figure 6. Pressure curves of 28.44 wt% starch slurry in progressive cavity pump. The used pump rotation speeds were 82, 204, and 326 rpm.

Table VII Flow rates and piping pressures of 36.69 wt% starch slurry in progressive cavity pump experiments. The used pump rotation speeds were 82, 204, and 326 rpm. Piping pressures were generated by control pressures of the actuator. Control pressures were 0.0, 2.0, 4.0, and 6.0 bar.

Pump rotation speed rpm	Flow rate m^3/h	Counter pressure bar	Piping pressure bar
82	2.03	0.0	-0.05
	1.59	2.0	1.56
	1.27	4.0	5.18
	0.88	6.0	8.48
204	4.45	0.0	-0.04
	3.99	2.0	2.22
	3.53	4.0	6.43
	2.90	6.0	10.76
326	6.89	0.0	-0.06
	6.60	2.0	2.22
	6.07	4.0	7.09
	5.41	6.0	11.28

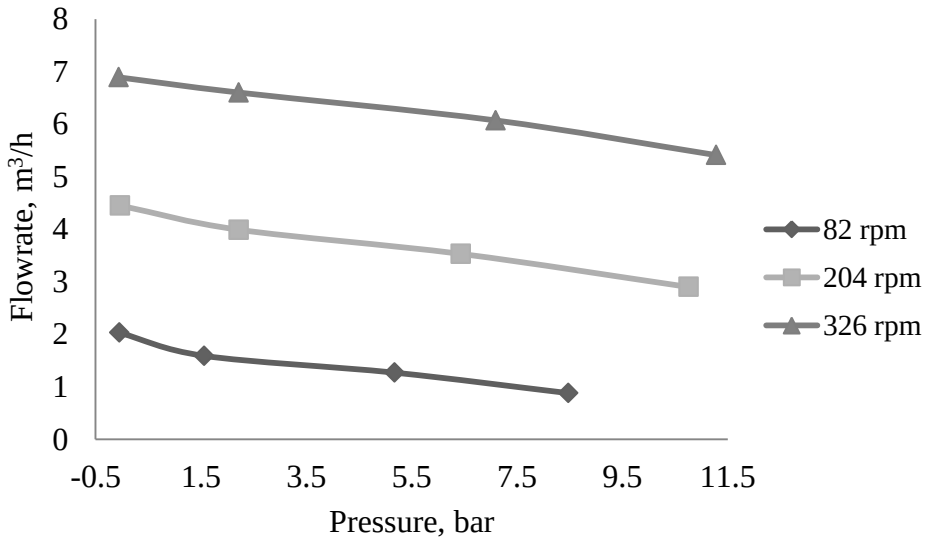

Figure 7. Pressure curves of 36.69 wt% starch slurry in progressive cavity pump. The used pump rotation speeds were 82, 204, and 326 rpm.

Table VIII Flow rates and piping pressures of 40.28 wt% starch slurry in progressive cavity pump experiments. The used pump rotation speeds were 82, 204, and 326 rpm. Piping pressures were generated by control pressures of the actuator. Control pressures were 0.0, 2.0, 4.0, and 6.0 bar.

Pump rotation speed rpm	Flow rate m^3/h	Counter pressure bar	Piping pressure bar
82	2.10	0.0	-0.09
	1.79	2.0	1.64
	1.35	4.0	5.49
	0.93	6.0	8.99
204	3.84	0.0	-0.07
	4.06	2.0	2.34
	3.56	4.0	6.37
	2.99	6.0	10.70
326	7.02	0.0	-0.06
	6.67	2.0	2.48
	6.21	4.0	6.73
	5.58	6.0	11.22

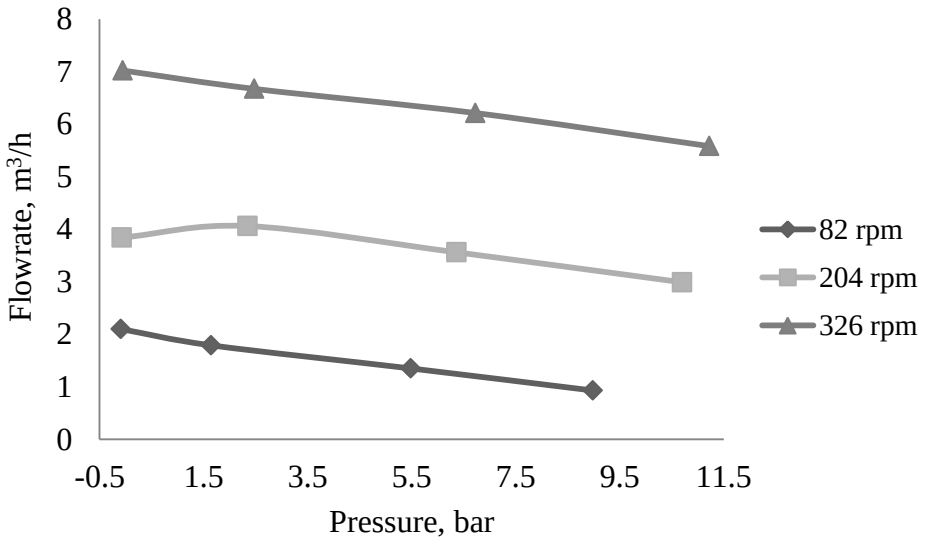

Figure 8. Pressure curves of 40.28 wt% starch slurry in progressive cavity pump. The used pump rotation speeds were 82, 204, and 326 rpm.

Table IX Flow rates and piping pressures of 44.38 wt% starch slurry in progressive cavity pump experiments. The used pump rotation speeds were 82, 204, and 326 rpm. Piping pressures were generated by control pressures of the actuator. Control pressures were 0.0, 2.0, 4.0, and 6.0 bar.

Pump rotation speed rpm	Flow rate m^3/h	Counter pressure bar	Piping pressure bar
82	2.17	0.0	-0.04
	1.86	2.0	1.55
	1.54	4.0	4.77
	1.09	6.0	9.20
204	4.32	0.0	-0.02
	4.20	2.0	1.99
	3.80	4.0	6.07
	3.30	6.0	10.32
326	6.90	0.0	-0.03
	6.67	2.0	2.57
	6.32	4.0	6.97
	5.72	6.0	10.99

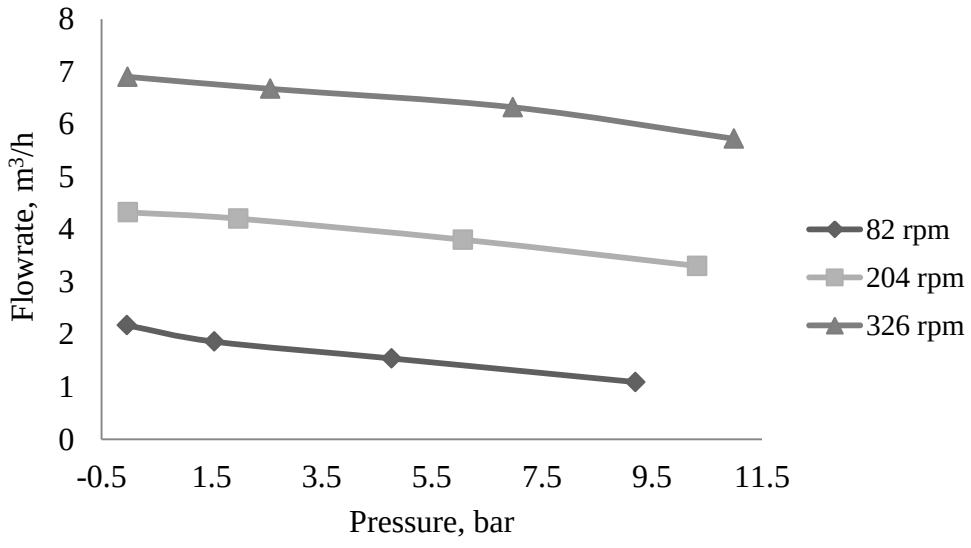

Figure 9. Pressure curves of 44.38 wt% starch slurry in progressive cavity pump. The used pump rotation speeds were 82, 204, and 326 rpm.